1990

Low-energy electron diffraction investigation of epitaxial growth: Pt and Pd on Pd(100)

Diane K. Flynn-Sanders
Iowa State University

Order Number 9100500

Low-energy electron diffraction investigation of epitaxial growth: Pt and Pd on Pd(100)

Flynn-Sanders, Diane K., Ph.D.

Iowa State University, 1990

U·M·I
300 N. Zeeb Rd.
Ann Arbor, MI 48106

Low-energy electron diffraction investigation of epitaxial growth: Pt and Pd on Pd(100)

by

Diane K. Flynn-Sanders

A Dissertation Submitted to the
Graduate Faculty in Partial Fulfillment of the
Requirements for the Degree of
DOCTOR OF PHILOSOPHY

Department: Chemistry
Major: Physical Chemistry

Approved:

Signature was redacted for privacy.

In Charge of Major Work

Signature was redacted for privacy.

For the Major Department

Signature was redacted for privacy.

For the Graduate College

Iowa State University
Ames, Iowa
1990

TABLE OF CONTENTS

Page

DEDICATION iii

GENERAL INTRODUCTION 1

PAPER I: USE OF LEED INTENSITY OSCILLATIONS IN MONITORING THIN FILM GROWTH 7

PAPER II: TEMPERATURE DEPENDENCE OF METAL FILM GROWTH VIA LOW-ENERGY ELECTRON DIFFRACTION INTENSITY OSCILLATIONS: Pt/Pd(100) 32

PAPER III: LEED INVESTIGATION OF Pd/Pd(100) EPITAXIAL GROWTH 56

PAPER IV: EFFECTS OF DIFFUSION ON EPITAXIAL THIN FILM GROWTH 113

PAPER V: PRACTICAL DETERMINATION OF THE OUT-OF-PHASE ENERGY FOR MONITORING INTENSITY OSCILLATIONS DURING THIN FILM GROWTH 178

APPENDIX: RECOATING LEED OPTICS 218

CONCLUSIONS 228

REFERENCES 232

ACKNOWLEDGEMENTS 234

DEDICATION

To my parents,

Jim and Mary Ann Flynn

GENERAL INTRODUCTION

Thin metal films often exhibit chemical, magnetic and electronic properties that are sometimes unlike those of the bulk material. Research on the properties of thin films has increased dramatically in recent years, not only because they are scientifically interesting, but also because they are commercially promising. Investigations of thin film properties are frequently explored via model systems involving epitaxial layers on single crystal, metal substrates (1,2).

One intense area of research is in relation to bimetallic catalysis (3). The presence of a second metal often enhances the rate or selectivity of a catalytic reaction. For example, model studies in the group of Somorjai (4-7) have shown that the dehydrogenation of cyclohexene to benzene on Au-covered Pt displays a fivefold increase in the reaction rate relative to the rate obtained on Pt itself. Similarly, one or two monolayers of Pt on Au exhibit accelerated reaction rates (4-6). This is remarkable, since Au itself is inert to cyclohexene dehydrogenation. This thin film system offers chemical properties unobtainable from either metal alone.

Unusual catalytic properties are also found in the Cu/Ru system. Cu films on Ru(001) (1,8) have been used extensively as a model catalyst in the investigation of geometric and electronic effects for various reactions: methanation (9), cyclohexane hydrogenolysis (8), and cyclohexane dehydrogenation to benzene (10,11). For the first two reactions, Cu serves as a diluent, blocking sites on a one-to-one basis

(1,8). In the last reaction, submonolayer quantities of Cu increase the reaction rate by an order of magnitude relative to that on Ru alone. Cu and Ru, if both exposed, could catalyze different steps in the dehydrogenation mechanism, leading to the augmented rate. Alternatively, the enhanced activity of this thin film system may stem from the unique geometric (10) or electronic (12) properties associated with the thin Cu film on Ru. The Cu/Ru system is particularly exciting due to the presence of a "true" interface electronic state - a state unique to the interface itself, for which the wave function has large amplitude near the metal atoms on both sides of the interface, and is discreet from any pure metal state (12).

Novel magnetic properties have been observed in thin film systems as well (13). Research in this area is motivated not only by the study of fundamental magnetic interactions, but has particular relevance to high-density recording applications. Much of this work has centered on epitaxial Fe films on Ag(001) (14). This research was prompted by the experimental observation that Fe films on Ag that are less than ca. 3 layers in thickness do not exhibit in-plane spin polarization. This is in marked contrast to theoretical predictions of enhanced Fe moments for such films. It is postulated that in this system, a large surface anisotropy forces the Fe moments to lie normal to the surface (15,16).

Applications of thin films in microelectronic devices and optical coatings has also received much attention recently. From superlattice electron-wave filters (17) to space mirrors (18), these exotic windows to the quantum and galactic universe exploit the unusual properties that are

manifested in thin films. The performance of these devices precisely depends on the detailed arrangement of atoms within the film. For example, with carefully tuned thicknesses of alternating layers of gallium arsenide and aluminum gallium arsenide, the superlattice electron-wave filter can yield 139 eV electrons with only a 0.003 eV spread (17). The mirrors of the Hubble space telescope (18) are yet another example where precisely defined thicknesses of thin film coatings are required for acceptable performance. With physical dimensions on the order of nanometers in these devices, the demand for perfection approaches the atomic level. Thus the morphology of thin films and structure of interfaces is increasingly important, and currently is a fervent area of study.

The spatial arrangement of atoms as a function of coverage during epitaxial growth is referred to as the growth mode. Understanding the growth mode is the first step in understanding the novel properties of the resulting thin film. Thermodynamic considerations (19) dictate that when the surface free-energy of the interface and growing film is less than or equal to that of the substrate, layer-by-layer growth results in the formation of smooth films. However, the epitaxial growth process often proceeds under nonequilibrium conditions. The actual growth *mechanism* can be dominated by kinetic limitations or local defects in the substrate, prohibiting the system from achieving macroscopic equilibrium. The resulting film structure can have chemical and physical properties that are vastly different from equilibrium films.

In this dissertation, we examine the epitaxial growth of Pt and Pd on Pd(100) via low-energy electron diffraction (LEED). We use these simple systems to gain a basic understanding of the growth process and resulting morphology. Since low-energy electrons (below ca. 400 eV) interact very strongly with solid materials, the LEED technique is very surface sensitive (20,21), thus suitable to the study of overlayer growth. Inelastic scattering limits the mean free path of the electrons to ca. 2 - 20 Å. Detected, elastically-scattered electrons are sensitive to the three-dimensional geometry and the chemical identity of atoms in the near-surface region. The symmetry of the LEED pattern is related to the symmetry of the surface structure. The shape of the diffracted beams contains information on imperfections and deviations in the long-range order of the surface structure. Thus, ordering or growth processes may be investigated by monitoring changes in the LEED pattern.

The equilibrium growth mode for both Pt and Pd on Pd(100) is layer-by-layer. One can envision layer-by-layer growth proceeding as the creation and annihilation of steps as each layer forms and completes. LEED is well-suited to monitor the development and completion of epitaxial layers, since the wavelength of the incident beam can be tuned to match the step height in such a way that diffraction from succeeding layers interferes destructively. The diffracted intensity thus oscillates as each layer forms and completes. Additionally, the LEED spot shape reflects the degree of perfection in the growing layers.

In particular, we monitor LEED spot profiles as a function of overlayer coverage, beam energy and substrate temperature during the

epitaxial growth of Pt and Pd on Pd(100). From the coverage-dependence of the profile lineshapes and intensities, we learn about deviations from perfect layer-by-layer filling. The energy-dependence of the diffracted intensity yields information on the physical dimension of overlayer structures. We extract activation barriers to surface diffusion from the temperature-dependence of the profiles. In addition, we model the growth process to clarify the role of diffusion in determining the ultimate morphology. Although LEED is a technique commonly available in surface science laboratories, it is quite uncommon to analyze the spot profile shapes and intensities during epitaxial growth, as we have done. We feel this is a significant study demonstrating the usefulness of spot profile analysis via conventional LEED.

Explanation of Thesis Format

This dissertation is arranged according to alternate-style format. Five papers are collected. Paper I, "Use of LEED Intensity Oscillations in Monitoring Thin Film Growth" by D. K. Flynn, W. Wang, S.-L. Chang and P. A. Thiel, is published in Langmuir, volume 4 on pages 1096-1100, 1988. Paper II, "Temperature Dependence of Metal Film Growth via Low-Energy Electron Diffraction Intensity Oscillations: Pt/Pd(100)" by D. K. Flynn, J. W. Evans and P. A. Thiel, is published in the Journal of Vacuum Science and Technology A, volume 7, on pages 2162-2166, 1989. Paper III, "LEED Investigation of Pd/Pd(100) Epitaxial Growth" by D. K. Flynn-Sanders and P. A. Thiel, will be submitted for publication in Physical Review B. Paper IV, "Effects of Diffusion on Thin Film Growth" by D. K.

Flynn-Sanders, P. A. Thiel and J. W. Evans, will be submitted for publication in Physical Review B. Paper V, "Practical Determination of the Out-of-Phase Energy for Monitoring Intensity Oscillations during Thin Film Growth" by D. K. Flynn-Sanders and P. A. Thiel, will be submitted for publication in Surface Science.

PAPER I:

USE OF LEED INTENSITY OSCILLATIONS IN MONITORING THIN FILM GROWTH

USE OF LEED INTENSITY OSCILLATIONS IN MONITORING THIN FILM GROWTH

D. K. Flynn, W. Wang, S.-L. Chang, M. C. Tringides and P. A. Thiel

Departments of Physics and Chemistry and Ames Laboratory-USDOE
Iowa State University
Ames, Iowa 50011 USA

ABSTRACT

We show that a conventional LEED apparatus may be used to observe oscillations in diffracted intensity during growth of Pt on Pd(100). The oscillations are due to successive filling of Pt layers, exactly analogous to the oscillations often observed with RHEED during semiconductor growth. In spite of the rather small coherence length of the apparatus, the spot profiles consist of two well-separated components, which are due to short-range and long-range order.

I. INTRODUCTION

In recent years, reflection high-energy electron diffraction (RHEED) has gained enormous popularity as a technique that can be used to measure the number of layers of material deposited during molecular beam epitaxy (MBE) of semiconductors. The technique rests upon the fact that the intensities of the reflected beams undergo periodic oscillations as a function of coverage during layer-by-layer growth which are caused by morphological changes on the surface (1-3). Intensity oscillations have been observed with RHEED during metal-on-metal growth as well (4-6). Henzler and co-workers also report the use of a high-resolution LEED instrument to measure intensity oscillations during growth of Si on Si(111) (7). In this paper we show that a *conventional* low-energy electron diffraction (LEED) apparatus may be used in an exactly analogous manner to ascertain the growth characteristics of a metal-on-metal system. LEED optics are usually configured for normal beam incidence, and this fact (typically) makes LEED less convenient than RHEED as a tool to monitor deposition processes. Nonetheless, it is a technique which might fruitfully be applied in many laboratories using existing equipment. This is particularly significant given the number of surface science groups currently initiating studies of metal-on-metal systems to understand bimetallic catalysts.

II. EXPERIMENTAL DETAILS

The sample is mounted on a liquid-nitrogen cold finger (8) and is heated resistively by passing current through two 0.010 in. diameter Ta wires spot-welded on one face or onto grooves cut in the edges of the sample. A W/5% Re vs. W/26% Re thermocouple is spot-welded to the edge.

The Pd(100) sample is cleaned by prolonged ion bombardment at $T \geq 500$ K to remove sulfur and traces of phosphorus (9-11), followed by repeated cycles of O_2 adsorption at room temperature and $CO_{(g)}$ formation under vacuum at $T \geq 600$ K. The absence of CO evolution is taken to signal a carbon-free surface. At this point Auger electron spectroscopy (AES) usually indicates that the surface is also oxygen-free. Upon adsorption of CO, this surface also shows the normal sequence of CO-related LEED patterns, including $(2\sqrt{2}x\sqrt{2})R45°$ at $\theta_{co} > 0.5$ (9-11).

The Pt evaporation source is based upon the design of DeCooman and Vook (12). It consists of a Pt droplet melted into a gap between 0.020 in. diameter tungsten rods, mounted on a commercial 2.75 in. o.d. flange with high-current feedthroughs. To avoid contamination during evaporation, and also to reduce undesirable evaporation onto other vacuum chamber surfaces, the Pt filament is surrounded by a double-walled, liquid-nitrogen-cooled shroud mounted on a double-side flange. A 1 cm orifice in the shroud allows Pt vapor to escape toward the sample. When the apparatus is operating at sufficiently high temperatures, the evaporation filament is relatively adiabatic and the resultant Pt film is quite clean. Lower evaporation rates (lower temperatures) lead to gross

carbon contamination. In a typical evaporation run the dc filament current is 47.5 A, and the pressure change is the chamber is about 5 x 10^{-10} Torr after 10 s. With the sample 1.5 cm away from the filament, the deposition rate at the sample is (2-5) x 10^{13} s^{-1} cm^{-2}. AES is used to check that the Pt distribution across the surface is uniform to within ± 10%. There is no detectable evidence for Si, S, P, or C contamination in our Pt films or in the Pd substrate after cleaning. In all of the work described here, the films are deposited at a substrate temperature of 300-350 K and are not annealed. The results of annealing are discussed elsewhere (13).

LEED spot profiles are measured with a computer-interfaced, silicon-intensified target video camera (14) and a standard set of Varian four-grid optics. The incident electron beam is normal to the surface within about 2°.

III. RESULTS AND DISCUSSIONS

During adsorption of Pt at 300-350 K, LEED indicates that the Pt films grow isomorphically; i.e., the (1x1) periodicity of the Pd(100) substrate is always preserved. However, the full-widths at half-maxima (FWHM) of the integral-order spot profiles vary strongly with incident beam voltage. The variation is such that at certain beam energies the spots for which $h + k = \pm 1, \pm 3, \ldots$ are very broad while the spots for which $h + k = 0, \pm 2, \ldots$ are very sharp. A photograph of the (1x1) pattern that illustrates this effect is shown in Figure 1. As the energy changes, the spots which are sharp broaden and vice versa. These observations are qualitatively identical with those published by Wagner and Ross (15) in a study of electrochemical roughening of Pt(100) surface. These observations are shown quantitatively in Figure 2 for an initial Pt coverage of 2.5 monolayers.

These data can be interpreted within the framework developed by Henzler (16) and elaborated upon by Wagner and Ross (15). Consider scattering from an island of atoms atop a square substrate, such as shown in Figure 3. We assume that the two-dimensional unit cell within each adlayer is identical, as shown. This is reasonable for the system under discussion. Scattering centers within the top layer are connected by a vector $\underline{g}$ to centers in the lower layer:

$$\underline{g} = x\underline{a} + y\underline{b} + \underline{c} \qquad (1)$$

Figure 1. LEED patterns of Pt/Pd(100)

Normal-incidence LEED patterns of ca. 1.5 ML Pt deposited on Pd(100) at room temperature.
Top: 120 eV, λ=1.12. [1,0] are approximately out-of-phase, whereas [1,1] are in-phase
Bottom: 80 eV, λ=1.37. [1,0] are approximately in-phase whereas [1,1] are out-of-phase.

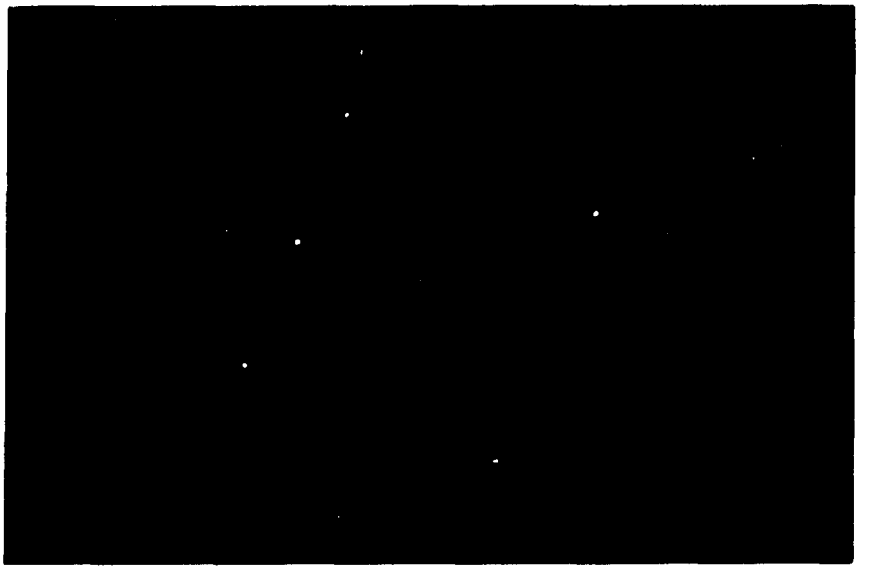

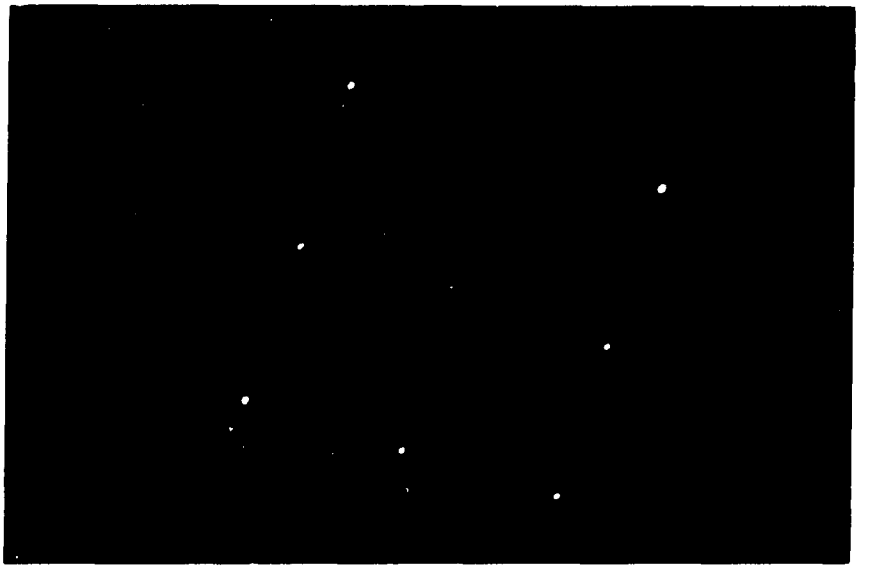

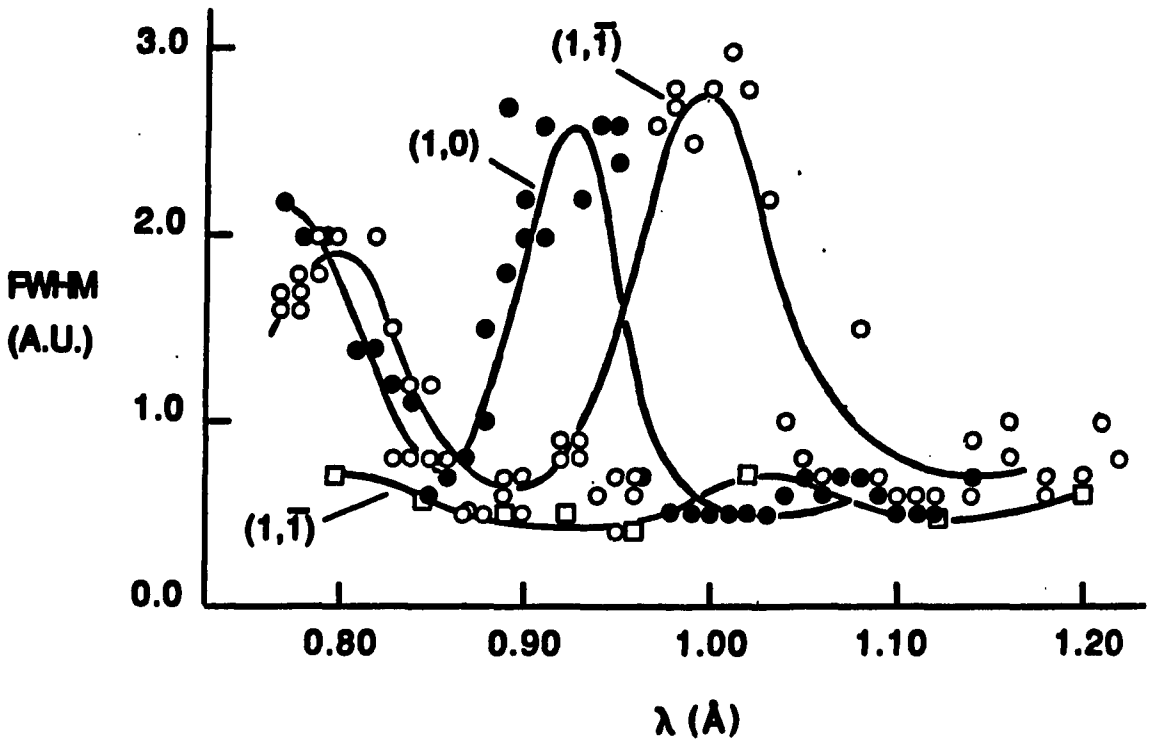

Figure 2. Energy dependence of FWHM

Variation in FWHM of spot profiles as a function of beam energy (electron wavelength) for a clean Pd(100) surface (squares) and after deposition of 2.5 monolayers of Pt at room temperature (circles). The FWHM are given in arbitrary units (A.U.).

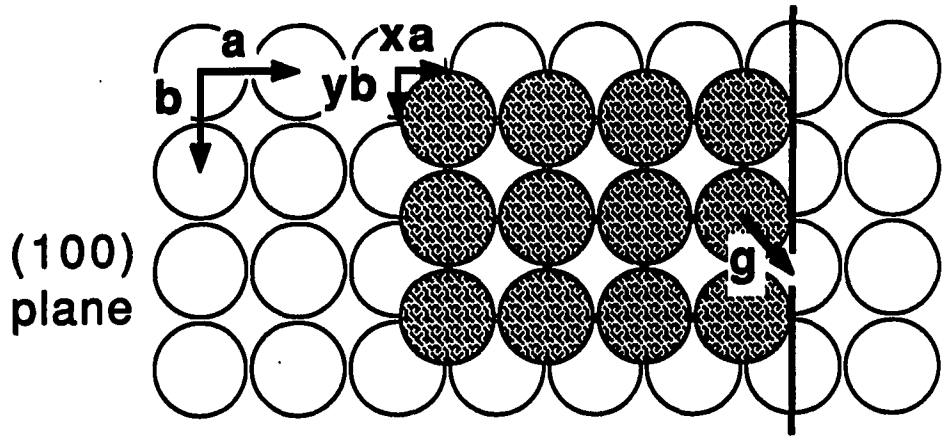

Figure 3. Schematic depiction of a fcc(100) surface (open circles) with an island of atoms in a top layer (shaded circles)

The real-space vectors are defined in the text.

where $\underline{a}$ and $\underline{b}$ are the two-dimensional unit cell vectors of either plane and $\underline{c}$ connects the top and bottom planes. For an fcc lattice, $|\underline{a}| = |\underline{b}| = \sqrt{2}|\underline{c}|$, and the angle between each pair of vectors is $\pi/2$.

The phase difference between adjacent terraces is given by

$$\underline{g} \cdot \Delta\underline{k} = 2n\pi \tag{2}$$

where $\Delta\underline{k}$ is the momentum-transfer wave vector. The parameter n is an integer for constructive interference or half-integer for destructive interference. Introducing the reciprocal-space vectors $\underline{a}^*$, $\underline{b}^*$, and $\underline{c}^*$ and setting

$$\Delta\underline{k} = h\underline{a}^* + k\underline{b}^* + l\underline{c}^* \tag{3}$$

equation (2) becomes

$$(x\underline{a} + y\underline{b} + \underline{c})(h\underline{a}^* + k\underline{b}^* + l\underline{c}^*) = 2n\pi \tag{4}$$

or

$$xh + yk + l = n \tag{5}$$

Here h and k must be integers, and l is determined by the component of $\Delta\underline{k}$ normal to the surface. In terms of experimental parameters, l is determined by the electron wavelength (beam energy) and by the diffraction spot indices, h and k. Henzler (16) has shown that, for normal incidence

$$l = \left(\frac{|\underline{c}|}{2\pi}\right)\left(|\underline{k}_0| + \left[|\underline{k}_0^2 - |(h\underline{a}^* + k\underline{b}^*)|^2\right]^{1/2}\right) \tag{6}$$

When $(h\underline{a}^* + k\underline{b}^*)^2$ is small compared with $\underline{k}_0^2$, then l is determined only by the beam energy, V_e, and equation (5) reduces to

$$V_e = \left(\frac{150.4}{4|\underline{c}|^2}\right)(n - xh - yk)^2 \tag{7}$$

It is easy to show that the patterns of in-phase and out-of-phase scattering shown in Figure 4 will result from the indicated choices of x and y, under these conditions. For instance, choose x = y = 1/2 in equation (5). The spot described by h = 0, k = 1 is in-phase when n = 1/2 + l is an integer, whereas coherent scattering at h = 1, k = 1 requires that n = 1 + l is an integer. In other words, when the (0,1) spot is in-phase the (1,1) spot is exactly out-of-phase (n differs by 1/2) for these choices of x and y. This provides a qualitative explanation for our results, which are most consistent with the choice x = y = 1/2. These values for x and y require that the Pt atoms occupy fourfold-hollow sites, which is physically reasonable for an fcc metal growing atop another fcc metal with an almost identical lattice constant.

However, in LEED it is not usually valid to assume that

$$(h\underline{a}^* + k\underline{b}^*)^2 \ll \underline{k}_0^2 \tag{8}$$

in equation (6). For the Pt on Pd system with x = y = 1/2, this means that the (0,1) spot is not in-phase at *exactly* the same energy where the

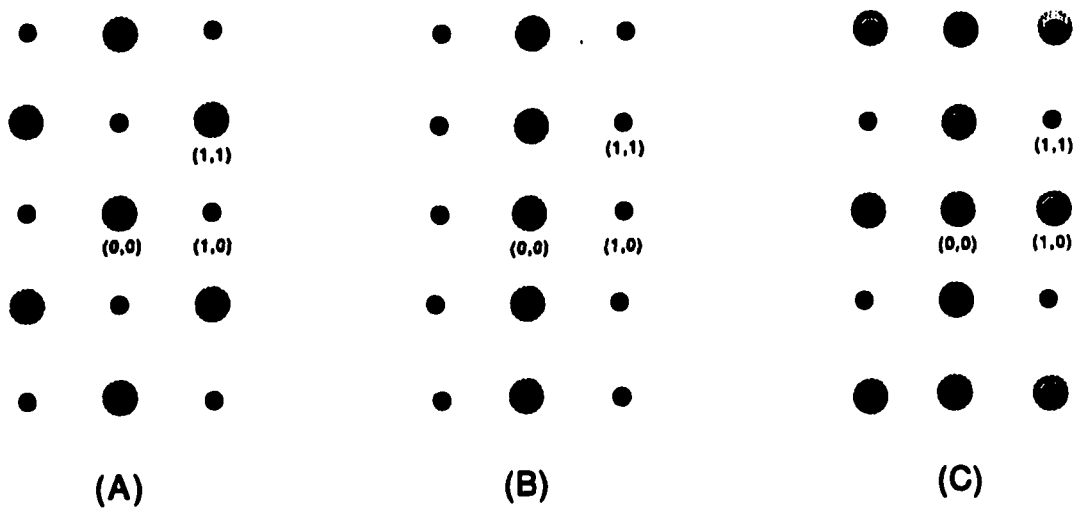

Figure 4. Schematic depiction of possible patterns of spot broadening induced by steps, as discussed in the text

(a) $x = y = 1/2$; fourfold-hollow sites occupied.

(b) $x = 1/2$, $y = 0$; one domain of twofold bridge sites occupied.

(c) $x = 1/2,0$ and $y = 0, 1/2$; two domains of twofold-bridge sites, patterns overlaid.

(1,1) spot is out-of-phase, for instance. Rather, there is a constant difference of about 10 eV between the energies where equation (5) predicts that these two conditions are met, in the range from 50 to 300 eV. The trend and symmetry shown in Figure 4a are preserved, however.

By concentrating on a single beam and measuring the angular profile half-width as a function of energy, we can extract information about the surface step height. When n is an integer, the half-width is expected to be a minimum since the scattered electrons interfere constructively (17); when n is a half-integer, maximum destructive interference occurs between terraces and the profile is broader. Thus the profile half-width oscillates with energy as observed in Figure 2. From the period of oscillations the step height, c, can be extracted. The resultant value is 2.0 ± 0.1 Å, identical within experimental uncertainty with the bulk value (1.96 Å for Pt). In the same figure at the bottom (using square symbols), we show similar measurements for clean Pd(100), but only very weak oscillations are seen. This probably means that the instrument coherence length, L (i.e., the maximal resolvable distance where coherent scattering occurs (18)), is smaller than the average terrace length, M. From the observed energy-independent half-width we estimate $L \approx 100$ Å and from the misorientation of the crystal (0.5°) ≈ 220 Å.

We can interpret our results in terms of a classic two-level system (19,20) resulting from overlayer deposition. The diffracted intensity exhibits oscillations, corresponding to a maximum when full layers are complete and a minimum at half-monolayers. More precisely, the angular

profile of a two-level system consists of a sharp instrument-limited part superimposed on a diffuse background (19,20). The sharp contribution results from coherent scattering of all the atoms present (both substrate and overlayer) and the broad part from incoherent scattering of the overlayer islands. As can be seen from Figure 5, the measured profiles indeed display such form, especially at coverages intermediate between completion of full layers. These measurements are performed on the $(1,\bar{1})$ beam at the out-of-phase condition, where sensitivity to the surface morphology is maximum. A good measure of the top-layer occupation (and therefore the Pt coverage) is the peak intensity, I_p, of the sharp portion. This quantity is represented schematically in the inset of Figure 6. It can be shown (19,20) that

$$I_p \propto (2\theta_{Pt} - 1)^2 \qquad (9)$$

where θ_{Pt} is the Pt coverage. It is clear from this expression that I_p is a maximum when $\theta_{Pt} = 0$ or 1 and a minimum when $\theta_{Pt} = 0.5$. This creates intensity oscillations with constant amplitude as more layers are deposited if perfect layer-by-layer filling (Frank van der Merwe growth) takes place. Oscillations are apparent in the data of Figure 6, supporting our previous report of layer-by-layer growth in this system (13). Actually, as can be seen from Figure 6, the oscillation amplitude is not constant, but rather decays with time (coverage), suggesting that more and more levels are partially occupied at the coverages corresponding to intensity maxima. The atoms on these levels scatter incoherently, reducing the maximum peak intensity. The points where the

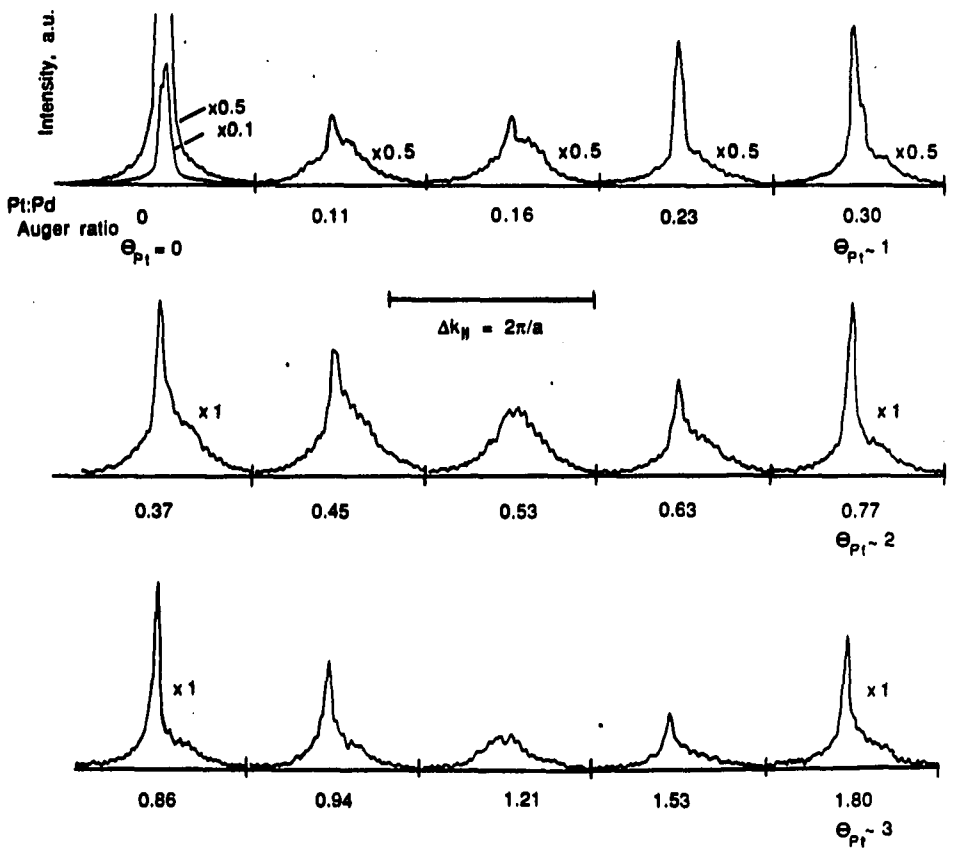

Figure 5. Profiles of the (1,$\bar{1}$) spot after successive Pt evaporations

Each profile is labeled with the Auger intensity ratio, denoted Pt:Pd (13). Profile intensities are given in arbitrary units. Coverages are also given for selected profiles. The Pt coverages are in excellent agreement with other work (13) in which Auger and ultraviolet photoemission spectroscopies are used to infer coverages, but not LEED.

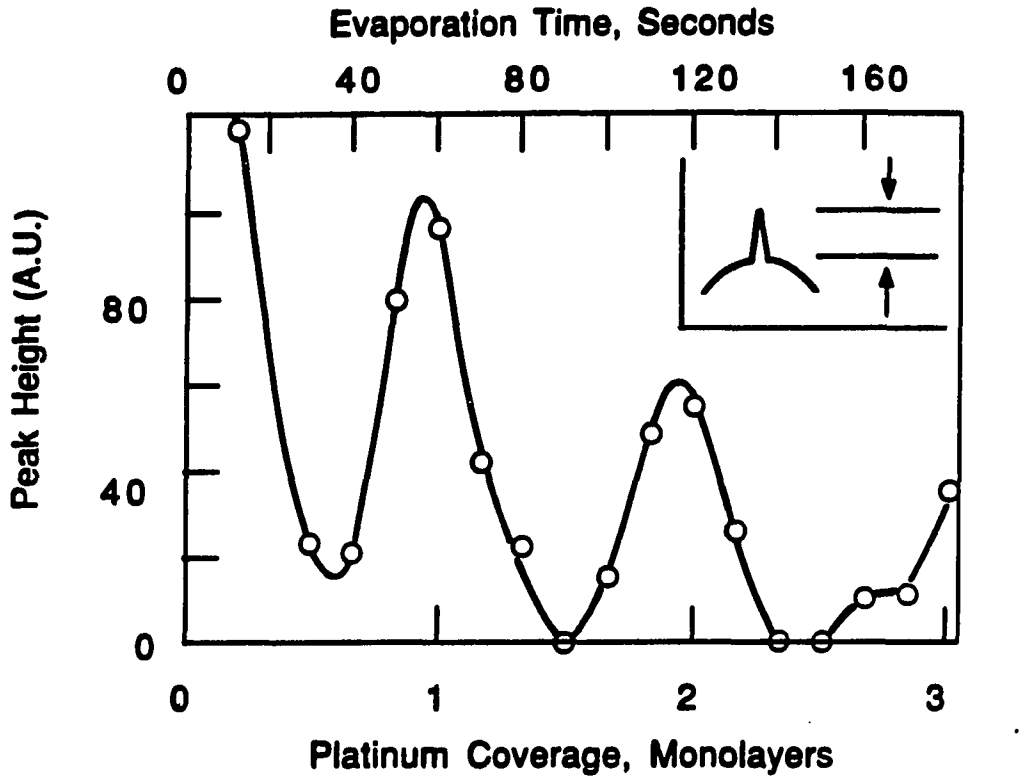

Figure 6. Variation of LEED spot intensity (given in arbitrary units) as a function of evaporation time and Pt coverage

The inset shows schematically how the peak height, I_p, is obtained from each profile.

intensity maxima occur suggest $\theta_{Pt} \sim 1, 2, 3$, etc., and they correspond to Pt:Pd Auger ratios (13) of 0.3, 0.8, and 1.2, respectively. This coverage calibration (in terms of the Auger ratios) is in excellent agreement with our previous coverage determination (13), which was based only on Auger and ultraviolet photoemission spectroscopies. Furthermore, the nearly linear variation of film coverage with evaporation time indicates that the Pt sticking coefficient is constant under these evaporation conditions, i.e., it is independent of changes in surface morphology and composition as the film grows. A constant sticking coefficient is usually assumed implicitly (and without justification) in studies of metal film growth.

It is interesting to notice that although the instrument has low resolving power we are still able to separate the coherent scattering from the diffuse part. This is because only small Pt islands from during film growth, as can be seen from the large half-width of the diffuse part (corresponding to an island diameter of only 10 Å), which stays invariant with coverage. Because this length is much smaller than the coherence of the instrument, the diffuse contribution is well separated.

One interesting aspect of the data is the presence of Lorentzian-like wings in the initial profile and in the profiles measured after completion of each Pt layer. This is not unreasonable after the completion of 1, 2, 3 ... layers because, as stated previously, there is an increasing tendency for some atoms to occupy higher levels, and this causes the oscillation amplitude to decrease by transferring diffracted intensity to the wings. However, wings are also present in the very fist

profile, which results from a clean surface. This profile should be instrumentally limited and therefore should be Gaussian, since the terrace length is larger than the coherence length. Perhaps some part of its Lorentzian-like shape is due to the presence of a small percentage of point defects on the clean Pd surface, but we do not believe this can account for all of its deviation from a Gaussian profile.

We conclude by considering some practical aspects of LEED, as it is typically configured, in terms of the convenience and data acquisition capabilities necessary for a study such as we describe here.

First, in order to obtain a set of data such as shown in Figure 5, our chamber configuration requires that we deposit a small amount of Pt film, turn the sample 180° to face the Auger spectrometer, measure the resultant film coverage, and then turn the sample again by 90° to face the LEED optics. This entire process, plus the measurement of eight spot profiles using the video camera and computer, takes about 5-6 min. Thus, where RHEED can be used to measure overlayer characteristics continuously during deposition, the analogous LEED measurement (at least in our apparatus) is a sequential one, and deposition cannot take place continuously. This is one of the disadvantages of LEED in comparison to RHEED. Continuous measurement during deposition is possible with RHEED because the glancing incident and exit angles allow the electron gun and detector to be positioned well out of way of the evaporation source, which can then face the sample directly. In principle, LEED could also be configured to permit constant spot profile measurement during continuous deposition, but most chambers currently in use would not

readily lend themselves to such an adaptation, because the LEED optics are arranged for normal incidence. A sequential experiment, such as we describe here, would often be possible, however.

Second, it is necessary to use some type of data acquisition system that is reasonably fast, i.e., a system that can gather the necessary spot profiles within a minute or two. This is because the sample is prone to contamination in the time between depositions. The data acquisition process should be relatively fast so as not to lengthen the experiment significantly. The video system which we use (14) is convenient, although many other techniques (e.g., photography or resistive anode networks) could certainly be used as well.

IV. CONCLUSIONS

In summary, we observe diffracted intensity oscillations in the growth of Pt on Pd(100) with a conventional LEED diffractometer. We demonstrate that a clear separation between the coherent and diffuse scattering in each profile is possible with a commercial instrument. Our observations are similar to the RHEED oscillations often observed in semiconductor MBE growth. We have shown that LEED spot profiles during thin film growth may be evaluated with standard equipment, providing a new tool for the study of epitaxial growth.

V. ACKNOWLEDGMENTS

This work is supported by a Presidential Young Investigator Award of the National Science Foundation, Grant No. CHE-8451317. We also acknowledge support from the Ford Motor Company. In addition, some equipment and all facilities are provided by the Ames Laboratory, which is operated by the U.S. Department of Energy by Iowa State University under Contract No. W-7405-ENG-82.

VI. REFERENCES

1. J. H. Neave, B. A. Joyce, P. J. Dobson and N. Norton, Appl. Phys. A 31 (1983) 1.
2. J. M. Van Hove, C. S. Lent, P. R. Pukite and P. I. Cohen, J. Vac. Sci. Technol. B 1 (1983) 741.
3. B. F. Lewis, F. J. Grunthaner, A. Madhukar, T. C. Lee and R. Fernandez, J. Vac. Sci. Technol. B 3 (1985) 1317.
4. M. Doyama, R. Yamamoto, T. Kaneko, M. Imafuku, C. Kokubu, T. Izumiya and T. Hanamure, Vacuum 36 (1986) 909.
5. E. Bauer, in Reflection High-Energy Electron Diffraction and Reflection Electron Imaging of Surfaces, edited by P. K. Larsen and P. J. Dobson (Plenum Press, New York, 1988).
6. S. T. Purcell, B. Heinrich and A. S. Arrott, Phys. Rev. B 35 (1987) 6458.
7. M. Horn and M. Henzler, J. Crystal Growth 81 (1987) 428; also R. Altsinger, H. Busch, M. Horn and M. Henzler, Surface Sci. 200 (1988) 235.
8. P. A. Thiel and J. W. Anderegg, Rev. Sci. Instrum. 55 (1984) 1669.
9. J. C. Tracy and P. W. Palmberg, J. Chem. Phys. 51 (1969) 4852.
10. R. J. Behm, K. Christmann, G. Ertl, and M. A. Van Hove, J. Chem. Phys. 73 (1980) 2984.
11. A. Ortega, F. M. Hoffmann, and A. M. Bradshaw, Surface Sci. 119 (1982) 79.
12. B. C. DeCooman and R. W. Vook, J. Vac. Sci. Technol. 21 (1982) 899.

13. S. L. Beauvais, R. J. Behm, S.-L. Chang, T. S. King, C. G. Olson, P. R. Rape, and P. A. Thiel, Surface Sci. 189/190 (1987) 1069.

14. J. W. Anderegg and P. A. Thiel, J. Vac. Sci. Technol. A 4 (1986) 1367.

15. F. T. Wagner and P. N. Ross, Jr., Surface Sci. 160 (1985) 305.

16. M. Henzler, Surface Sci. 22 (1970) 12.

17. M. G. Lagally, D. Savage and M. C. Tringides in Reflection High-Energy Electron Diffraction and Reflection Electron Imaging of Surfaces, edited by P. K. Larsen and P. J. Dobson (Plenum Press, New York, 1988).

18. T.-M. Lu and M. G. Lagally, Surface Sci. 99 (1980) 695.

19. C. S. Lent and P. I. Cohen, Surface Sci. 139 (1984) 121.

20. J. M. Pimbley and T.-M. Lu, J. Appl. Phys. 57 (1985) 1121.

PAPER II:

TEMPERATURE DEPENDENCE OF METAL FILM GROWTH VIA LOW-ENERGY ELECTRON DIFFRACTION INTENSITY OSCILLATIONS: Pt/Pd(100)

TEMPERATURE DEPENDENCE OF METAL FILM GROWTH VIA LOW-ENERGY ELECTRON DIFFRACTION INTENSITY OSCILLATIONS: Pt/Pd(100)

D. K. Flynn, J. W. Evans and P. A. Thiel

Department of Chemistry and Ames Laboratory-USDOE
Iowa State University
Ames, Iowa 50011 USA

ABSTRACT

A commercial, conventional LEED apparatus is used to monitor Bragg intensity oscillations during the growth of Pt on Pd(100). The effect of substrate temperature between 80 and 400 K is investigated. Between 80 and 300 K, two to three Bragg oscillations are observed. The oscillation amplitude damps out quickly as film coverage increases at fixed temperature, but damp out less quickly at the higher substrate temperatures. Above ca. 350 K, reconstruction of the Pt overlayer interferes with the oscillations. These data indicate that a kinetic barrier, most probably the barrier to surface diffusion, inhibits the system from achieving macroscopic equilibrium, and that the true equilibrium growth mode for this system is layer-by-layer. A new, analytical procedure is used to determine the coverage distribution within the layers from the Bragg intensities during growth. Bragg oscillations are predicted to occur at low substrate temperatures where surface diffusion is minimal and deposition is essentially random, but restricted to the fourfold-hollow adsorption sites.

I. INTRODUCTION

Metal films on metal substrates can exhibit unusual catalytic, chemisorptive and magnetic properties (1). To understand these properties, it is important to understand how the film is spatially distributed on the surface, e.g., does the film form two-dimensional layers or three-dimensional clusters? The spatial arrangement as a function of coverage is referred to as the growth mode. In this paper, we present new experimental and theoretical approaches to determining details of the growth mode of Pt films on Pd(100).

In layer-by-layer (Frank-van der Merwe) growth, each layer fills completely before the next layer is populated. One can think of this phenomenon as the formation and annihilation of steps as each layer forms. The expected LEED spot profiles at non-integral coverages consist of two parts: a broad, Lorentzian-like distribution indicative of short-range order and the presence of steps, summed with a Bragg peak indicative of long-range order (2). LEED is most sensitive to surface disorder at the out-of-phase condition, where the diffracted intensities from atoms in consecutive layers interfere destructively. At these energies, for *perfect* layer-by-layer growth, the normalized Bragg intensity oscillates between 1 and 0 for completely-filled and half-filled layers, respectively. Both reflection high-energy electron diffraction (RHEED) and low-energy electron diffraction (LEED) have been used to follow growth of overlayers by monitoring the Bragg intensity as a function of coverage (3).

Previous Auger electron and ultraviolet photoemission spectroscopic studies of Pt on Pd(100) at 300-350 K have indicated that Pt grows isomorphically with the substrate in a layer-by-layer fashion up to at least three atomic layers (4). Since Pt and Pd have the same bulk structure, with lattice constants agreeing to within 0.8 % (5), there is little interfacial strain. This promotes layer-by-layer growth (6). A subsequent study of this system (7) showed that LEED could be used to observe oscillations in the Bragg intensity as the Pt film was deposited at 300 K. This confirmed the earlier hypothesis of layer-by-layer growth. However, the oscillation amplitude decreased as coverage increased, indicating an increasing number of partially-occupied layers as thickness increased, i.e., imperfect layer-by-layer growth.

In this work, we analyze deviations from equilibrium growth of the Pt overlayer on Pd(100), by investigating the effect of substrate temperature. We use a commercial LEED apparatus to monitor variations in the Bragg intensity as a function of Pt coverage and substrate temperature between 80 and 400 K. We outline a new, analytical procedure for obtaining the coverage distribution among layers as a function of total coverage from these data.

II. EXPERIMENTAL DETAILS

Experiments are performed in a stainless steel UHV chamber equipped with a Pt evaporator (8), standard Varian four-grid LEED optics, single-pass CMA, mass spectrometer and ion gun. LEED spot profiles, taken at normal incidence, are measured with a computer-interfaced, silicon-intensified-target video camera (9). The Pd(100) sample is cleaned of bulk contaminants to within the detection limit of Auger analysis (10).

In a typical experiment, Pt is dosed for 10 seconds while the Pd sample is held at constant temperature. The pressure in the chamber typically rises to ca. 6×10^{-10} Torr during this dose. The Pt 64 eV and Pd 327 eV Auger peaks are measured at three positions to ensure uniformity of the film. The sample is next turned toward the LEED optics and selected spot profiles are measured at given energies. Each Pt dose, followed by AES and LEED measurements, takes a total period of 4-5 minutes. Repeating the evaporation and subsequent measurements, spot profiles are accumulated as a function of Pt coverage. Alternatively, spot profiles are recorded as a function of energy at a given coverage. We discuss results of both types of experiment.

III. EXPERIMENTAL RESULTS

To follow the formation of layers during growth, the Bragg oscillations are analyzed at an energy where diffraction is sensitive to the presence of steps, i.e., an energy where the scattering from atoms in different levels is out-of-phase. We determine an out-of-phase condition for the Pt-Pd system by measuring the full-width at half-maximum (FWHM) of the $(1,\bar{1})$ beam as a function of energy, for Pt-covered Pd, at room temperature. A maximum occurs at ca. 145 eV. For comparison, we calculate out-of-phase energies for Pt-on-Pt and Pd-on-Pd from the equation given by Henzler (11). We assume the fourfold-hollow is the adsorption site, and use bulk values for the interlayer spacings. This calculation indicates an out-of phase condition at 140.5 eV for Pt-on-Pt and 142.5 eV for Pd-on-Pd (11). These values agree favorably with our experimental data for Pt-on-Pd. Thus, both the experimental data and the calculation show that 145 eV represents an energy at, or very nearly at, an exact out-of-phase condition for this system.

It is fortunate that the $(1,\bar{1})$ reflex has appreciable intensity at this energy, enabling clear separation of the diffracted peak from the background. For the (1,0) beam, out-of-phase conditions coincide with extreme minima in the I-V curves, or occur at inconvenient energies. We thus confine our discussion to the $(1,\bar{1})$ reflex.

The $(1,\bar{1})$ spot profiles are shown in Figure 1 as a function of cumulative evaporation time. In experiments of this type, the substrate temperature is held constant except during LEED data acquisition. During

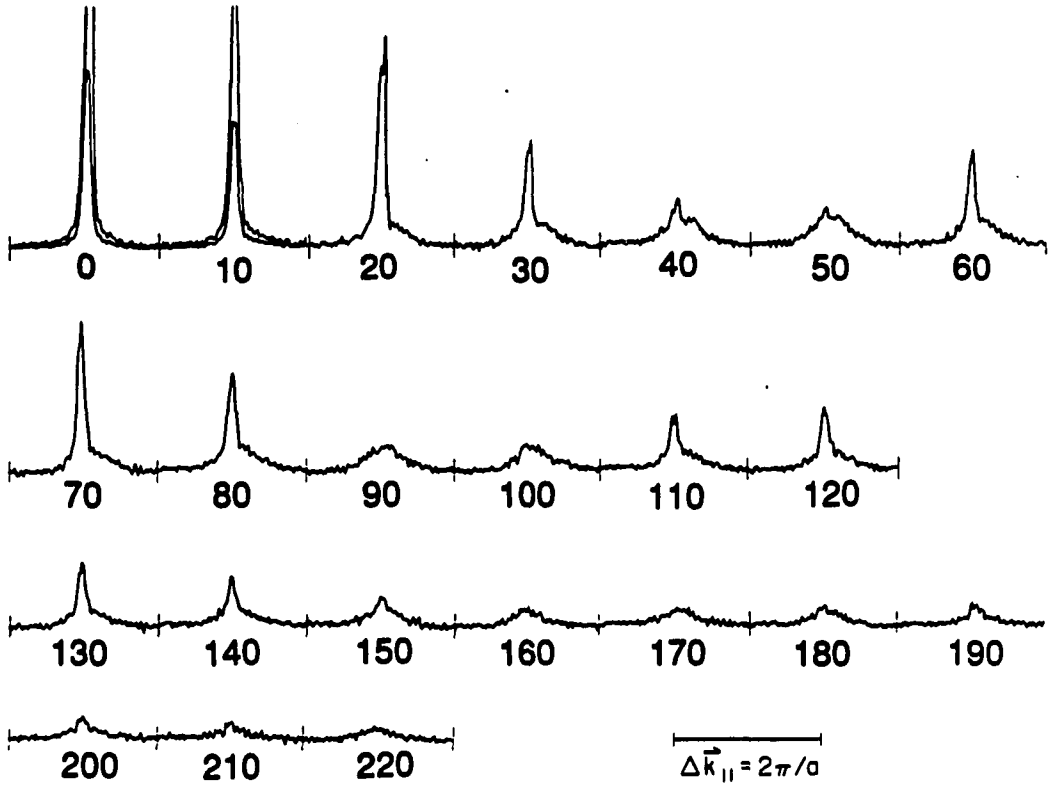

Figure 1. $(1,\bar{1})$ spot profiles as a function of cumulative evaporation time at 145 eV

The substrate temperature is 250 K. The first profile is that of the clean substrate. The second profile is taken after a 10 second Pt dose. The 10 second dose is repeated before each of the following profiles. The profiles are divided into three rows, each row roughly showing the filling of a Pt layer.

this time the heating current is chopped, so as not to distort the diffraction pattern. (The temperature drop during chopping does not exceed 12 K. The average temperature drop for substrate temperatures between 80 and 350 K is 4 K.)

At zero Pt coverage (first profile, Figure 1) the sharp spot profile reflects the intrinsic order of the substrate and the instrumental response function. As Pt coverage increases, no new LEED spots are observed, but the integral-order spots take on a new shape. These profiles are clearly separable into two parts: a sharp, narrow Bragg peak, summed with a broader, Lorentzian-like distribution. The intensity of the Bragg peak oscillates in a manner similar to that expected for layer-by-layer growth, although it never regains its full initial intensity.

In order to interpret the intensity behavior one must consider the effect of the difference in scattering factors of Pt and Pd. If there is an appreciable difference, the intensity would first be characteristic of the scattering factor of Pd, and then reflect that of Pt as the coverage increases. However, the ratio of atomic scattering amplitudes, calculated on the basis of the partial wave analysis equation (12) at 145 eV, is 0.987, i.e., essentially unity.

We obtain profiles similar to those of Figure 1 for substrate temperatures between 80 and 400 K. Bragg intensities, normalized to the Bragg intensity of clean Pd, are shown in Figure 2 for temperatures between 80 and 350 K. When depositing at 350 K and above, Pt overlayer

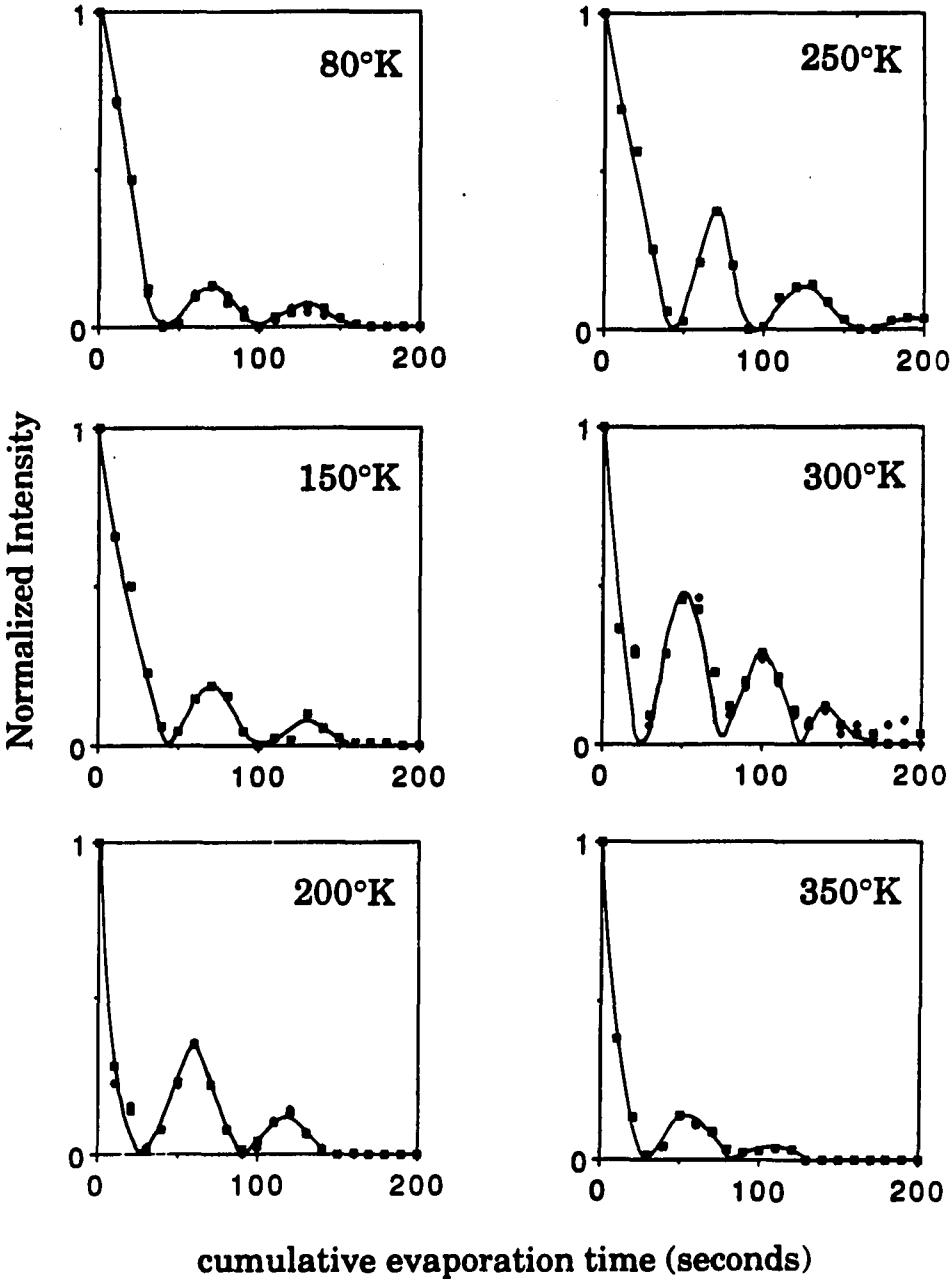

Figure 2. Normalized Bragg intensity as a function of cumulative evaporation time for the temperatures indicated

The beam energy is 145 eV. Curves between data points are drawn in to guide the eye.

reconstruction interferes with the oscillations (4). The temperature regime above 300 K, and the associated reconstructions, are not discussed further in this paper.

IV. DISCUSSION

We observe distinct oscillations in the Bragg intensity at substrate temperatures between 80 and 300 K. For perfect layer-by-layer growth, the maxima should occur at full-layer coverages with unit amplitude. The reduction of the measured Bragg intensity at each maximum, relative to zero Pt coverage, indicates incomplete filling of one layer before the next layer begins to grow. Figure 2 shows that the amplitude at a given oscillation increases with increasing substrate temperature, up to 300 K. This is more clearly shown in Figure 3, where the Bragg intensities at the first, second and third maxima are plotted as functions of substrate temperature. This demonstrates the trend toward more perfect layer-by-layer growth with increasing substrate temperature. The data of Figures 2 and 3 indicate that at substrate temperatures exceeding ca. 150 K, diffusion plays an important role in smoothing the film. The top curve of Figure 3, which represents the intensity at the first maximum, demonstrates this most clearly. The sharp increase at ca. 150 K indicates that at this temperature the Pt adatoms have sufficient thermal energy to overcome the barrier to surface diffusion, leading to a more perfect (smoother) film. The temperature at which diffusion begins to play a role suggests that the surface diffusion barrier is on the order of 10 kcal/mol. These data indicate that Pt adatoms are *kinetically* trapped in upper layers as the film grows at low temperatures ($T \leq$ 150 K), and the true *equilibrium* growth mode for this system is layer-by-layer.

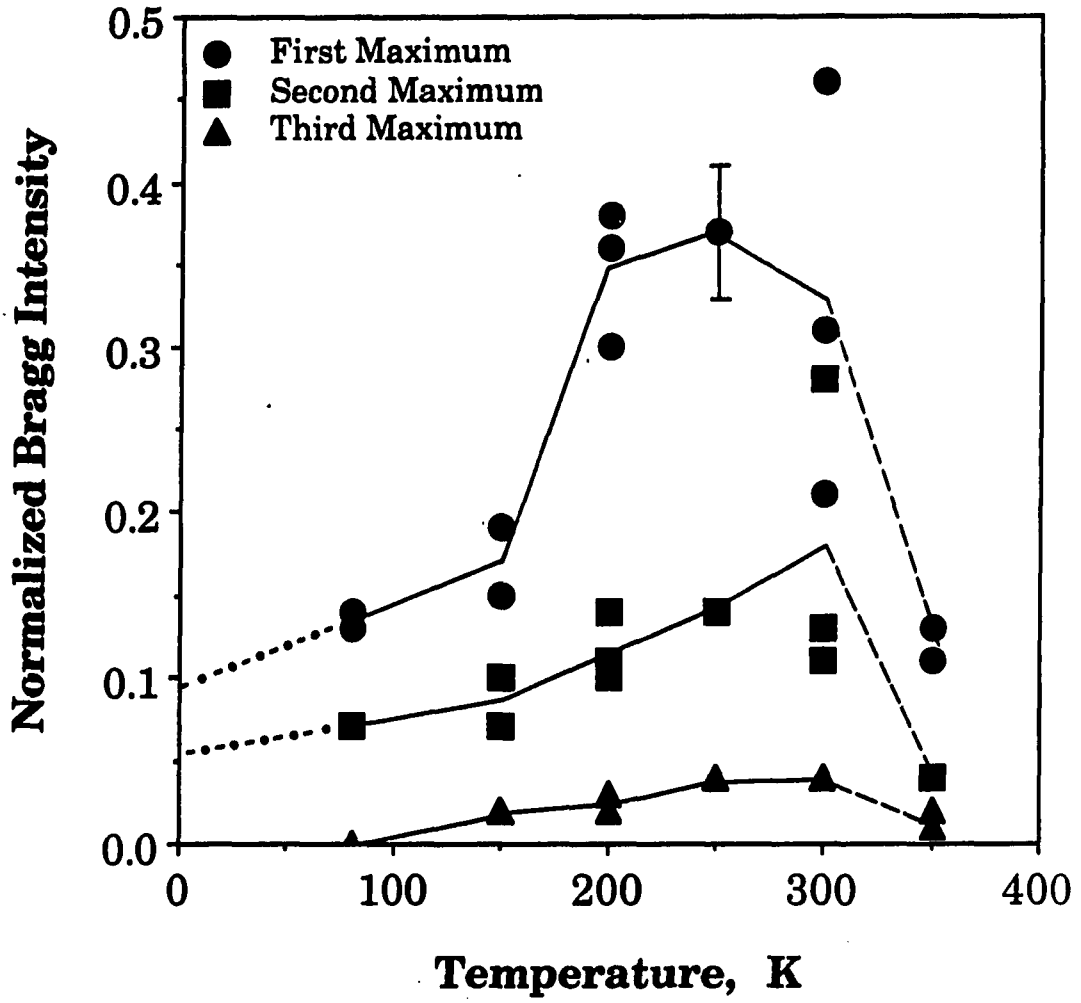

Figure 3. Normalized Bragg intensity for the first, second and third maxima as function of substrate temperature

Straight lines, which connect the average value of intensity at each coverage, are shown for clarity. Dashed lines indicate temperatures at which Pt reconstruction interferes with the oscillations. Dot-dash lines show the extrapolation to 0 K.

V. BRAGG INTENSITY ANALYSIS

We are interested in the relationship between the coverage distribution among the layers and the Bragg intensity during growth. Only in perfect layer-by-layer growth is this relationship well understood: the maxima in the Bragg intensity correspond to coverages of completed layers. Here, we explore the more complicated case of imperfect growth.

The key assumptions of the analysis are:

1) *The fourfold-hollow is the adsorption site.* Adsorption into this site maintains the fcc structure, resulting in isomorphic growth. Besides being the physically intuitive site for fcc(100) growth, this site is supported the symmetry of the LEED pattern (4,7), and the agreement between the measured out-of-phase energy and the calculation using the fourfold site.

2) *The Bragg intensity is given by the kinematic approximation.* Kinematic theory has been used frequently to analyze disorder in epitaxial growth (13,14). In kinematic scattering, the intensity at an out-of-phase condition is given by:

$$I = \frac{(N_0 - N_1 + N_2 \ldots)^2}{\sum_i N_i^2} \qquad (1)$$

In this equation, N_i is the effective number of *exposed* atoms in layer i, and i=0 corresponds to the surface substrate layer. We assume that each adatom effectively blocks scattering from a *net* of one atom in the layer

below (15), so N_i is calculated as the difference in coverage between layers i and i+1.

The kinematic approximation has recently been used to analyze the occupations of each layer based on the energy-dependence of the intensity (16). Multiple scattering presumably has less influence on the coverage-dependence (which we are concerned with here) than on the energy-dependence. Certainly, a full dynamical calculation would lead to a better understanding of the behavior of the Bragg intensity. Ideally this would provide the effective scattering factors for exposed atoms with different local environments, i.e., isolated atoms, atoms at the edge or interior of islands, and those that are partially covered by the next layer. One could then check the above assumptions and modify the kinematic calculation as necessary. However, such large dynamic calculations are not within the scope of this project.

First, we consider the microscopic model for film growth at T=0 K, as developed in reference 15. We assume adsorption occurs at a constant impingement rate with an equal probability of filling any fourfold-hollow site. In this model, adsorption occurs every time an atom impinges within an area determined by the centers of four neighboring atoms comprising the fourfold-hollow site. If an atom strikes an area not so defined, (i.e., an incomplete fourfold-hollow site) it does not adsorb. The T=0 K assumption implies that there is no diffusion. One can set up and analytically solve the master equations for this model, when they are expressed as a set of coupled kinetic rate equations. The mathematical details are presented elsewhere (15). From these equations, the partial

occupation of each layer and the Bragg intensity is *exactly* calculated as a function of total coverage or time. Figure 4 shows the Bragg intensity as a function of time, calculated from the above assumptions. Distinct oscillations are evident. For contrast, random deposition onto *atop* sites leads to *no* oscillations. In this case, the Bragg intensity simply decays monotonically with coverage (15). The difference between these two cases is easily explained in terms of the number of atoms required for the adsorption of an adatom. For adsorption into atop sites, *every* exposed atom may serve as the starting point for the growth of an upper layer. Columns of atoms grow independently and diffraction quickly becomes out-of-phase. However, in the case of the fourfold-hollow adsorption site, it is necessary to have a square arrangement of four neighboring atoms in the lower layer, thus *creating* the adsorption site for an atom in the next layer. This imposes a severe restriction on the filling of upper layers, which enhances layer-by-layer growth.

To assess the applicability of this model, we compare the intensities at the maxima of the calculated oscillations (at T=0 K) with our experimental data at low temperatures, as shown in Table 1. The calculated intensities, *at* 0 K, agree well with the low temperature, experimental intensities *extrapolated to* 0 K. (See Figure 3.) This convergence supports the validity of our assumptions.

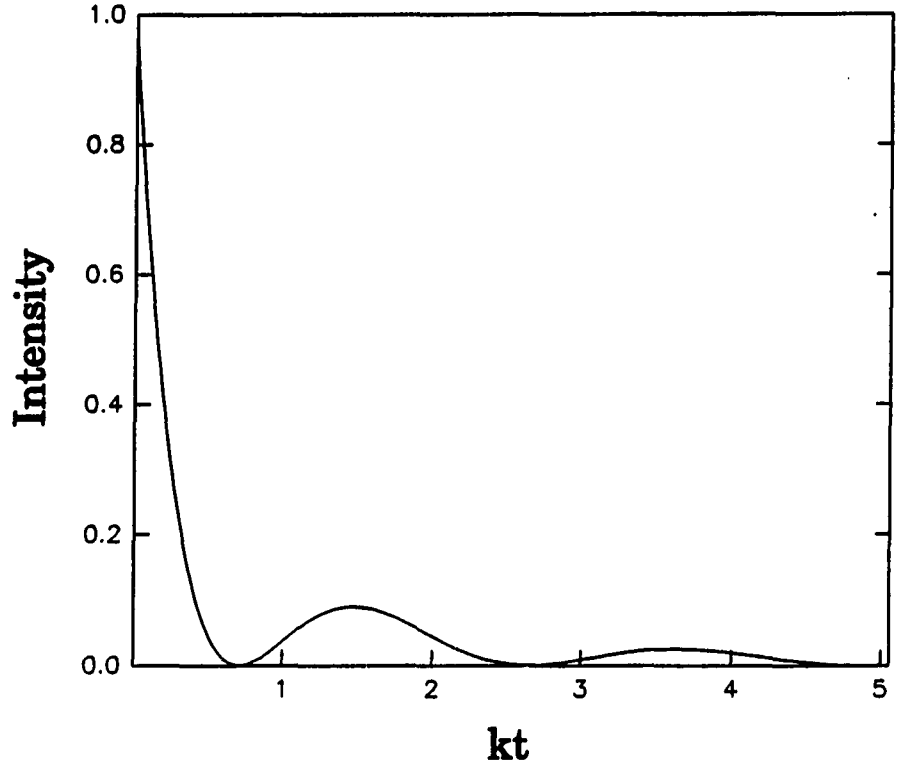

Figure 4. Calculated Bragg intensity as a function of kt

k is the impingement rate and t is time. The calculation assumes random adsorption into fourfold-hollow sites at T=0 K.

Table 1. Calculated (0 K) and measured (80 and 150 K) Bragg intensities at the first and second maxima

Temperature	First Maximum	Second Maximum
0	0.09	0.03
80	0.14	0.07
150	0.17	0.09

Table 2. Calculated coverage distribution at the first Bragg oscillation maximum

The temperatures are given in degrees Kelvin, and the coverages are given in monolayers, as defined in the text. The estimated error in the calculations at nonzero temperatures is ±0.04 ML.

Temperature	First Layer	Second Layer	Total
0	0.77	0.12	0.89
80	0.78	0.09	0.87
150	0.79	0.08	0.87
200	0.90	0.10	1.00
250	0.90	0.10	1.00

For growth at 0 K, the model predicts 0.89 monolayer (ML) coverage at the first maximum of the Bragg intensity. (We define one monolayer, θ=1, as one adatom per Pd(100) surface atom.) Here, the coverage distribution is 0.77 ML in the first layer (θ_1), 0.12 ML in the second layer (θ_2), and all upper layers are essentially empty. This is quite far from perfect layer-by-layer growth, in which the first maximum corresponds to θ_1=1 and θ=0 for all upper layers. Yet, the model predicts oscillations in the Bragg intensity. Thus, oscillations will occur for isomorphic fcc(100) growth, even in the absence of diffusion (i.e., T=0 K), by virtue of the requirement of a fourfold-hollow adsorption site.

There is a discrepancy in the time-dependence of the calculated and experimental oscillations. The time required to reach the first maximum, relative to that for the second maximum, is substantially smaller for the model than it is for the experiment. (See Figures 2 and 4.) In the model, we assume an atom adsorbs only if it strikes a fourfold-hollow adsorption site (as defined above). Since the number of these sites decreases with time, so does the sticking coefficient. In reality, it is likely that atoms which do not strike a fourfold-hollow site are accommodated through local equilibration, rather than reflected from the surface. This would lead to a sticking coefficient that is more constant with time. We will address this issue in future work.

In a separate paper (10), we develop a generic procedure to approximately, but simply, extract the coverage distribution from the Bragg intensity for arbitrary temperatures. This procedure focuses on

the dependence of θ_2 on θ_1, i.e., $\theta_2 = f_1(\theta_1)$. For a given choice of the function, f_1, and by using a scaling hypothesis to calculate the analogous functions, f_i, which determine the coverages of higher layers, one can calculate the Bragg intensity as a function of total coverage (15). We vary f_1 to fit the first and second maxima of the experimental data at each temperature, between the limits of T=0 K (which is *exactly* solvable for the random deposition model) and perfect layer-by-layer growth (θ_2=0 for all $\theta_1 \neq 1$).

The resultant values of θ_1 and θ_2 at the first maximum of the Bragg intensity are given in Table 2 for selected temperatures. In these cases, we find third-layer occupation is negligible. As temperature increases, the coverage in the first layer increases, and the coverage in the second layer decreases. In general, the coverages at the maxima do not correspond to the ideal full-layer values, and the absolute deviation from the ideal values increases with each successive maxima. We find that as temperature increases, the total coverage approaches the ideal layer-by-layer value of unity at the first maximum. This analysis supports the postulate that diffusion does not play a significant role in smoothing the film until the substrate temperature exceeds 150 K.

VI. CONCLUSIONS

We use a conventional LEED apparatus to measure Bragg oscillations during growth of Pt films on Pd(100). At 350 K and above, intensity associated with Pt reconstruction interferes with the oscillations. Between 80 and 300 K, Pt adatoms simply continue the (1x1) fcc structure set by the Pd(100) template. The oscillations are severely damped at all temperatures, but the higher substrate temperatures of this regime lead to oscillations of increased amplitude. These data indicate the true equilibrium growth mode is layer-by-layer. Damping occurs because the Pt adatoms are kinetically trapped during growth. The barrier to surface diffusion, which is on the order of 10 kcal/mol, inhibits the system from achieving macroscopic equilibrium in these experiments.

In general, Bragg oscillations for isomorphic fcc(100) growth are predicted to exist, even in the absence of diffusion, mainly due to the site requirement for the growth of additional layers. Experimental Bragg oscillation amplitudes for Pt on Pd(100) are analyzed to yield the partial occupation in each layer throughout growth. This analysis clearly demonstrates the trend toward perfect layer-by-layer growth as the temperature increases in this system.

VII. ACKNOWLEDGEMENTS

We are grateful to W.-D. Wang, and W.-Y. Leung for help with the experiments and to M. C. Tringides for useful discussions. This work is supported by a Presidential Young Investigator Award of the National Science Foundation, Grant No. CHE-8451317, the Ford Motor Company and the Division of Chemical Sciences, Office of Basic Energy Sciences. J. W. E. is supported by the Ames Laboratory. In addition, some experimental equipment and all facilities are provided by this Laboratory, which is operated for the U. S. Department of Energy by Iowa State University under contract No. W-7405-ENG-82.

VIII. REFERENCES

1. For example: C. H. F. Peden and D. W. Goodman, J. Catalysis 100 (1986) 520; M. W. Ruckman and M. Strongin, Phys. Rev. B 29 (1984) 7105; M. F. Onellion, C. L. Fu, M. A. Thompson, J. L. Erskine and A. J. Freeman, Phys. Rev. B 33 (1986) 7322.
2. P. R. Pukite, C. S. Lent and P. I. Cohen, Surface Sci. 161 (1985) 39.
3. For example: B. A. Joyce, J. Zhang, J. H. Neave and P. J. Dobson, Appl. Phys. A 45 (1988) 255; J. M. Van Hove, C. S. Lent, P. R. Pukite and P. I. Cohen, J. Vac. Sci. Technol. B 1 (1983) 741; R. Altsinger, H. Busch, M. Horn, and M. Henzler, Surface Sci. 200 (1988) 235; S. T. Purcell, B. Heinrich and A. S. Arrott, Phys. Rev. B 35 (1987) 6458 also J. Vac. Sci. Technol. B 6 (1988) 794.
4. S. L. Beauvais, R. J. Behm, S.-L. Chang, T. S. King, C. G. Olson, P. R. Rape and P. A. Thiel, Surface Sci. 189/190 (1987) 1069.
5. C. Kittel, Introduction to Solid State Physics, Fifth edition (Wiley, New York, 1976), p. 31.
6. J. H. van der Merwe, CRC Crit. Rev. Solid State Mater. Sci. 7 (1978) 209.
7. D. K. Flynn, W. Wang, S.-L. Chang, M. C. Tringides, and P. A. Thiel, Langmuir 4 (1988) 1096.
8. B. C. De Cooman, and R. W. Vook, J. Vac. Sci. Technol. 21 (1982) 899.

9. J. W. Anderegg and P. A. Thiel, J. Vac. Sci. Technol. A 4 (1986) 1367.

10. D. K. Flynn-Sanders, P. A. Thiel and J. W. Evans, Departments of Chemistry and Physics, Iowa State University, manuscript in preparation, (1990).

11. M. Henzler, Surface Sci. 22 (1970) 12. See also reference 7. Equations 5 and 6 of reference 7 are used to obtain the given result, using n=3.5 in equation 6.

12. E. Merzbacher, Quantum Mechanics, Second edition (Wiley, New York, 1970) p. 234. Phase shifts are obtained from M. Van Hove, Lawrence Berkeley Lab., Berkeley, California, private communication.

13. C. S. Lent and P. I. Cohen, Surface Sci. 139 (1984) 121.

14. J. M. Pimbley and T.-M. Lu, Surface Sci. 139 (1984) 360.

15. J. W. Evans, Phys. Rev. B, 39 (1989) 5655.

16. M. Horn, U. Gotter and M. Henzler, J. Vac. Sci. Technol. B 6 (1988) 727.

PAPER III:

LEED INVESTIGATION OF Pd/Pd(100) EPITAXIAL GROWTH

LEED INVESTIGATION OF Pd/Pd(100) EPITAXIAL GROWTH

D. K. Flynn-Sanders and P. A. Thiel

Department of Chemistry and Ames Laboratory - US DOE

Iowa State University

Ames, Iowa 50011

ABSTRACT

We investigate the epitaxial growth of Pd on Pd(100) via spot profile analysis using conventional LEED. This work demonstrates the wealth of information which can be extracted from spot profiles acquired with conventional LEED. For Pd on Pd(100) at 100 K, the growth process is nondiffusive, and islands of 1 to 4 atoms in width result. The profile analysis points to a surface diffusion activation barrier of ca. 13 kcal/mol for Pd/Pd(100), with an onset temperature of ca. 170-200 K. Between 200 and 400 K, the LEED profiles exhibit ring-structure, which is indicative of a periodic distribution of islands in the overlayer. The development of ring structure in the LEED profiles is correlated with the onset of diffusion. By 500 K, growth appears to proceed by step propagation. We report, for the first time, oscillations in the ring intensity as a function of coverage for growth at intermediate temperatures. These oscillations are associated with the detailed filling of individual layers. We also propose that, in the limit of one to several atoms, the interlayer spacing for a growing island is dependent on the number of atoms in the island.

I. INTRODUCTION

The physical and chemical properties of thin films can be greatly influenced by the structure of the interface initially formed during growth. In many applications, epitaxial growth proceeds under conditions that are far from equilibrium (1,2). The exact final state of the system is not necessarily the most stable state, but is determined by the relative rates of deposition, diffusion, condensation and evaporation. The kinetics of initial nucleation and island growth are crucial to the development of smooth, epitaxial layers.

The formation of epitaxial layers can proceed by creation and annihilation of steps, as islands form and merge within the growing layer. Low-energy electron diffraction (LEED) is very sensitive to the presence of steps (3). Information on the morphology at the atomic scale is contained in the LEED pattern, particularly in the profile shape. Thus LEED is a technique well-suited to the study of initial growth.

We describe the coverage-, temperature- and energy-dependence of LEED spot profiles during the initial stages of homoepitaxial Pd(100) growth. A homoepitaxial system is ideal for this study, since the equilibrium growth mode is necessarily Frank-van der Merwe (4) (layer-by-layer). Any deviation from this growth mode reflects a kinetic limitation of the system.

II. EXPERIMENTAL DETAILS

Experiments are performed in a conventional, ultrahigh-vacuum chamber, with a base pressure of 6×10^{-11} Torr. After daily sample cleaning procedures, and prior to deposition experiments, the operating pressure of the chamber is below 2×10^{-10} Torr. The chamber is equipped with an ion gun, single pass CMA for Auger spectroscopy and mass spectrometer to examine sample cleanliness. A standard, Varian four-grid LEED apparatus is used in conjunction with a computer-interfaced, video data acquisition system (5) to obtain single-pixel-width spot profiles. The evaporator is a resistively-heated source, based on the design of DeCooman and Vook (6). It is enclosed in a liquid-nitrogen-coolable shroud. A 1 cm orifice in the shroud allows metal vapor to escape toward the Pd(100) face. A rotatable shutter permits the sample to be shielded from the vapor flux. The sample is mounted on a rotatable, liquid-nitrogen-coolable coldfinger (7). Temperatures between ca. 90 and 1500 K are controlled via a feedback circuit (8) and a W-5%Re/W-26%Re thermocouple spotwelded to the back of the crystal.

Sequential deposition experiments at constant substrate temperatures are performed as follows. LEED spot profiles at various energies are measured prior to deposition. (The heating current is chopped during profile acquisition to alleviate current-induced distortions of the diffraction pattern.) The sample is rotated to face the evaporator, which is degassed for 10 s (shutter up). The shutter is moved to expose the substrate for 10 s. The sample is then turned toward the LEED optics and profiles are again measured. This process is continued to obtain

coverage-dependent spot profiles at constant temperature and constant energy. Similar experiments are performed for substrate temperatures between 95 and 500 K. Alternatively, after a predefined dose, the energy, from 50 to 300 eV, is scanned to obtain constant coverage, constant temperature profiles as a function of energy.

III. GENERAL LEED PATTERN

A. Results

Evaporation of Pd onto the Pd(100) substrate above ca. 100 and below ca. 500 K results in a LEED pattern in which each original spot is surrounded by a region of enhanced intensity. This region of enhanced intensity, or profile "foot" is either Lorentzian-like (homogeneously-broadened) or ring-shaped depending on the coverage and substrate temperature. The profile foot is evident at energies corresponding to out-of-phase conditions for each spot symmetry (9,10). Out-of-phase conditions are met when scattering from successive layers interferes destructively. These energies are most sensitive to the layer occupations and the presence of steps. Alternatively, steps are not reflected in the LEED pattern at in-phase scattering conditions, where all layers scatter coherently. At these energies, and at all temperatures in these experiments, each spot remains sharp, without additional structure.

At out-of-phase energies, when depositing at 100 K, the foot is homogeneously broad and very weak. The LEED pattern generally exhibits a high background. Between ca. 200 and 400 K, the foot takes the form of a ring around each spot. For deposition at 500 K, no additional structure is observed in the profiles at any energy.

Representative profiles demonstrating the energy- and temperature-dependence of profiles are shown in Figure 1 for the (1,-1) spot at ca.

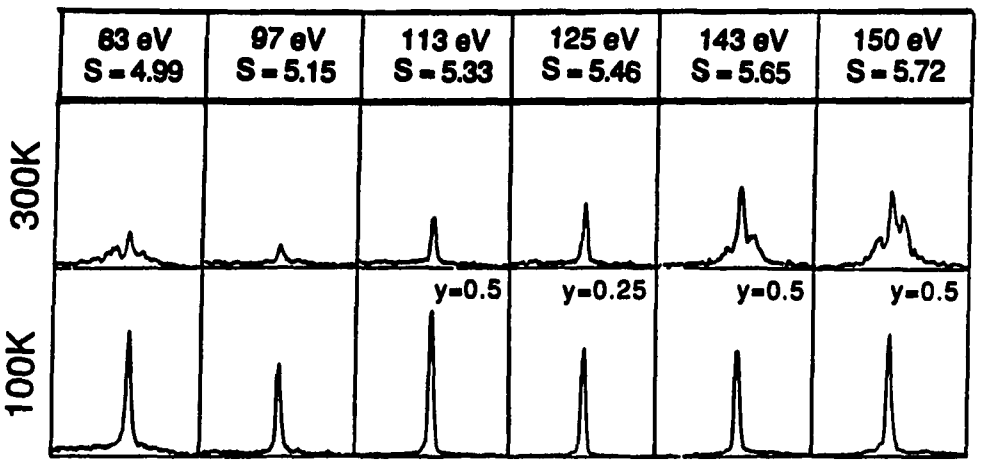

Figure 1. (1,-1) spot profiles for ca. 1/2 ML Pd deposited on Pd(100) at 100 and 300 K, demonstrating the energy- and temperature-dependence of the foot

The phase, S, is calculated according to the equation given by Henzler (9), which is based on the kinematic approximation.

1/2 ML Pd/Pd(100). At 300 K, certain energies (out-of-phase) clearly demonstrate the two, separable components: a central-spike and foot-component (which is ring-like), while at other energies (in-phase) only a single feature is evident. At 100 K, the foot is very weak and broad. Note there is some disagreement between the experimentally observed and kinematicaly-predicted (9) out-of-phase condition, demonstrating the importance of experimentally determining the out-of-phase condition (10). In this report, we choose the experimental out-of-phase condition to coincide with maximized foot-structure.

B. Discussion

The LEED spot profile provides information on atomic steps and island growth (11). A sharp spot is representative of a flat surface. Defects on an otherwise flat surface cause characteristic changes in the LEED spot profile. A homogeneously-broadened profile is indicative of random steps. Many levels are exposed, with steps in uncorrelated directions and terraces of uncorrelated size. Such a surface is typical after sputtering, from which homogeneously-broadened profiles have been observed (9,12). A profile consisting of a broad foot, with centrally superimposed sharp-spike, indicates a random island distribution. Typically two, or only a few, layers are exposed, with islands of a limited range of sizes and separations. Ring-structured spots denote a more structured distribution. Again, islands are of restricted height, but are characterized by either a constant (or very narrow range of) island size or island separation (13,14).

The symmetry of the LEED pattern produced by Pd deposition on Pd(100) indicates that the Pd adatoms occupy fourfold-hollow adsorption sites (15). The basic shape of the profiles indicate that for deposition at ca. 100 K islands of restricted height, but of varying widths, result. When the substrate temperature is increased to between ca. 200 and 400 K, the deposited overlayer assumes an arrangement with some long-range periodicity in the distribution. The ring pattern observed at these temperatures indicates that islands are of nearly constant size or of constant separation. The sharp profiles obtained when depositing at high temperature (500 K) indicate that large terraces are maintained throughout growth.

IV. ENERGY-DEPENDENCE AT CONSTANT COVERAGE AND TEMPERATURE

A. Results

Changes in the LEED spot profile with coverage or energy provide information on the structure of the surface during epitaxial growth. For a quantitative evaluation, a "characteristic distance" is measured in terms of the full-width at half-maximum (FWHM) for sharp or homogeneously-broadened profiles. For two-component profiles, the characteristic distance is measured by the foot FWHM or the ring diameter. These measures (in reciprocal space) are indicative of the terrace widths, island sizes or island separations in real space. We therefore distinguish a "reciprocal-space characteristic distance", which denotes a FWHM or ring diameter of a LEED spot profile; and a "real-space characteristic distance", which denotes the corresponding size or separation on the surface. Because of instrumental limitations, a maximum lateral distance of ca. 200 Å can be resolved with most commercial LEED optics. This means that perfect terraces wider than this do not produce correspondingly sharper LEED spots. Thus, deviations from perfection on a scale greater than this cannot be detected. The height of the steps, or islands, may be derived from the energy-dependence of the profile (9). In this section, we examine the energy-dependence of the (0,-1) and (1,-1) profile shapes (reciprocal-space characterisitic distances) for ca. 1/2 ML Pd deposited at 100 and 300 K, to derive information on the island height and distribution at these two temperatures.

First we inspect the energy-dependence of the initial substrate profiles. Figure 2 shows the FWHM of (0,-1) and (1,-1) profiles between 50 and 300 eV at 100 and 300 K. We subtract a constant background from each profile before measuring the full-width, and then normalize to the spot separation at each energy. Filled (empty) arrows in Figure 2 indicate an out-of-phase (in-phase) scattering condition, predicted by the kinematic analysis given by Henzler (9). The minimum FWHM value of ca. 0.017 indicates a transfer width of our instrument of ca. 160 Å. Small oscillations *may* be evident in Figure 2, suggesting the possibility of a low concentration of steps (i.e., we may detect some terraces less than ca. 160 Å, but because of the scatter in the data it is difficult to conclusively determine the reliability of this observation). This transfer width sets the scale for the dimension of islands that are distinguishable with our LEED optics. Given a maximum crystal miscut angle of 0.5 ° terraces should be no less than 200 Å, a typical size for polished, single crystal metal samples.

Next, we analyze the energy-dependence of the profiles obtained upon deposition. This requires division of the sharp-component from the foot. For basis of comparison, we choose to linearly extrapolate the foot to the region beneath the central-spike. The profile is separated at the first deviation of the central-spike from a regular, Gaussian-like lineshape. We acknowledge a large uncertainty associated with the extraction of the foot when it occurs with weak intensity. It is not always an obvious choice between a low-amplitude foot (with measurable width or diameter) and no component at all (i.e., a sharp, one-component

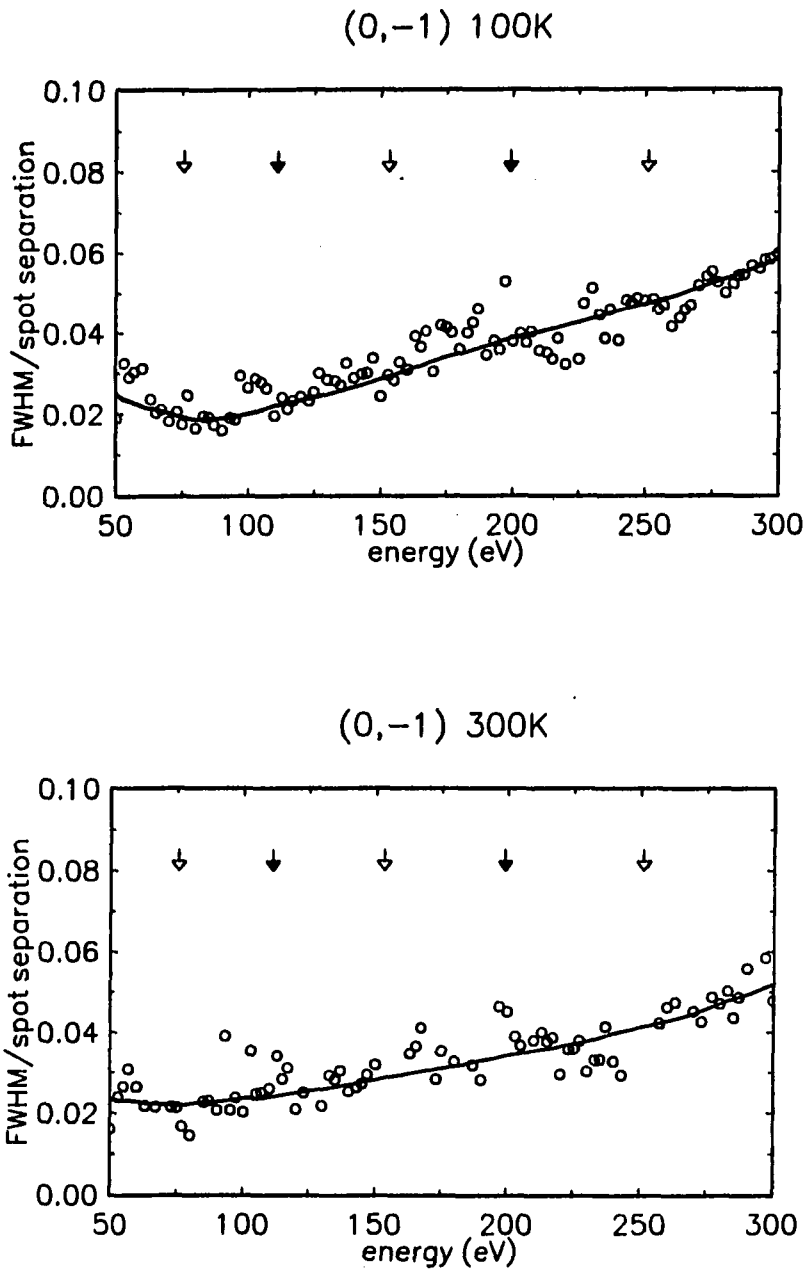

Figure 2. FWHM of clean substrate profiles as a function of energy

Arrows defined in text

(a) (0,-1) 100 and 300 K

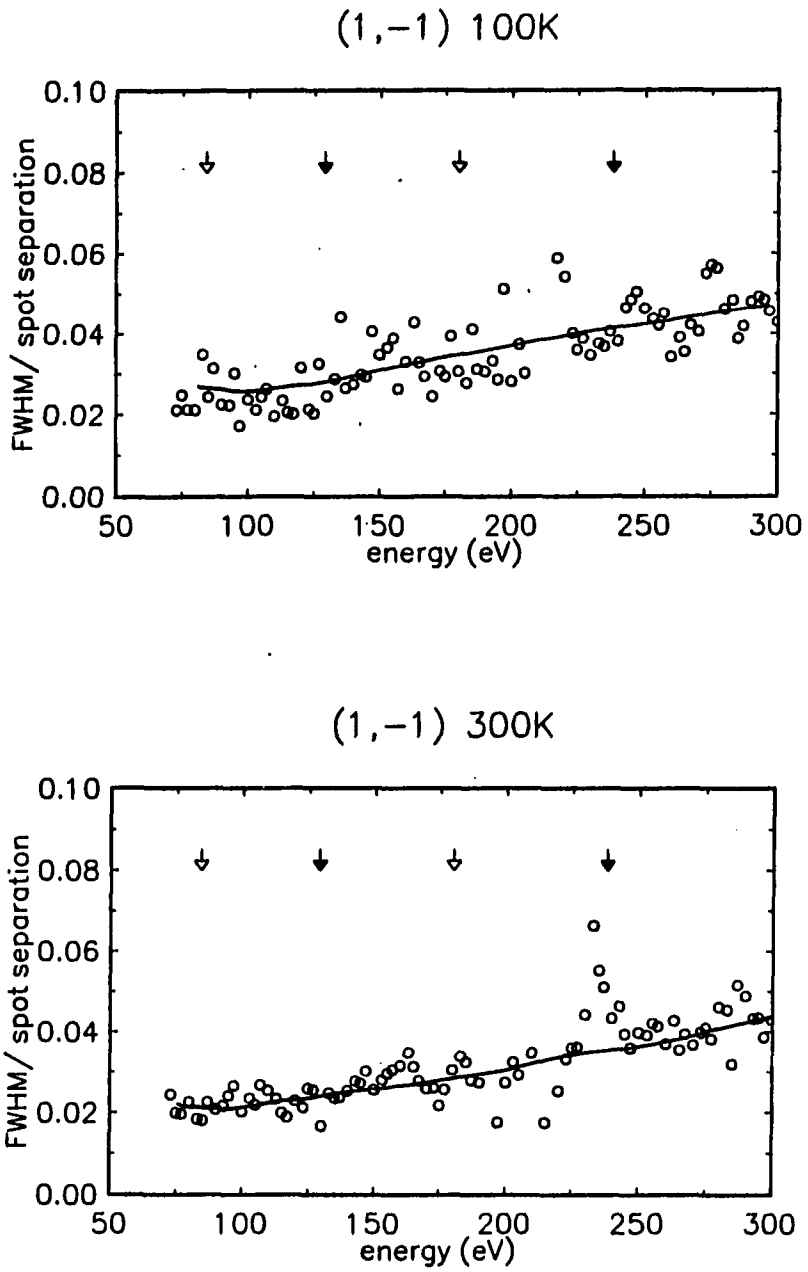

Figure 2. (continued)

(b) (1,-1) 100 and 300 K

profile).

The filled circles of Figure 3 show the FWHM of the sharp-component of the (0,-1) and (1,-1) profiles, from a surface with ca. 1/2 ML Pd deposited at 100 and 300 K. For comparison, we superimpose the data from the initial ("clean") surface (from Figure 2) with open circles. These results show that, within experimental uncertainty, there is no broadening of the central-spike, as has been theoretically predicted (14,16,17).

We now consider the foot reciprocal-space characteristic distance ca. 1/2 ML Pd/Pd(100) profiles at 100 and 300 K. Figure 4 shows the foot FWHM or ring diameter, whichever is appropriate to the profile under consideration (at 100 K, the foot is Lorentzian-like, at 300 K, the foot is generally ring-structured.) No measurement is shown for energies at which a foot is not discernable. This results in "gaps" in Figure 4 - energy regions where baseline structure (homogeneously broadened or ringlike foot) is evident and regions where the profile is characteristically sharp, having only one component.

B. Discussion

Figure 5 shows (1,-1) profiles at 147 eV during deposition. It is interesting to note that the "wing structure" of the clean surface profiles (θ = 0 ML) resembles the baseline structure at higher coverages at this energy. This observation complicates the interpretation of the data presented in Figure 4. For well-ordered surfaces, "wing-structure" is usually associated with inelastic scattering (18). Often

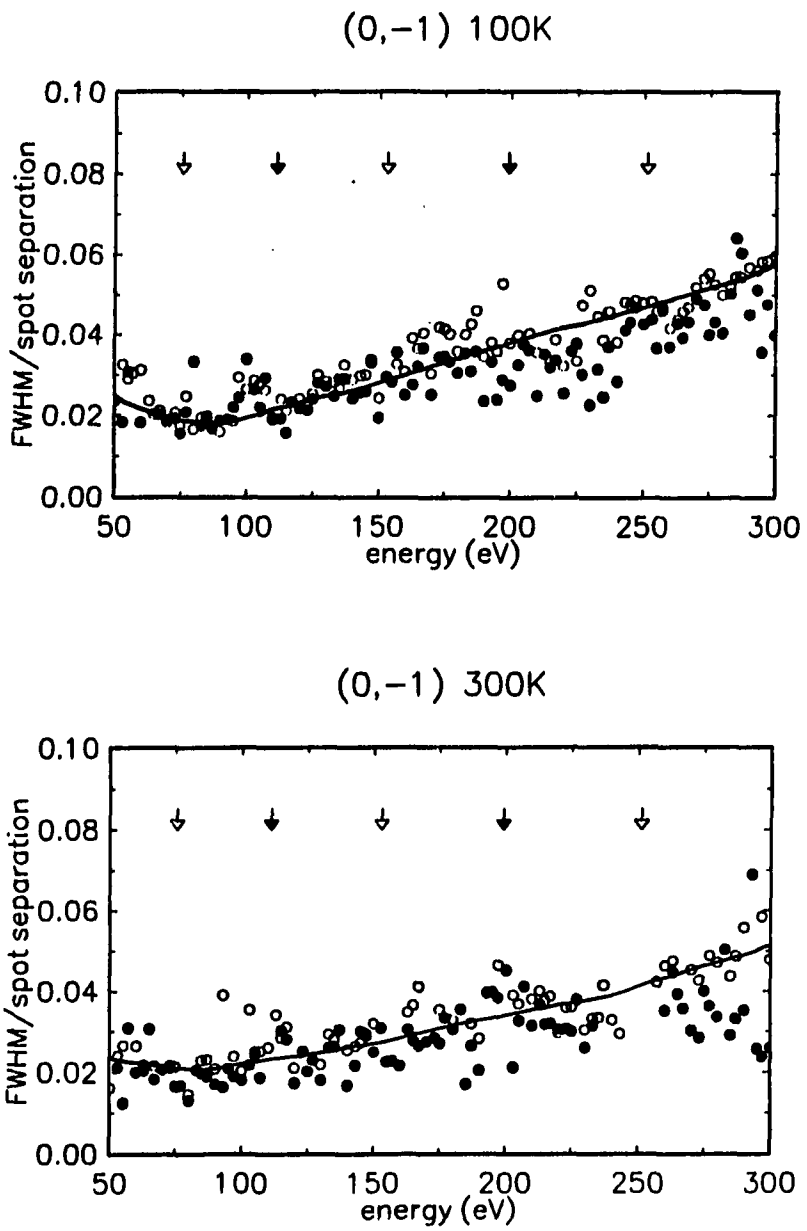

Figure 3. **FWHM of sharp component of profiles from ca. 1/2 ML Pd deposited on Pd(100) at 100 and 300 K (filled circles)**

The data of Figure 2 are shown for comparison (open circles). Arrows are defined in the text.

(a) (0,-1)

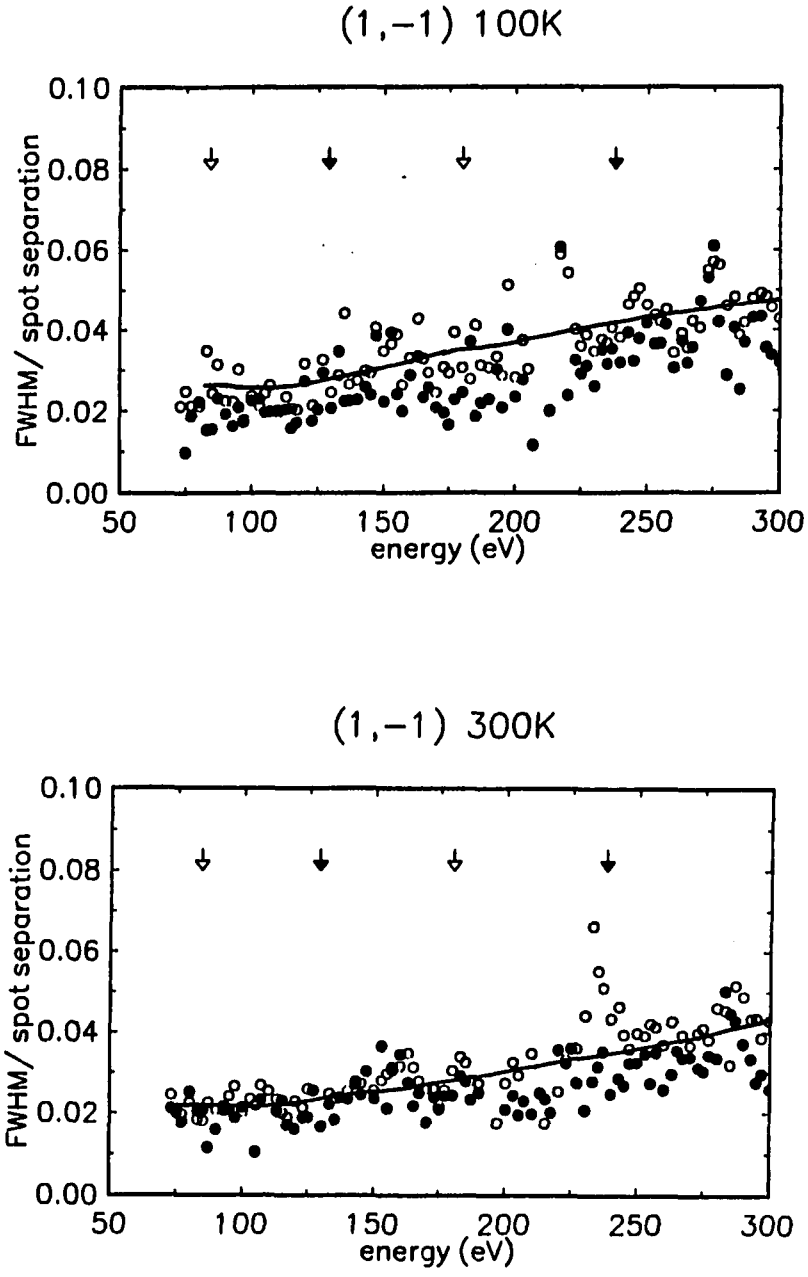

Figure 3. (continued)

(b) (1,-1)

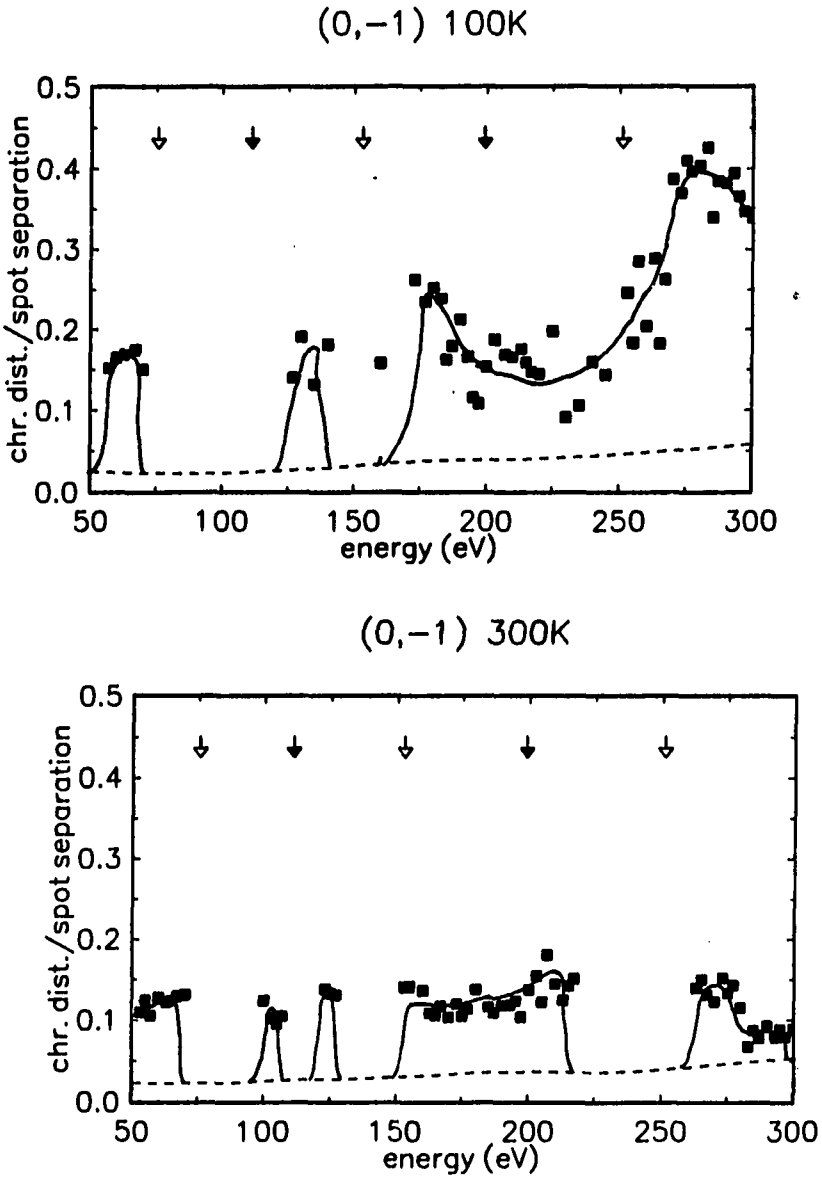

Figure 4. Reciprocal-space characteristic distances of ca. 1/2 ML Pd deposited on Pd(100) at 100 and 300 K

The data of Figure 2 determine the instrument response, shown as the dashed line. Arrows are defined in the text. The solid line is drawn to guide the eye.
(a) (0,-1)

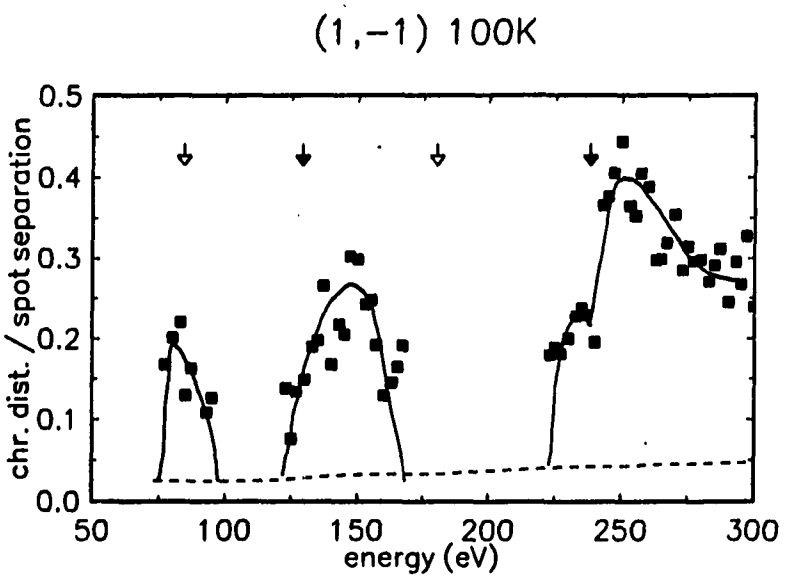

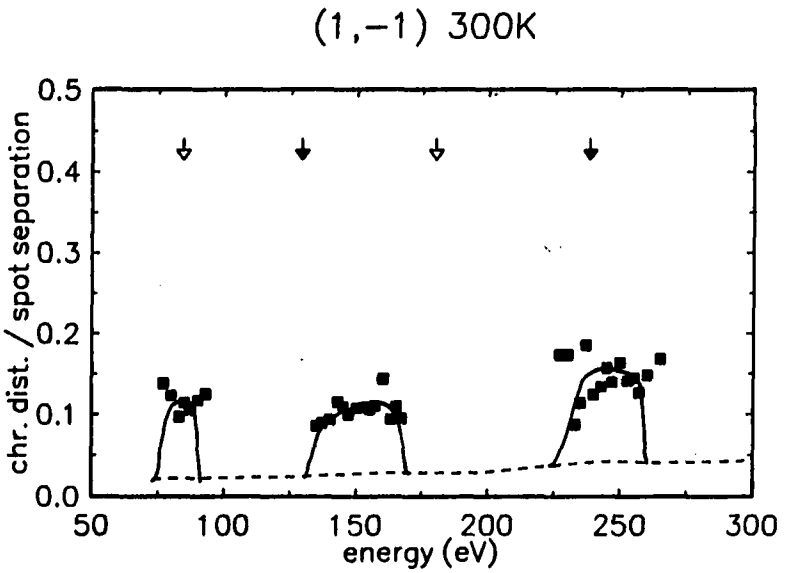

Figure 4. (continued)

(b) (1,-1)

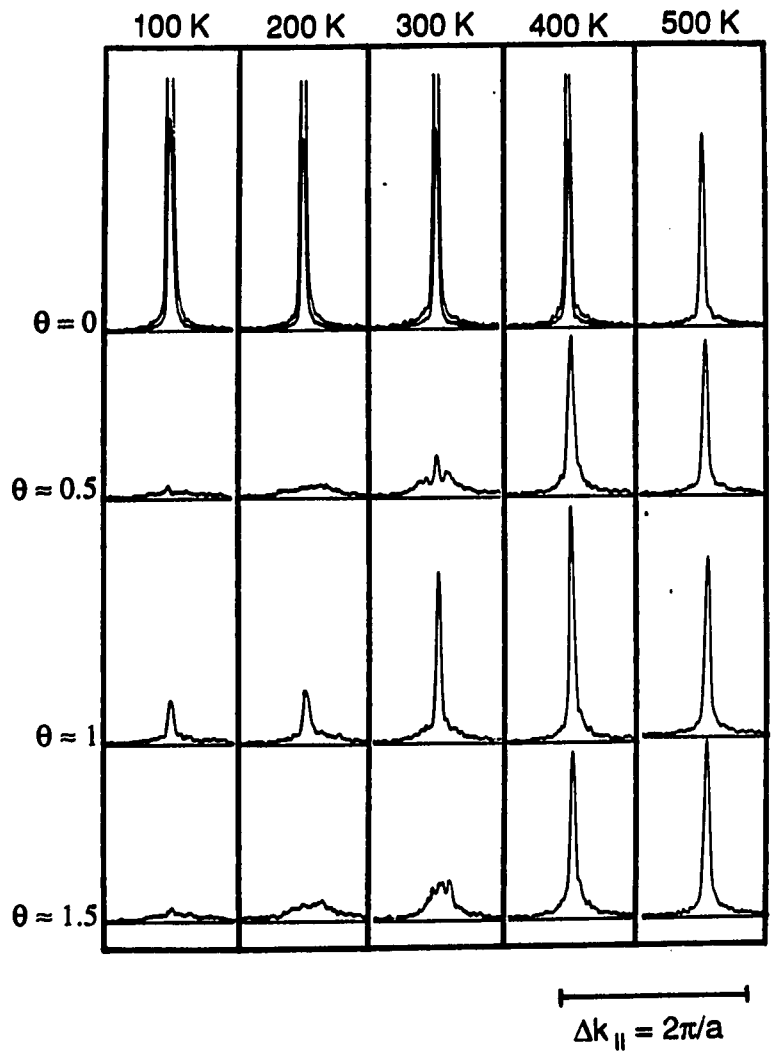

Figure 5. Out-of-phase (1,-1) spot profiles during deposition at various temperatures

The beam energy is 147 eV. The length of each profile is approximately 2/3 a^*. The θ = 0, 100 through 400 K profiles are shown on both y = 1 and 1/2 scales. These profiles correspond to extrema in the intensity vs. coverage (oscillation) curves (presented in section V), from which the approximate coverages are derived.

considered part of the instrumental response, it is not separated from the true angular profile. However, the similarity between the "wing-structure" of clean surface profiles and the foot of higher coverages compels us to examine the energy-dependence of "wing-structure" in more detail. We must question whether the foot actually contains information on a real-space characteristic distance or is simply "wing-structure", i.e., the remainder of scattering after (kinematic) Bragg cancellation.

We cannot justify decomposition of the initial substrate profiles in the same manner as those profiles resulting from deposition. That is to say, we cannot attach the same physical meaning to a characteristic distance derived from a profile "mechanically" separated by the same criterion. Our spectrometer has a coherence length of ca. 160 Å, which is less than the terrace length of our crystal. Therefore any observed "structure" in the baselines of initial substrate profiles should not have its origin in an average island distribution. Although we cannot undeniably exclude every possibility of defect contribution, i.e., the presence of some steps or mosaic structure, we expect such a contribution, if present, to be very small. Nonetheless, we impose the extraction criterion described in the previous section to profiles of the initial substrate, to determine which energies of Figure 4 may be affected. We are interested in the extent (if any) to which the substrate governs the profile shape after deposition without overlooking imperfections in, or other contributions from, the substrate.

The criterion we established for extraction is somewhat arbitrary. Difficulties in the deconvolution arise when the foot component is very

weak (as already discussed) and additionally when the central-spike is very intense. This is because we separate profiles at the first deviation from a regular, Gaussian lineshape, and distortions in the lineshape are more evident when the profiles are very intense, leading to an overestimated foot. Nonetheless, the extraction is consistent, thus useful in comparing initial and covered surfaces at each temperature.

Figure 6 shows results for the initial substrate (open squares) superimposed on the data of Figure 4 (filled squares) at 100 and 300 K. Again, when no discernible baseline structure is present (single-component profiles), no measurement is shown. At both temperatures, near experimental out-of-phase energies, both the initial and covered surfaces show reciprocal-space characteristic distances significantly higher than the instrumental response (dashed line). We note that there are occurrences of baseline-structure for the covered surface that are not associated with the initial surface. The initial surface yeilds "wing-structure" FWHMs of ca. 0.1 to 0.2 at both 100 and 300 K. For the covered surface, while the 300 K experiment shows a reciprocal-space characteristic distance of 0.1 - 0.2, the 100 K experiment shows a much broader range of values.

The fact that the covered surface shows the same reciprocal-space characteristic distance as the initial substrate at 300 K means either that, at this temperature, the ultimate island distribution within the overlayer is determined by the original surface, or there is a lower limit to which this distance may be reliably measured. Reciprocal-space characteristic distances of 0.1 to 0.2 correspond to ca. 27.5 - 13.8 Å in

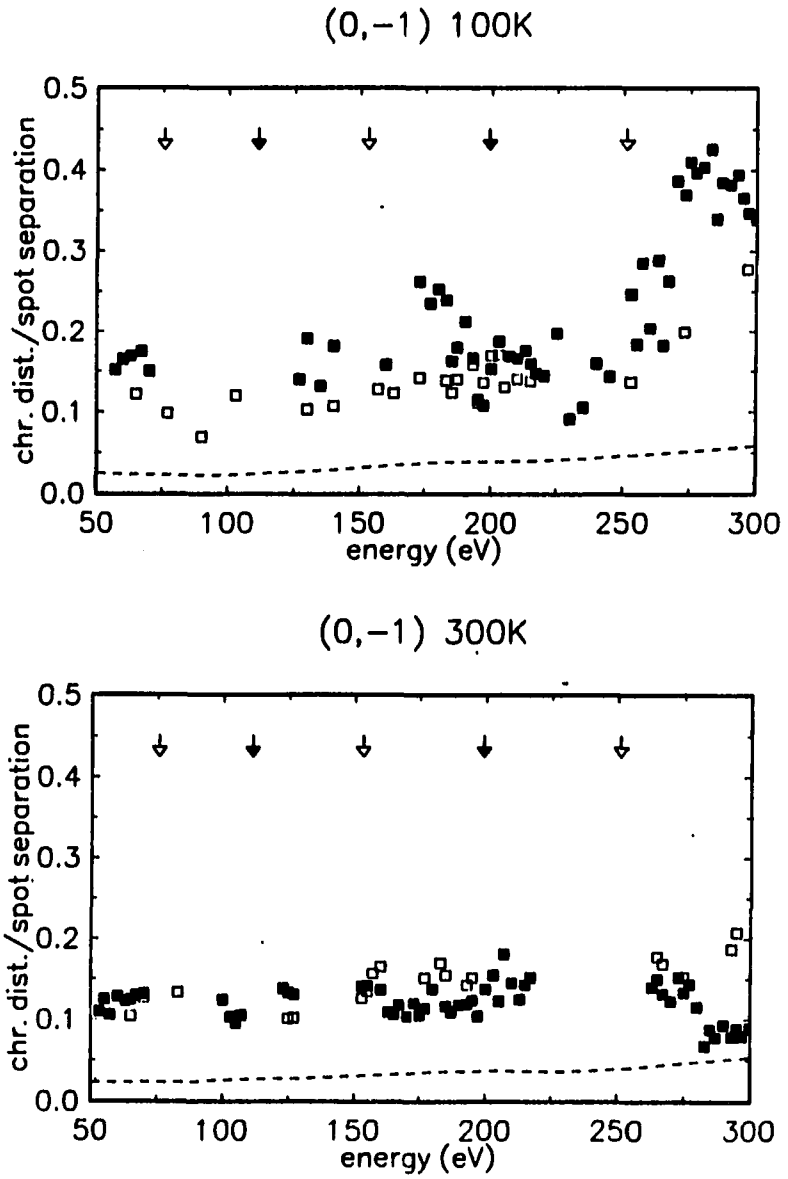

Figure 6. Comparison of baseline structure of initial substrate profiles (□) to reciprocal-space characteristic distances of profiles from the surface with ca. 1/2 ML deposit (■)

The dashed line shows the instrument response, as determined from Figure 2. Arrows are defined in the text. Profiles without discernible baseline structure are not represented. (a) (0,-1) 100 and 300 K

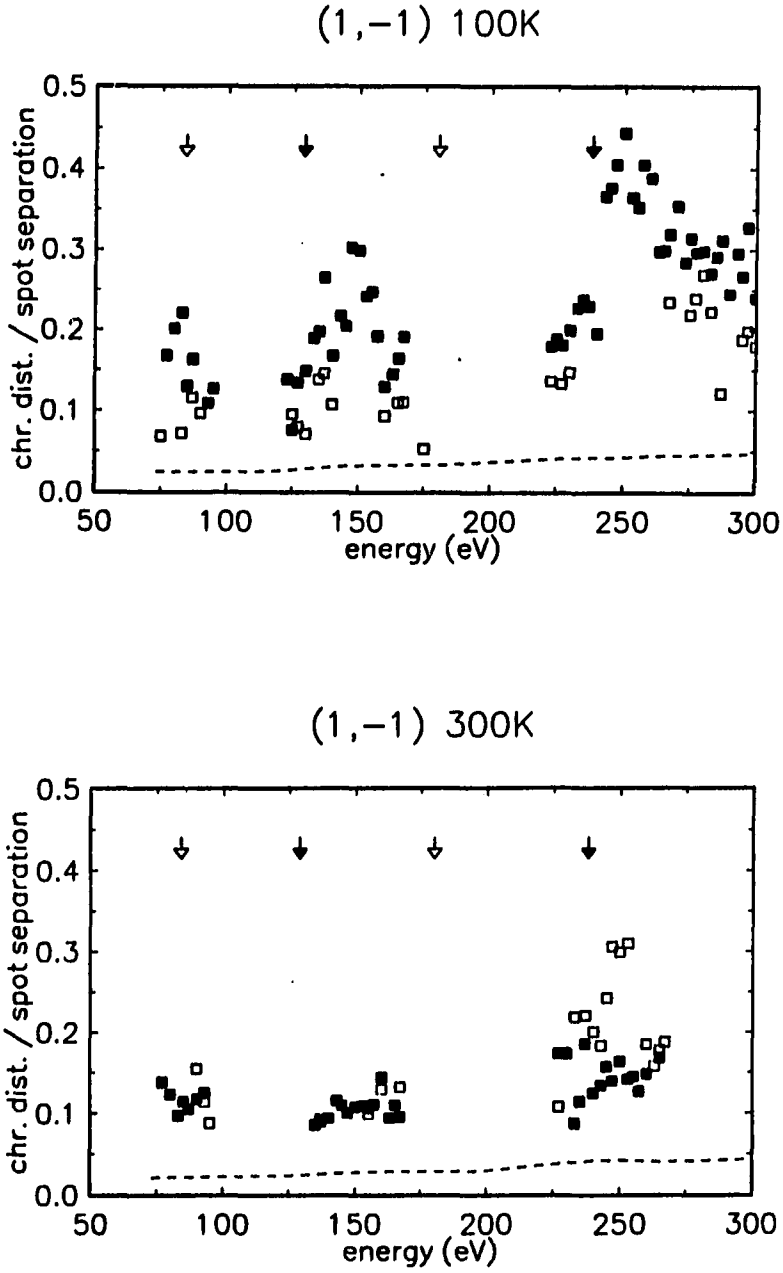

Figure 6. (continued)

(b) (1,-1) 100 and 300 K

real space. Since the substrate undergoes several cleaning and annealing cycles prior to deposition (annealing temperature = ca. 1500 K), it is unreasonable to assume such small islands reproducibly exist and *are stable* on our initial surface. This is further justification that we cannot attach meaningful physical significance to the value of the reciprocal-space characteristic distance of a clean surface profile in terms of an average island size. "Wing-structure" *must* be derived from other sources, such as inelastic scattering. We conclude that in this study when the amplitude of the foot nears that of the initial substrate "wing-structure", the derived average island size (or separation) is reliable *only* when the reciprocal-space characteristic distance *exceeds* ca. 0.1. Since the 300 K profiles of the covered surface exhibit clear ring-structure, with amplitude greater than the initial substrate wing-structure, we conclude that overlayer islands are characterized by a ca. 17.5 ± 3.5 Å periodic distance (width or separation). It may be fortuitous that this value is nearly equal to the FWHM of the initial substrate wing-structure, and we cannot rule out the possibility that some substrate characteristic or defect (other than an average island size) ultimately determines the overlayer distribution, without another technique to examine the substrate perfection. The lack of structure in Figure 2 leads us to believe this is not the case, however.

The amplitude of the foot of profiles from Pd deposited at 100 K is *not* much greater than the wing structure of the clean substrate profiles. Furthermore, these profiles do not exhibit ring-structure. Therefore we expect a reliable estimate of the island size only when the reciprocal-

space distance is greater than ca. 0.1. The range of the 100 K data of Figure 6 indicates average island sizes between 7 and 27.5 Å, or islands approximately 2 to 10 atoms in width result from deposition at this temperature. We note that the average island size determined from background-subtracted profiles are skewed to larger sizes, since isolated atoms are not included in the calculation. (A constant background is normally associated with point defects or isolated atoms (19,20).) This is particularly a problem at low temperatures, where low adatom mobility inhibits significant condensation. This suggests that at 100 K, most islands are much less than 10 atoms in width.

The step height may be calculated from the period of the FWHM data of Figure 6. The 300 K (0,-1) and (1,-1) data yield an average step height of 1.91 ± 0.15 Å, in good agreement with the Pd(100) first-layer spacing (1.94 Å) (21).

Lastly, we note that obtaining the energy-dependent profiles with our data acquisition system typically takes ca. 2 - 2 1/4 hours. Temporal effects may be a factor in these experiments. At 300 K, there may be some "self-annealing" of the deposited overlayer during data acquisition. There may also be some contribution from residual-gases, for both the initial and covered surfaces, particularly at low temperatures where typically sticking coefficients are high and desorption rates are low. We expect adsorbed residual-gases to affect mainly the central-spike intensity, with a lesser effect on the foot. The profiles are accumulated in a nonlinear energy sequence, identical in all experiments, in an effort to average over temporal effects.

V. SEQUENTIAL DEPOSITION EXPERIMENTS

A. Intensity Oscillations

1. Results

We examine the profile shape as a function of coverage at various temperatures. Figure 7 shows (1,-1) spot profiles obtained for incremental Pd deposition at 300 K. The beam energy is 147 eV, which corresponds to an out-of-phase scattering condition. The first profile is of the initial surface ($\theta = 0$). It is characteristically sharp, indicative of a very low step density. As Pd is deposited, two components become apparent in the profiles, a sharp-component and the foot. Figure 7 shows the intensity of the central-spike oscillates with coverage.

Figure 8 shows a comparison of the coverage-dependence of the central-spike height of the (0,-1) and (1,-1) beams for out-of-phase and in-phase scattering conditions at various temperatures. Each temperature represents one experiment. Both symmetries show oscillations as a function of coverage at the out-of-phase condition. However, these spots show dissimilar coverage-dependence at the in-phase condition.

2. Discussion

Perfect layer-by-layer growth is accurately described as a two-level system for growth on an ideally flat substrate. At most, one incomplete layer exists at any time. The development of an epitaxial layer requires the formation of steps, as islands form on the flat substrate. As the layer nears completion, the number of steps is reduced. Within the

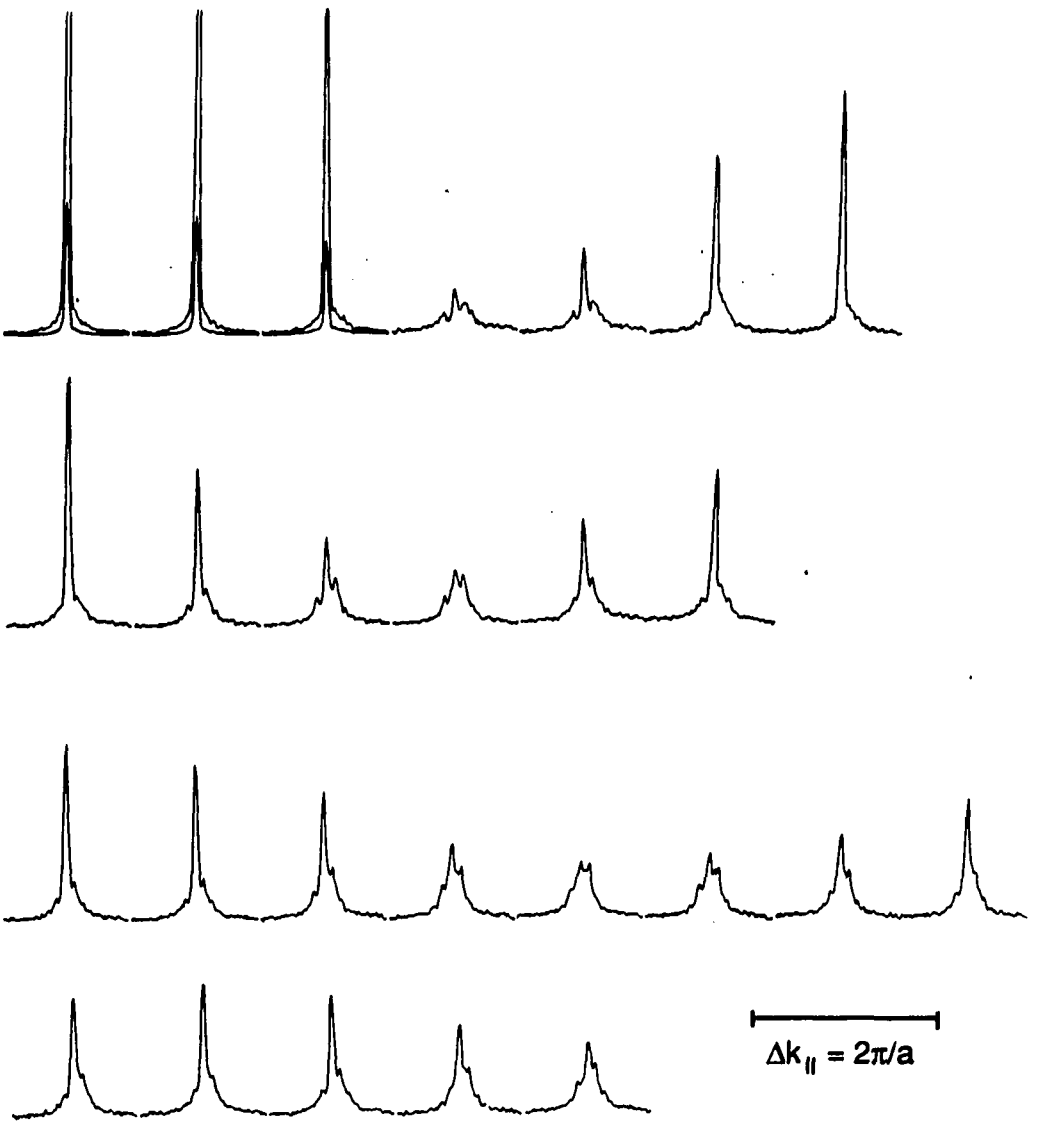

Figure 7. Profiles of the (1,-1) spot after successive evaporations at 147 eV

The substrate temperature is 300 K. The first profile is that of the clean substrate. The second profile is taken after a 10 s Pd dose. The 10 s dose is repeated before each of the following profiles. The profiles are divided into four rows, each roughly showing the filling of a new layer.

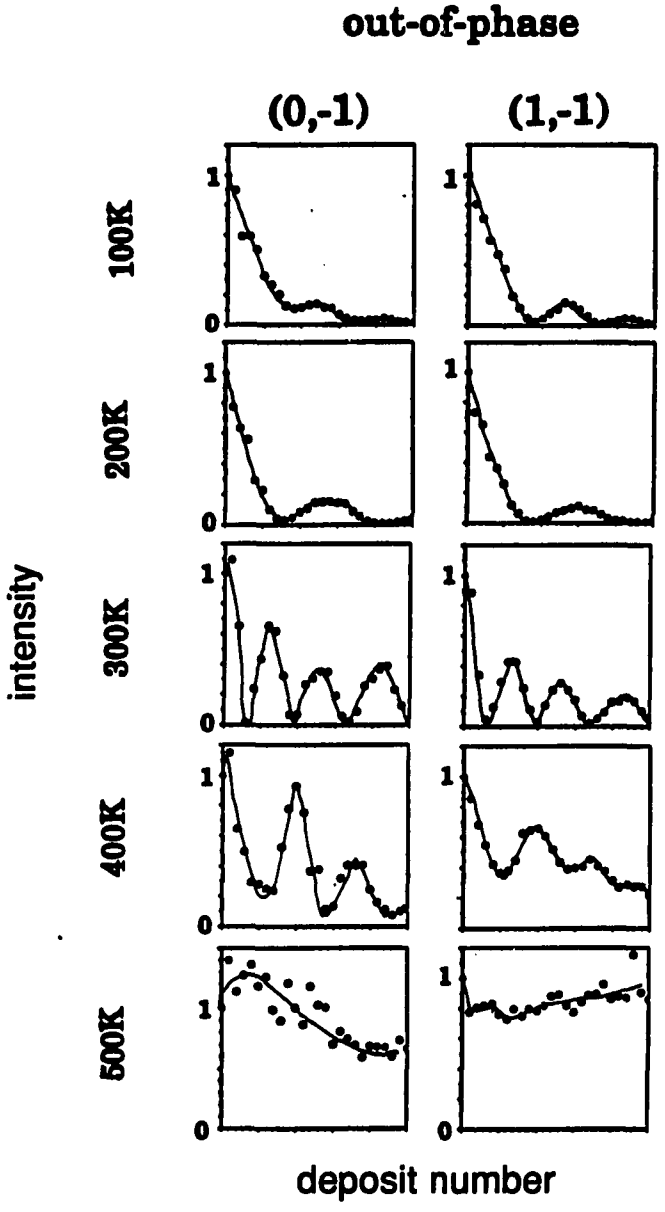

Figure 8. Normalized central-spike intensity as a function of deposit number for the temperatures indicated

Each deposit consists of a 10 s Pd dose.

(a) left: (0,-1) 53 eV, out-of-phase
right: (1,-1) 147 eV, out-of-phase

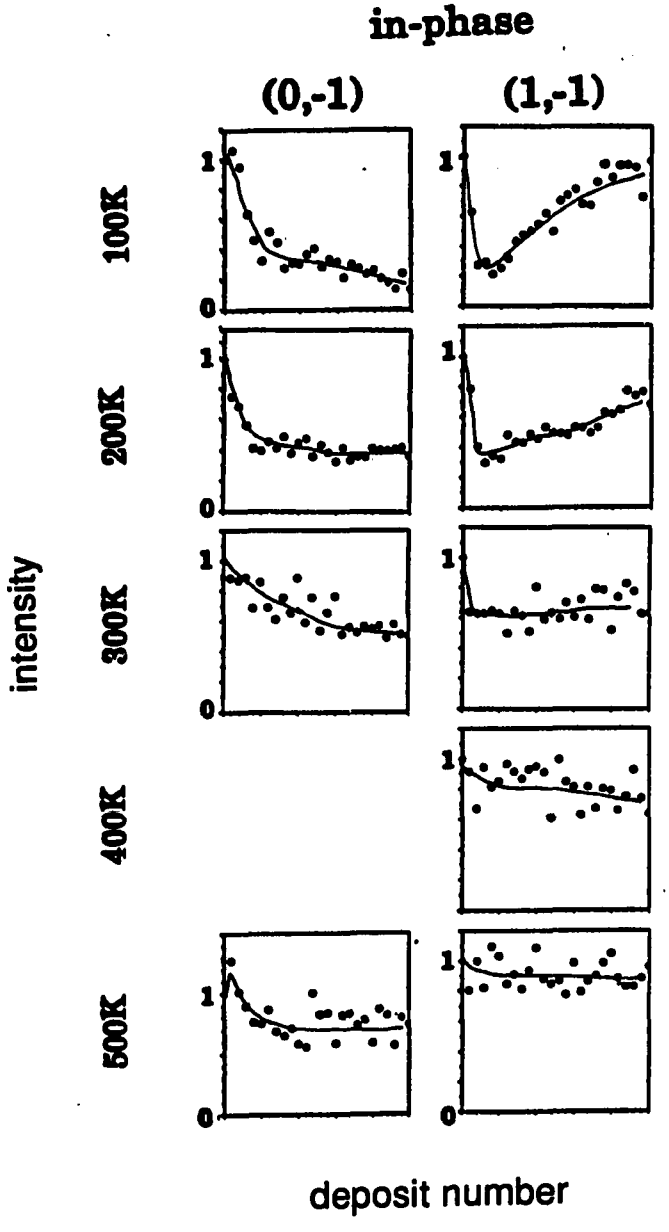

Figure 8. (continued)

(b) left: (0,-1) 133 eV, in-phase
right: (1,-1) 113 eV, in-phase

kinematic approximation, scattering from successive layers interferes destructively at an out-of-phase condition, and it has been shown that the intensity for a two-level system varies with coverage according to (14,17):

$$I = (2\theta - 1)^2 \qquad (1)$$

where θ is the fractional coverage of the growing layer. The intensity oscillates between zero and unity, for half-layer and full-layer coverages. This behavior directly results from the destructive interference of scattering from successive layers, and is depicted in Figure 9. The cusp-like appearance at the maxima stems from the abrupt transition between the filling of successive layers for this idealized growth.

The out-of-phase data of Figure 8a show damped oscillations for Pd(100) epitaxial growth below 500 K. The equilibrium growth mode for this homoepitaxial system is necessarily Frank-van der Merwe, but we do not observe perfect layer-by-layer filling at any temperature in these experiments. Clearly idealized equilibrium is not attained during this growth process.

During equilibrium growth, entropy would prohibit a layer from attaining perfect flatness, even at T = 0 K. Also, due to kinetic limitations, the lower layer may not be complete before the next layer begins to fill. With more than two levels present, the ideal oscillation curve of Figure 9 is smoothened and to some extent dampened. Oscillations of this sort have been experimentally observed with various

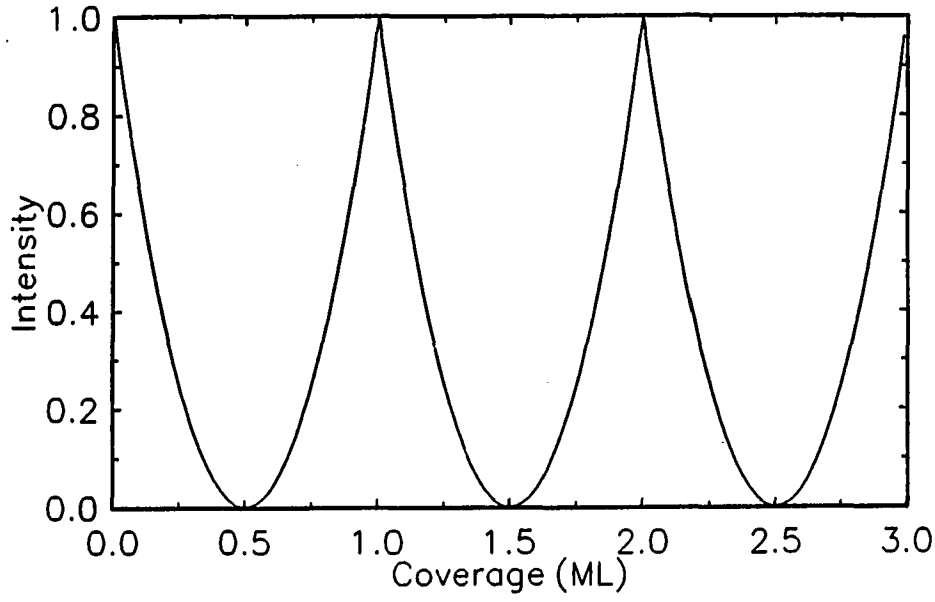

Figure 9. Coverage-dependence of the diffracted intensity during perfect layer-by-layer growth

diffraction techniques for many epitaxial systems (22-26).

The *existence* of oscillations for the Pd/Pd(100) system (Figure 8a) indicates that there is *some* layer-by-layer quality to the growth, but there is an increasing number of unfilled layers as growth proceeds. The oscillatory nature of the curve is clearest at 300 K. Below this temperature, the oscillations are more damped, and above this temperature, the minima of the oscillations are no longer zero.

The behavior at and below 300 K is easily explained in terms of limited surface diffusion. Previous studies have shown that nondiffusive, random deposition into fourfold-hollow adsorption sites results in damped, low amplitude intensity oscillations (27,28). As adatoms become mobile (via thermally-activated surface diffusion) the oscillation amplitude increases. Our experiments show that at ca. 200 K, diffusion is operable to an extent sufficient to reduce the number of growing layers, relative to growth at lower temperatures. However, this "annealing effect" is not complete, and damping is still evident in the oscillations.

This picture suggests that if we could increase the surface temperature enough, perfect layer-by-layer oscillations, like those of Figure 9, should result. Figure 8a shows this is not what we observe. At 400 K, oscillations at the out-of-phase condition are still evident; however, the minima are nonzero. At 500 K oscillations are no longer apparent. (These two points are clear from the 400 and 500 K profiles in Figure 5.) We expect these experimental observations are associated with preexisting steps on the surface. Since the substrate is not perfectly

flat, ideal layer-by-layer growth is prevented. The rather constant coverage-dependence of the intensity at 500 K suggests diffusion is essentially unlimited on the timescale of the deposition. Deposited atoms are mobile enough to migrate to existing step edges between deposition events, a phenomenon called "step propagation". Nucleation of new layers occurs only on very large terraces. Consequently, the initial surface morphology is more or less conserved throughout the growth process, yielding little change in intensity as coverage increases. The initial (low coverage, short time) intensity drop indicates diffusion is not *completely* unlimited on the timescale of this experiment, even at 500 K. The slow increase thereafter may indicate a continuous annealing process as the experiment proceeds.

We show the coverage-dependence of the in-phase beams in Figure 8b. A rapid, initial decrease in the intensity is observed at low coverages, followed by a more gradual decrease (for the (0,-1) beam) or increase (for the (1,-1) beam) as coverage increases. With increasing substrate temperature, the initial intensity drop is less severe, and the subsequent behavior less dramatic. By 500 K, the intensity is fairly constant with coverage.

The in-phase condition results when the wavelength of the incident beam matches the three-dimensional lattice spacings in the crystal. As a logical extension of this definition, the observed initial in-phase intensity drop indicates that some of the deposited atoms do not occupy regular, three-dimensional lattice positions. We envision two extremes, either (some) deposited atoms are kinetically trapped in alternate, two-

dimensional, lattice positions (parallel to the surface), or the growing layer experiences a relaxation unlike that of a complete layer. Recent molecular dynamics simulations of epitaxial fcc(100) growth (21,22) have shown that deposited atoms occupy the nearest fourfold site, regardless of the exact point of impact inside the unit cell, even when the substrate temperature is 80 K. Therefore a two-dimensional displacement is not expected. However, the results of Sanders and DePristo (21) for Pd on Pd(100) show that single atoms are *vertically* displaced, contracted 14 % relative to the first interlayer spacing.

In our deposition experiments, a large fraction of isolated atoms are presumably present at low coverages, and particularly at low temperatures. Based on the results of reference 21, we expect the initial, in-phase intensity to be reduced via incoherent scattering between substrate and deposited (isolated) atoms occupying contracted positions. Indeed, the reduction of intensity is most dramatic at low coverages. As the coverage increases and isolated atoms form growing islands, we expect the interlayer spacing to rather quickly approach its equilibrium value as lateral interactions increase. This may account for for the less striking decrease observed in (0,-1) in-phase intensity as the coverage increases. Since the initial intensity never recovers with increasing coverage, we conclude there is always some fraction of isolated atoms (and *very* small islands) present during growth.

The proposed variation of the interlayer spacing in the limit of very small islands is also consistent with the observed temperature-dependent trends. We expect a larger impact on the intensity at lower

temperatures, where limited migration reduces the probability for coalescence within a layer. At higher temperatures the effect is less dramatic, presumably because single atoms more readily attach to larger, preexisting terraces, even at low coverage. These trends are evident in the (0,-1) data of Figure 8b.

We believe residual-gas effects account for the intensity rise of the in-phase (1,-1) intensity in the later stages of the experiment (see Figure 8b). Taking 1.5 to 2 hours, background-gas adsorption is inevitable in these experiments. This is a particular problem at low temperatures, since sticking coefficients usually vary inversely with temperature. The dependence on temperature and deposit number (proportional to coverage and time) is explained if scattering from an adsorbed species is particularly intense at the energy studied. Thermal desorption experiments show that approximately 1/3 ML H_2 will adsorb during the course of an experiment at 100 K, but H_2 itself is usually a weak scatterer and is not thought to contribute appreciably to the intensity. A comparison of spot intensity as a function of energy at 100 and 300 K for the clean surface reveals that over the course of 1.5 - 2 hours, a fivefold increase in the intensity of the (1,-1) beam is evident at energies near in-phase scattering (near 113 eV) at low temperature relative to high. Correspondingly, for the (0,-1) beam (near 133 eV) the intensity increase is less than 1.5 times. This indicates temperature affects the (1,-1) and (0,-1) beams differently at their in-phase energies, suggesting a residual-gas component. Additionally, when comparing the clean and 1/2 ML covered surfaces at one temperature, there

is little intensity difference. This suggests that the disparity in the coverage-dependence of the two measured in-phase symmetries is not strongly influenced by multiple-scattering effects, but rather has origins in residual-gas contributions.

B. Onset of Diffusion

1. Results

We examine profiles of the sequential deposition experiments in further detail, to distinguish changes associated with the onset of diffusion. In Figure 5, we show profiles at the first minimum, first maximum, and second minimum of the intensity oscillation curves (Figure 8a) compared to the initial profiles. Respectively, these points approximately represent Pd coverages of 1/2, 1, 1-1/2 and 0 ML. Figure 10 shows the reciprocal-space characteristic distance as a function of temperature at the first and second minima for experiments like, and including, those of Figure 5. The circles represent data from the first minimum, squares from the second. Open symbols denote a FWHM of a foot, filled symbols denote diameter of a ring. Above 200 K, *only* ring-structure is observed at these half-integral coverages. The characteristic distance at the second minimum is always less than that which is measured at the first minimum.

Figure 11 shows the intensity of the sharp-component at the first oscillation maximum (see Figure 5) plotted as a function of substrate temperature. Little temperature-dependence is observed below ca. 200 K,

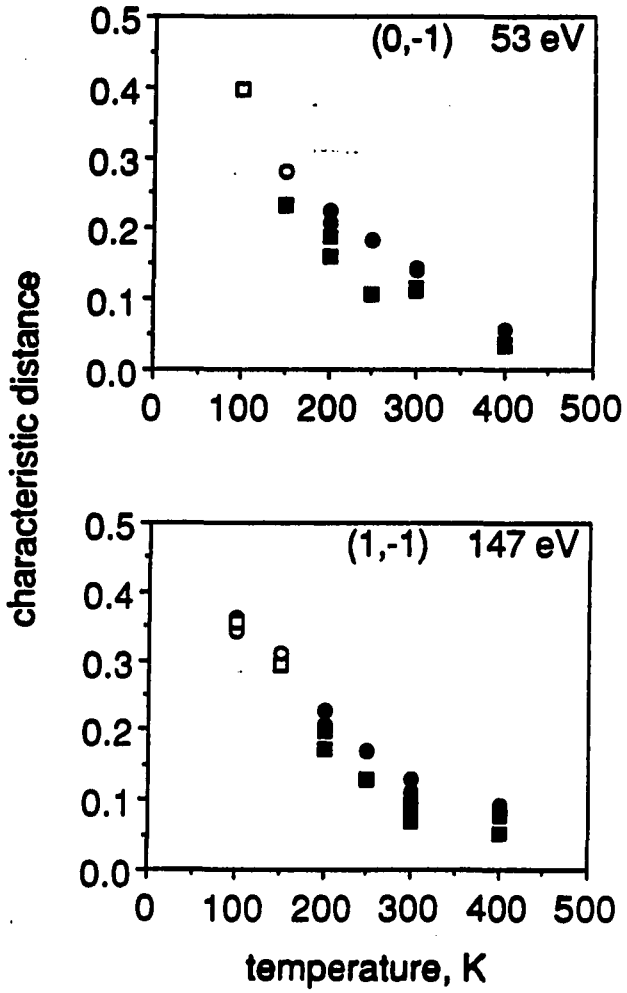

Figure 10. Reciprocal-space characteristic distance as a function of temperature at the first and second minima of the oscillation curves

- o FWHM at the first minimum
- ● ring diameter at the first minimum
- □ FWHM at the second minimum
- ■ ring diameter at the second minimum

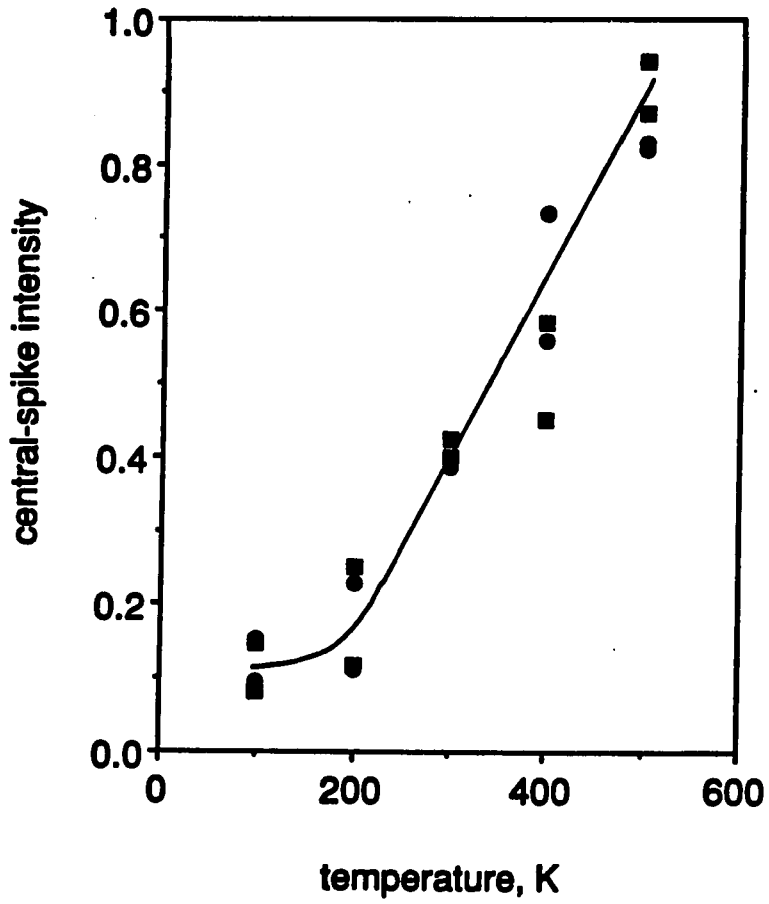

Figure 11. Normalized intensity of the first maximum ($\theta \approx 1$) as a function of substrate temperature

but a striking increase in the intensity is observed above this temperature.

2. Discussion

Ring-structure is evident in the LEED spot profiles at substrate temperatures at and above 200 K, indicating that islands are distributed in an ordered fashion, either with constant (or limited range of) separation or size. Below 200 K, the LEED profiles are characterized by a homogeneously-broadened foot, suggesting islands of random size and random separation. The change in the basic nature of the LEED profile indicates a fundamental change in the growth process near 200 K. The emergence of a more regular (rather than random) growth is consistent with the onset of thermally-activated diffusion. The overall decreasing trend of the reciprocal-space characteristic distance with increasing substrate temperature (Figure 10) indicates that for the same approximate coverage, the islands are spaced *further apart* at higher temperatures (13). This can only be true if there are *fewer* islands. Thus, significant condensation must occur at the higher temperatures.

Further evidence for the onset of diffusion near 200 K lies with the temperature-dependence of the sharp-component (Figure 11). The low slope of the curve below 200 K indicates growth is nearly temperature-independent, thus diffusion is *not* operative. Above 200 K, a strong temperature-dependence is observed, with increasing tendency toward perfect layer-by-layer growth as temperature increases. The change in slope between ca. 170 and 200 K suggests thermally-activated surface

diffusion "turns on" in this temperature regime. Assuming a prefactor of 10^{13} s^{-1}, this onset temperature suggests an activation barrier of ca. 12.7 kcal/mol. This value is in reasonable agreement with surface diffusion barriers on other unreconstructed fcc(100) surfaces: 11 kcal/mol activation barrier for Cu/Cu(100) (26), and 14.6 kcal/mol for Ni/Ni(100) (30). Our result is also in agreement with field-ion microscopy studies of Pd on Ta(110) which show Pd atoms become mobile at 180 K with an activation energy of 11.3 kcal/mol (31).

C. Coverage-Dependence of Ring-Structure

1. Results

The coverage-dependence of the ring-structure at the out-of-phase condition is examined in more detail. Figure 12 shows the ring diameter and intensity, along with the central-spike oscillations, for three different temperatures. The ring diameter is normalized to the spot separation, and the ring intensity is normalized to the intensity of the initially sharp spot at zero coverage. At very low coverages (first 1-3 deposits) a ring is not observable in the profile lineshape, but usually appears by ca. θ = 0.25 ML.

2. Discussion

At low coverages, and approximately during the filling of the first layer, the ring diameter decreases with coverage, indicating islands generally grow further apart as coverage increases. This is consistent with the idea that at these temperatures, after initial nucleation there is significant condensation of isolated atoms (and perhaps even of small

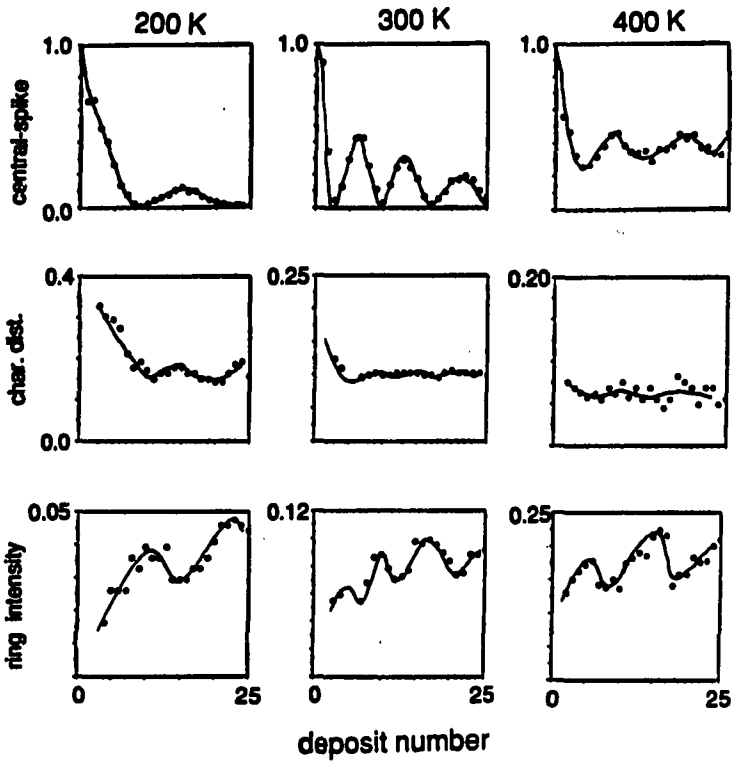

Figure 12. Central-spike intensity, reciprocal-space characteristic distance and ring diameter of (1,-1) profiles as a function of deposit number for various temperatures

The beam energy is 147 eV, representing an out-of-phase scattering condition. The central-spike and ring intensities are normalized to the intensity from the initial substrate. The reciprocal-space characteristic distance is normalized to the spot separation. Lines through the data are drawn for clarity.

clusters) to the larger, immobile islands (13). This implies an irreversible attachment of small, mobile species at island edges. As the first-layer completes, and throughout the filling of the second-layer, the average separation remains constant, as evidenced by the nearly constant ring diameter at these coverages. This suggests the second-layer island separation is governed by that of the first, as would be expected. The superimposed, weak oscillations in the ring diameter seem to suggest maximum separation near half-layer coverages and closest separation near full-layer coverages. However, repetitive experiments do not always produce these superimposed oscillations, suggesting an extreme sensitivity of the ring characteristics to the exact coverage distribution. However, the general trend in, and limiting value of, the ring diameter with temperature is reproducible. The decreasing difference between the initial and asymptotic ring diameter with increasing temperature further illustrates the enhanced mobility at higher temperatures.

We see from Figure 12 that the normalized ring intensity oscillates roughly out-of-phase with the central-spike intensity. In contrast to the central-spike intensity, the ring intensity generally increases with coverage. We gain insight to the coverage-dependence of the ring intensity by considering an idealized system with islands of constant size and constant separation, as shown in Figure 13. For growth where all islands monotonically increase, we expect the ring intensity to scale with the size of the islands at low coverages, but scale with the gaps between islands at high coverages. Thus the ring intensity should

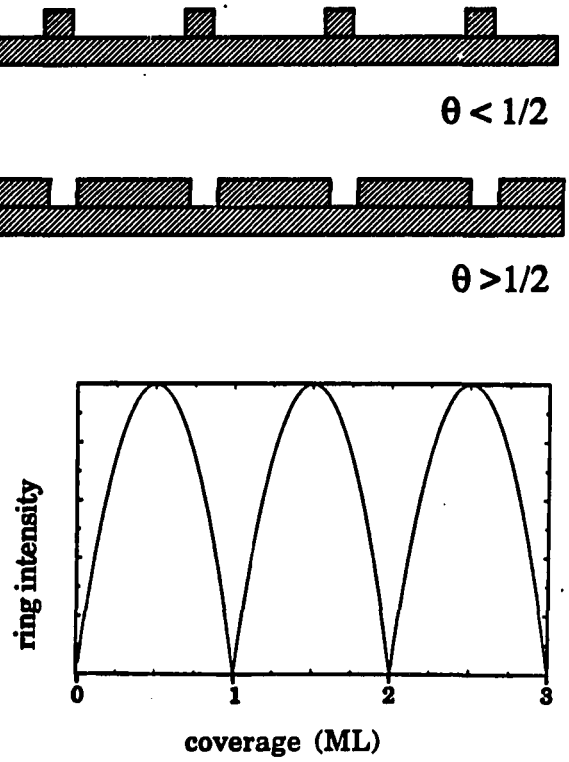

Figure 13. Idealized island growth of constant size and constant separation

TOP: nucleation of equally spaced islands results in ringed profiles, and ring intensity should be indicative of island size

MIDDLE: as layer completes, the ring intensity should be indicative of the gaps between islands

BOTTOM: predicted coverage-dependence of the ring intensity

oscillate with coverage as shown in Figure 13.

The experimental coverage-dependence of the ring intensity (Figure 12) follows the predicted behavior fairly well, demonstrating the successive filling of layers during growth. Even at 200 K, there must not be substantial filling of the second layer before the first completes. The general increase in ring intensity with coverage reflects the increasing size of the islands. The intensity increase with increasing substrate temperature is consistent with enhanced mobility and coalescence at higher temperatures, resulting in the formation of larger islands (more atoms per island).

D. Sticking Coefficient

Figure 14 shows the temperature-dependence of the deposit at which the second maximum of the out-of-phase oscillation curve is reached, relative to that of the first, for several beam symmetries and energies. (One deposit consists of a 10 second Pd dose.) These data are extracted from the sequential deposition experiments at constant temperature, including those of Figure 8. Within experimental uncertainty, there is no change of phase for the first two oscillations, indicating unit sticking coefficient, invariant with temperature. Since the binding energy in metal systems is typically 60-85 kcal/mol, evaporation from the metal surface at these temperatures is negligible. Thus, unit sticking coefficient is expected.

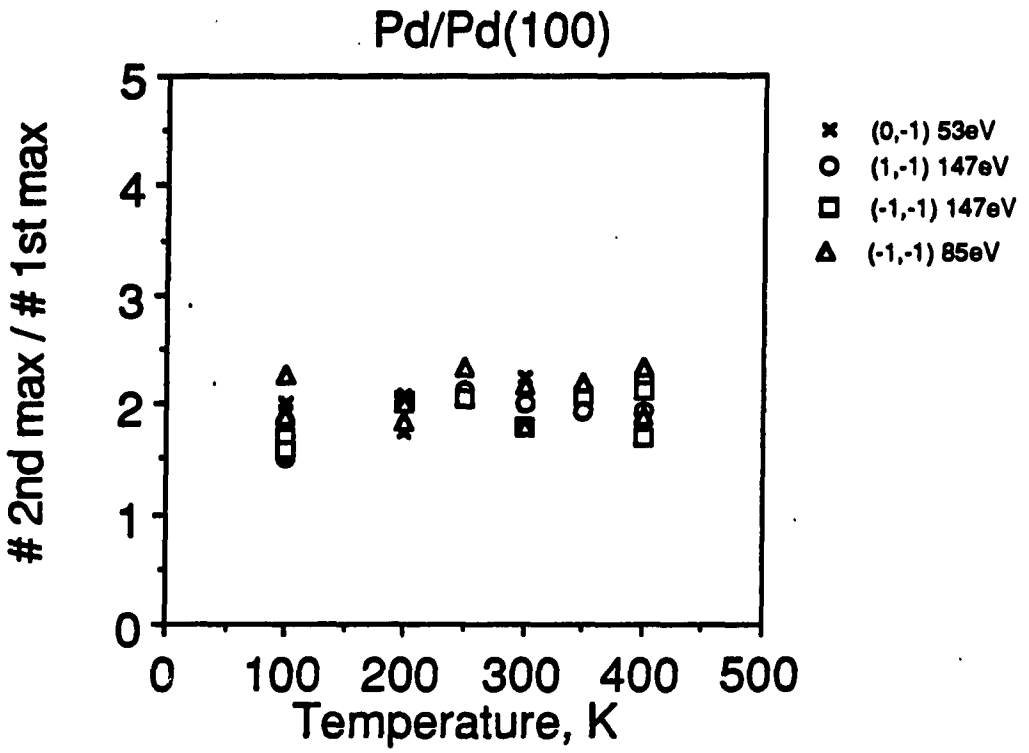

Figure 14. Sticking coefficient

The deposit number of second maximum ($\theta \approx 2$ ML) in the oscillation curve relative to that of the first ($\theta \approx 1$ ML), for various beam energies and symmetries for a number of experiments. The constant value of 2 indicates a sticking coefficient of unity for the first two layers in the temperature range studied.

E. Multiple-Scattering Effects

The (-1,-1) beam is monitored at two different out-of-phase energies during the sequential deposition experiments, 85 and 147 eV. In any one experiment, the lower-energy spot generally produces a maximum in the oscillation curve at a lower coverage (deposit number) than the higher-energy spot, as shown in Figure 15. A "phase difference" between beams of the same symmetry implies different degrees of imperfection are sensed *for the same overlayer morphology*. This difference must be associated with a multiple-scattering effect, since kinematic theory is independent of spot symmetry and predicts the same behavior for all spots at all out-of-phase energies. Therefore the observed "phase difference" presumably depends on the details of the layer distribution (e.g., step density and the local geometry describing a step edge) in addition to the layer coverages. Figure 15 also shows that there is a greater coverage disparity between the oscillation maxima at low temperature which levels off as temperature increases. At low temperatures, random deposition results in a large number of steps. At higher temperatures, thermally-activated diffusion tends to smoothen the overlayer, thus the number of multiple-scattering events at steps is reduced. Similar, albeit much grosser, effects have been observed in RHEED studies of molecular beam epitaxially grown semiconductors, where in some cases, multiple-scattering leads to phase doubling (32).

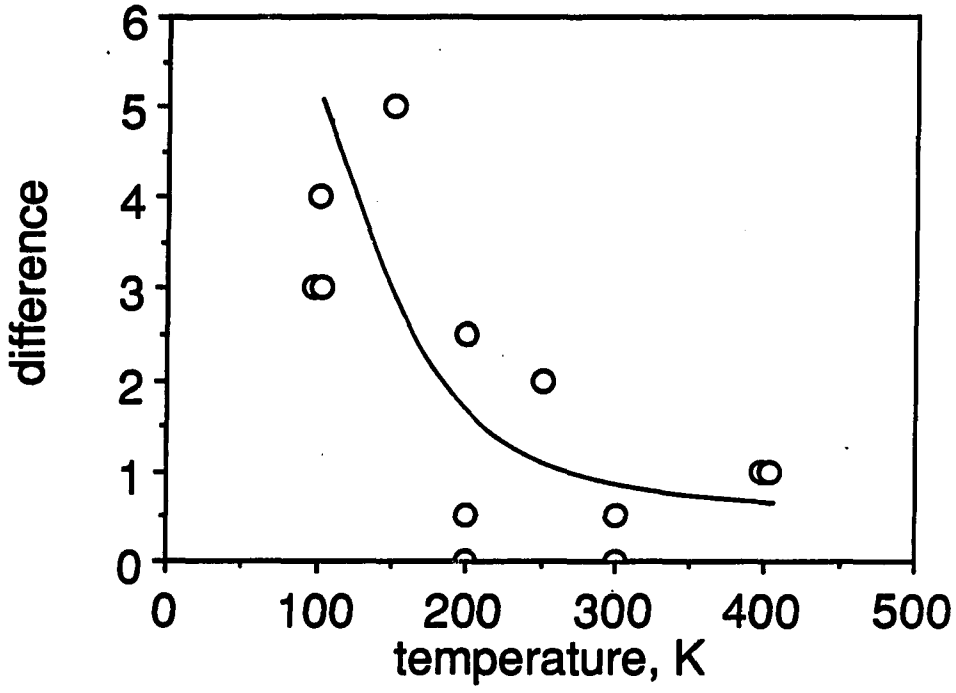

Figure 15. Multiple-scattering effects

Difference in the deposit number (proportional to coverage) of the first maximum in the oscillation curve between the (-1,-1) profiles at 85 and 147 eV. Both energies represent an out-of-phase scattering condition.

VI. COMPARISON WITH OTHER WORK

We investigate the homoepitaxial growth of Pd(100) between 100 and 500 K via LEED spot profile analysis. At low temperature, the growth is characterized by islands of random size and separation, and one, to a few, layers in height. At intermediate temperatures (ca. 200 - 400 K), islands of are regular distribution, which results from limited diffusive processes being operative at these temperatures. At higher temperatures (500 K), the growth process is better characterized by step propagation.

The results obtained herein for Pd deposition on Pd(100) between 200 and 400 K are generally consistent with those obtained by Hahn and coworkers, for the epitaxial growth of W on W(110), between 300 and 430 K (13). In the W/W study, the following observations were made:

(1) ring structure was present in the LEED profiles for $\theta > 0.1$ ML,

(2) ring intensity was maximized at out-of-phase energies and minimized at in-phase energies,

(3) ring intensity increased with coverage,

(4) ring diameter was invariant with energy,

(5) ring diameter increased up to θ = ca. 0.5 ML, then was invariant with coverage (up to 2 ML),

(6) ring diameter varied inversely with temperature.

It was concluded that for W/W(110) at these temperatures, after initial nucleation, only growth of existing islands occurs. From (3) it was concluded that the second-layer begins to fill well before the first is completed, as these authors noted the ring intensity would decrease for θ

> 0.5 otherwise. On the basis of nucleation theory and observation (5), Hahn and coworkers (13) argued that the ring diameter is representative of the island separation.

The observations for W/W(110) are generally consistent with our data for Pd/Pd(100) between 200 and 400 K. However, contrary to the W/W(110) system, we observe an initial *decrease* in the ring diameter with coverage; from the coverage at which it first appears, as well as oscillations in the ring intensity as a function of coverage. The initial decrease in ring diameter with coverage for Pd on Pd(100) is consistent with an increasing island separation at low coverages, as would be expected if significant island coalescence (including incorporation of isolated atoms) occurs. This is compatible with our idea of growth in the temperature regime in which diffusion is operative. No interpretation is offered in the W/W(110) study for the low coverage ring diameter behavior. Our report of ring intensity oscillations during epitaxial growth is, to our knowledge, the first of its kind. Perhaps oscillations were missed in the W/W study, since only a few coverages were examined, or perhaps the layer-by-layer growth of W/W(110) is sufficiently less layer-by-layer-like than that of Pd/Pd(100), preventing oscillations in the ring intensity.

VII. CONCLUSIONS

We use LEED spot profile analysis to investigate the homoepitaxial growth of Pd on Pd(100) between 100 and 500 K. Random, nondiffusive growth results at low temperature, with LEED spot profiles consisting of a central-spike and a superimposed, homogeneously-broadened foot. Deposition at intermediate substrate temperatures (ca. 200 to 400 K) leads to ring-structured profiles, indicative of a regular island distribution, the formation of which is mediated by limited surface diffusion. Sharp profiles are maintained throughout growth at high temperatures, indicative of a step propagation mechanism.

Deposited atoms occupy fourfold-hollow adsorption sites, but isolated atoms are vertically displaced. Our data suggest this vertical displacement is dependent upon the number of atoms per island. The change in the interlayer spacing as the island grows is not thermally-activated. In the limit of an isolated atom, recent molecular dynamics simulations demonstrated that a single Pd atom is contracted 0.27 Å relative to the first Pd(100) interlayer spacing (21). We propose that isolated atoms maximize bonding interactions by "sinking into" the substrate. As lateral interactions increase with the coalescence of atoms, the "plane" of the island moves out toward the equilibrium first layer spacing. We expect only a few lateral neighbors are necessary for the island to attain the equilibrium spacing.

Our data show the onset of thermally-activated diffusion on Pd(100) near ca. 200 K, indicating an activation barrier of ca. 13 kcal/mol. The

appearance of ring-structure in the LEED spot profiles is correlated with the onset of diffusion. At temperatures low enough that surface diffusion is inoperative, the growth mechanism is dominated by the random deposition process. LEED profiles for deposition at 100 K show a foot that is homogeneously-broadened, indicative of a random size distribution. At intermediate temperatures (200 to 400 K), diffusional processes overcome this random distribution. At these temperatures, after initial nucleation, there is little new nucleation. Rather, islands initially formed grow continuously via condensation, maintaining relatively constant separation between the growing islands.

Oscillations of the ring intensity during epitaxial growth are reported for the first time. The ring intensity is ideally associated with the number of atoms within a (two-dimensional) island. These data reflect the growth of islands within an individual layer and the successive filling subsequent layers. The observation of ring intensity oscillations demonstrates the relatively small deviation from idealized layer-by-layer growth for Pd on Pd(100), even at 200 K.

We demonstrate the importance of considering "wing structure" in the zero coverage profiles when interpreting island sizes or separations from the reciprocal-space characteristic distances observed during epitaxial growth. For growth of Pd on Pd(100), islands of ca. 17.5 ± 3.5 Å separation are observed at 300 K in this study. This distance coincides with the FWHM of the initial profile wing structure, so the influence of the substrate in determining the overlayer island separation cannot be unequivocally established. At 100 K, Pd deposition on Pd(100) results in

islands of 1 to at most 10 atoms wide. Our data show an average step height of 1.91 Å at 300 K.

By evaluation of the spot profile shape, and the changes in the profile as a function of coverage, substrate temperature and energy, we gain information on the growth process, onset of diffusion, interlayer spacing, sticking coefficient, multiple-scattering effects, average island size, average island separation and step (island) height during epitaxial growth. Spot profile analysis has been exploited by Henzler and coworkers, using a specially-designed, high-resolution LEED system (33-35). We note the use of a conventional spectrometer in the present investigation. Although the spot profile evaluations are not as detailed as those of Henzler's studies, we believe this is a significant study demonstrating the usefulness of spot profile analysis via conventional LEED.

VII. ACKNOWLEDGEMENTS

We are grateful for experimental assistance from O. L. Warren. We are also grateful to M. C. Tringides for helpful discussions of the data. Additionally, we thank D. E. Sanders for discussions of unpublished work. The experimental component of this work is supported by a Presidential Young Investigator Award of the National Science Foundation, Grant No. CHE-8451317, Camille and Henry Dreyfus Teacher-Scholarship (P.A.T.) and by the Ford Motor Company. Also, some experimental equipment and all facilities are provided by the Ames Laboratory, which is operated for the US Department of Energy by Iowa State University under Contract No. W-7405-ENG-82.

VIII. REFERENCES

1. J. D. Weeks and G. H. Gilmer, in Advances in Chemical Physics, Vol. 40, edited by I. Prigogone and S. A. Rice (Wiley, New York, 1979) p. 157.
2. A. A. Chernov, in Crystal Growth and Characterization, edited by R. Ueda and J. B. Mullin (North-Holland, Amsterdam, 1975), p. 33.
3. M. Henzler, Surface Sci. 19 (1970) 159; Surface Sci. 36 (1973) 109; Appl. Phys. 9 (1976) 11.
4. E. Bauer and J. H. van der Merwe, Phys. Rev. B 33 (1986) 3657.
5. J. W. Anderegg and P. A. Thiel, J. Vac. Sci. Technol. A 4 (1986) 1367.
6. B. C. DeCooman and R. W. Vook, J. Vac. Sci. Technol. 21 (1982) 899.
7. J. W. Anderegg and P. A. Thiel, Rev. Sci. Instrum. 55 (1984) 1669.
8. H. Herz, H. Conrad and J. Küppers, J. Phys. E 12 (1979) 369.
9. M. Henzler, Surface Sci. 22 (1970) 12.
10. D. K. Flynn-Sanders and P. A. Thiel, Iowa State University, Chemistry Dept., manuscript in preparation (1990).
11. M. Henzler, Surface Sci. 73 (1978) 240.
12. G. Schulze and M. Henzler, Surface Sci. 73 (1978) 553.
13. P. Hahn, J. Clabes and M. Henzler, J. Appl. Phys. 51 (1980) 1079.
14. J. M. Pimbley and T.-M. Lu, J. Appl. Phys. 57 (1985) 1121.
15. D. K. Flynn, W. Wang, S.-L. Chang, M. C. Tringides and P. A. Thiel, Langmuir 4 (1988) 1096.
16. J. M. Pimbley and T.-M. Lu, J. Appl. Phys. 59 (1986) 2439; 57 (1985) 4587.

17. C. S. Lent and P. I. Cohen, Surface Sci. 139 (1984) 121.

18. M. G. Lagally, in Methods in Experimental Physics: Solid State Physics: Surfaces, Volume 22, edited by R. L. Park and M. G. Lagally (Academic Press, Orlando, 1985) p. 273.

19. M. Henzler, Appl. Surface Sci. 11/12 (1982) 450.

20. M. Henzler, Appl. Phys. A 34 (1984) 205.

21. D. E. Sanders and A. E. DePristo, Iowa State University, Chemistry Department, manuscript in preparation (1990).

22. Thin Film Growth Techniques for Low-Dimensional Structures, edited by R. F. C. Farrow, S. S. P. Parkin, P. J. Dobson, J. H. Neave and A. S. Arrott (Plenum Press, New York, 1987).

23. Reflection High Energy Electron Diffraction and Reflection Imaging of Surfaces, edited by P. K. Larson and P. J. Dobson (Plenum Press, New York, 1988).

24. S. T. Purcell, A. S. Arrott and B. Heinrich, J. Vac. Sci. Technol. B 6 (1988) 794.

25. D. K. Flynn, J. W. Evans and P. A. Thiel, J. Vac. Sci. Technol. A 7 (1989) 2162.

26. J. J. De Miguel, A. Cebollada, J. M. Gallego, J. Ferrón and S. Ferrar, J. Crystal Growth 88 (1988) 442.

27. J. W. Evans, D. K. Flynn and P. A. Thiel, Ultramicroscopy 31 (1989) 80.

28. J. W. Evans, Vacuum (1990) in press.

29. J. W. Evans, D. E. Sanders, P. A. Thiel and A. E. DePristo, Phys. Rev. B 41 (1990) 5410.

30. R. T. Tung and W. R. Graham, Surface Sci. 97 (1980) 73.

31. P. R. Schwoebel and G. L. Kellogg, Phys. Rev. B 38 (1988) 5326.

32. J. Zhang, J. H. Neave, P. J. Dobson and B. A. Joyce, Appl. Phys. A 42 (1987) 317.

33. K. D. Gronwald and M. Henzler, Surface Sci. 117 (1982) 180.

34. R. Altsinger, H. Busch, M. Horn and M. Henzler, Surface Sci. 200 (1988) 235.

35. M. Horn, U. Gotter and M. Henzler, J. Vac. Sci. Technol. B 6 (1988) 727.

PAPER IV: EFFECTS OF DIFFUSION ON EPITAXIAL THIN FILM GROWTH

EFFECTS OF DIFFUSION ON EPITAXIAL THIN FILM GROWTH

D. K. Flynn-Sanders, P. A. Thiel and J. W. Evans

Departments of Chemistry and Physics and Ames Laboratory - US DOE
Iowa State University
Ames, IA 50011

ABSTRACT

We investigate the growth of Pt and Pd films on Pd(100), using a conventional LEED apparatus. Distinct oscillations in the central-spike intensities are observed, even at 80 K where thermally-activated surface diffusion is negligibly slow. We have shown previously that low-temperature oscillations result from the requirement of a fourfold-hollow adsorption site. The experimental data suggest that surface diffusion switches on at ca. 150 K for Pt and ca. 170 K for Pd. We extend our fourfold-hollow site, random deposition model to the temperature range where diffusion begins. We present an analysis of the master equations which incorporate diffusion and the appropriate adsorption site requirement. The model predicts that, typically, growth becomes more layer-by-layer like with the onset of diffusion, mimicking the experimental data for Pt and Pd on Pd(100). The role of diffusion is complex, since lateral (intralayer) diffusion leads to two-dimensional clustering, which creates more adsorption sites and can diminish layer-by-layer growth. Downward, or interlayer diffusion has a clustering component as well, but generally enhances the layer-by-layer quality of the growth. We develop a novel representation of the layer-coverage distribution, from which the deviation from perfect layer-by-layer growth and the onset of diffusion are quite evident. Lastly, we consider the issue of "transient mobility" and show that it is not necessary to invoke such an assumption to describe low-temperature growth.

I. INTRODUCTION

Thin metal films have a pervasive presence in today's technology: from printed circuit boards to potato chip bags, bimetallic catalysts to biomedical devices. In all these applications, continuous, uniform films are desired. Although the physical parameters which must be controlled to achieve technical grade films in these cases are known (e.g., flux, temperature), the underlying principles governing the physical processes during thin film growth are still debated (1,2).

Understanding the growth mode is of primal importance in any epitaxial system. Thermodynamic criteria based on surface/interface free energy relations have been established for the equilibrium growth modes: Frank-van der Merwe (layer-by-layer), Volmer-Weber (island) or Stranski-Krastanov (layer then island) (3-5). For the production of thin, atomically smooth films, Frank-van der Merwe growth is the preferable mode. Here, the surface free energy of the growing film and the interface must be less than or equal to that of the substrate. To maintain this mode throughout growth, this condition must be fulfilled as each layer completes. Thus, Frank-van der Merwe is necessarily the equilibrium growth mode for homoepitaxial systems (6). For heteroepitaxial systems, Frank-van der Merwe growth can only occur when the overlayer and substrate have very similar surface free energies and the free energy of the interface is negligible.

During thin film deposition, however, growth often proceeds under nonequilibrium conditions. Oftentimes, the actual growth *mechanism* is governed by kinetic limitations or local defects; thermodynamic

equilibrium is not achieved. For example, in systems that exhibit equilibrium Frank-van der Merwe growth, low surface mobility may trap atoms in upper layers before lower layers are completed, resulting in a rapid divergence of the interface width. Clearly, the extent of diffusion plays a key role in determining the final structure of the deposited film in this example.

Diffraction techniques, such as reflection high-energy electron diffraction (RHEED) (7-9), low-energy electron diffraction (LEED) (10,11) and thermal-energy atom scattering (TEAS) (12,13) have been used to study the epitaxial growth of metal films, since they are all sensitive to the "smoothness" of the growing film. These techniques rely on the oscillatory nature of the diffracted intensity with increasing coverage, which is intimately related to the changing morphology during growth. Often, experiments are performed at elevated temperatures, presumably because kinetic barriers to surface diffusion are sufficiently surmountable and growth can proceed in a layer-by-layer fashion (8). However, oscillations have recently been observed for metal on metal systems at low temperatures (1,11,14) where diffusive processes are seemingly negligible. Thus, the extent that the existence of oscillations is a measure of layer-by-layer growth and the role of surface diffusion in determining the quality of growth are not yet clarified.

In this paper, we consider two systems that display (equilibrium) Frank-van der Merwe growth, under *nonequilibrium* conditions. In particular, we examine Pd/Pd(100) and the initial growth of Pt/Pd(100).

We explore, experimentally and theoretically, the effects of diffusion on growth, and the extent to which lack of diffusion alters the growth mechanism at low temperature. We present a detailed account of a general model for epitaxial fcc(100) growth, schematically described in previous publications (11,15). Experimental LEED results for Pd/Pd(100) (16) and Pt/Pd(100) (10,11) are presented and discussed in sections II and III. A discussion of the onset of diffusion is given in section IV. The growth model, analysis of the rate equations, and associated resuilts are described in section VI. We continue in section V by describing a novel representation of the relationships between the layer coverages, diffracted intensity and onset of diffusion for the initial stages of growth. Lastly, we consider the issue of "transient mobility", a term used to describe surface diffusion which may result from the inability of a deposited atom to instantaneously dissipate its adsorption energy (1,17).

II. EXPERIMENTAL DETAILS

Experiments are performed in a stainless-steel, ultrahigh-vacuum chamber equipped with an evaporator and shutter, standard four-grid LEED optics, Auger spectrometer, mass spectrometer and ion gun. The base pressure is ca. 6×10^{-11} Torr. LEED spot profiles are measured at normal-incidence, with a computer-interfaced, silicon-intensified target video camera (18).

The Pd sample is grown, cut and polished at the Ames Laboratory, and is oriented to within ±0.5 ° of the (100) face. The sample is mounted on a liquid-nitrogen coolable coldfinger (19). The temperature is measured with a W-5%/Re/W-26%/Re thermocouple (spotwelded to the back of the crystal) and controlled via a feedback circuit (20). Sulphur and phosphorous are removed by cycles of ion-bombardment and annealing, followed by cleaning in oxygen to remove carbon.

The evaporator is home-built, based on the design of DeCooman and Vook (21). A small length Pt or Pd wire is wrapped around a 1 mm gap in a tungsten holder. The holder is mounted on a high current feedthrough, which is surrounded by a liquid-nitrogen-cooled shroud. During deposition, the sample is situated ca. 72 mm from the evaporator source. The maximum pressure rise by the end of a 10 second dose is to 6×10^{-10} Torr for Pt; and ca. 2.5×10^{-10} Torr for Pd. The evaporation rate is ca. 0.014 monolayer (ML)/s for Pt, and ca. 0.007 ML/s for Pd.

To dose the sample, the Pd(100) face is placed in front of the evaporator, with the shutter up. Following a 10 s, full-current outgassing period, the shutter is rotated down. Metal (Pt or Pd) is

deposited in a 10 s increment at normal-incidence. The sample is then turned toward the LEED optics and (single-pixel width) spot profiles are taken. The sample is held at constant temperature during the evaporation, but heating current is chopped to remove current-induced distortions during LEED data acquisition. Repeating the dose and LEED measurements, profiles are acquired as a function of cumulative evaporation time. The entire experiment is repeated at various temperatures. In an alternative experiment, a given coverage of metal is deposited at ca. 90 K. The sample is then annealed to successively higher temperatures for 1 minute each. Between each anneal, the sample is quenched to low temperature and LEED spot profiles are acquired. This gives temperature-dependence of the profiles at constant coverage. Results of both types of experiment are discussed.

For LEED profiles, a constant background, set equal to the minimum value of each profile, is subtracted. The profiles are not compensated for "grid structure" from the LEED optics, and they are not smoothed. Intensities are then measured as the height of the central-spike component of each profile, as depicted in Figure 1a.

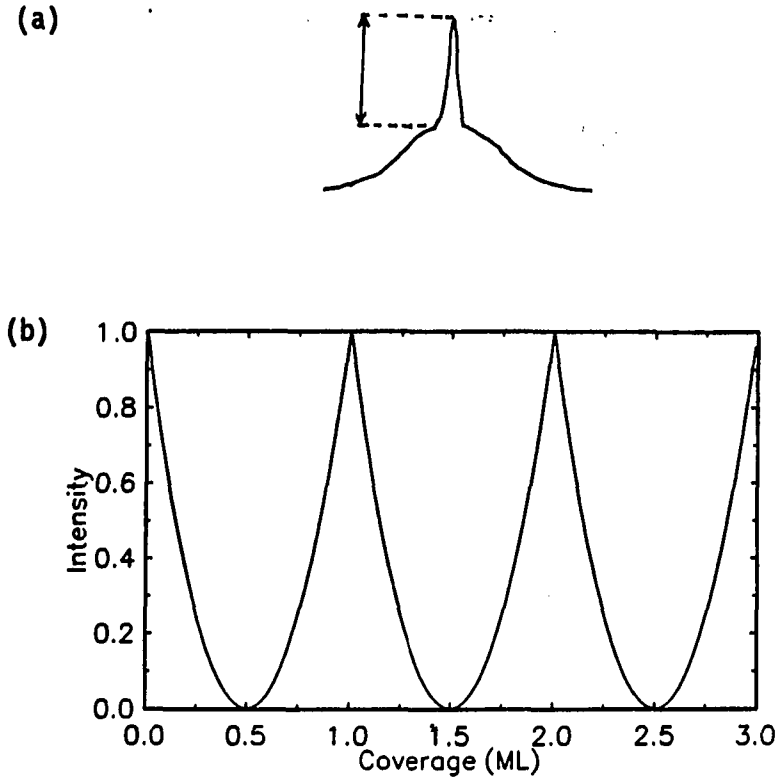

Figure 1. Idealized intensity oscillations

(a) Depiction of central-spike height measurement from a profile.

(b) Idealized intensity oscillations as a function of coverage for perfect layer-by-layer growth.

III. EXPERIMENTAL RESULTS AND DISCUSSION

In this section, we summarize LEED results previously published for the epitaxial growth of Pt on Pd(100) (10,11) and present new results for Pd/Pd(100) (16).

A. LEED Results

As growth proceeds in a layer-by-layer fashion, the diffracted intensity oscillations reflect the successive filling of layers. The intensity is monitored at an energy where scattering from adjacent layers interferes destructively. At this energy, denoted as the out-of-phase energy (22), the intensity is maximized at full-layer coverages and minimized at half-layer coverages. Figure 1b shows the idealized behavior of the diffracted intensity as a function of coverage for perfect layer-by-layer growth. The curve shown is calculated within the kinematic approximation, according to $I \propto |2\theta-1|^2$, where θ is the fractional coverage of the growing layer (23,24).

The central-spike intensity as a function of cumulative evaporation time (proportional to coverage) is shown in Figures 2a and 3a for Pt and Pd deposition, respectively, on Pd(100) at various substrate temperatures. (1,-1) and (-1,-1) profiles are measured at 145 eV for Pt, and at 147 eV for Pd, energies corresponding to experimental out-of-phase conditions (10,11,16). Although the equilibrium growth mode for both metals on Pd(100) is layer-by-layer, the behavior of the central-spike intensity seems far from that depicted in Figure 1b. In neither case are

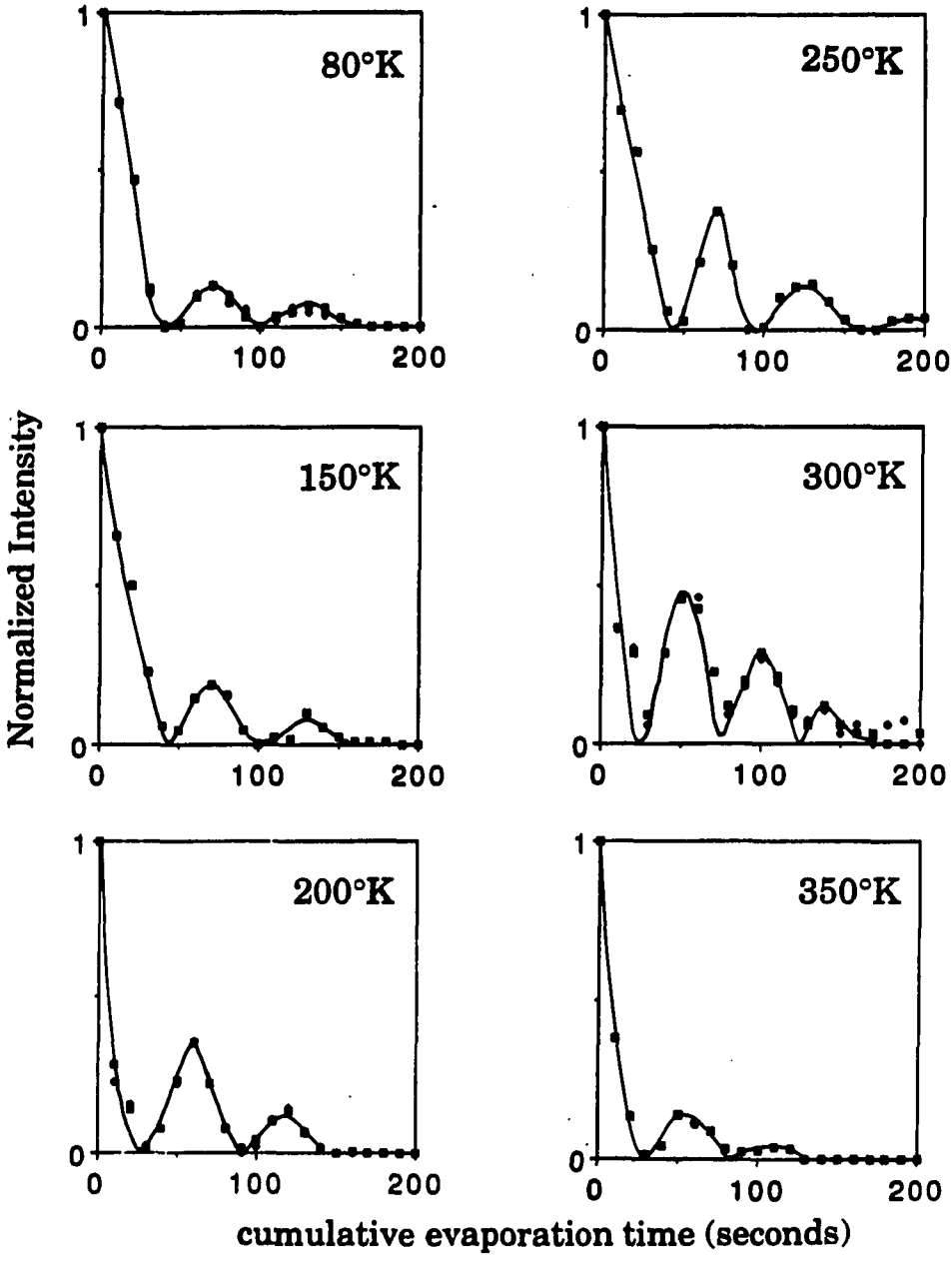

Figure 2. Pt/Pd intensity oscillations

(a) Normalized central-spike intensity of Pt/Pd(100) as a function of cumulative evaporation time, t, at various temperatures. The beam energy is 145 eV. Curves between data points are drawn in to guide the eye.

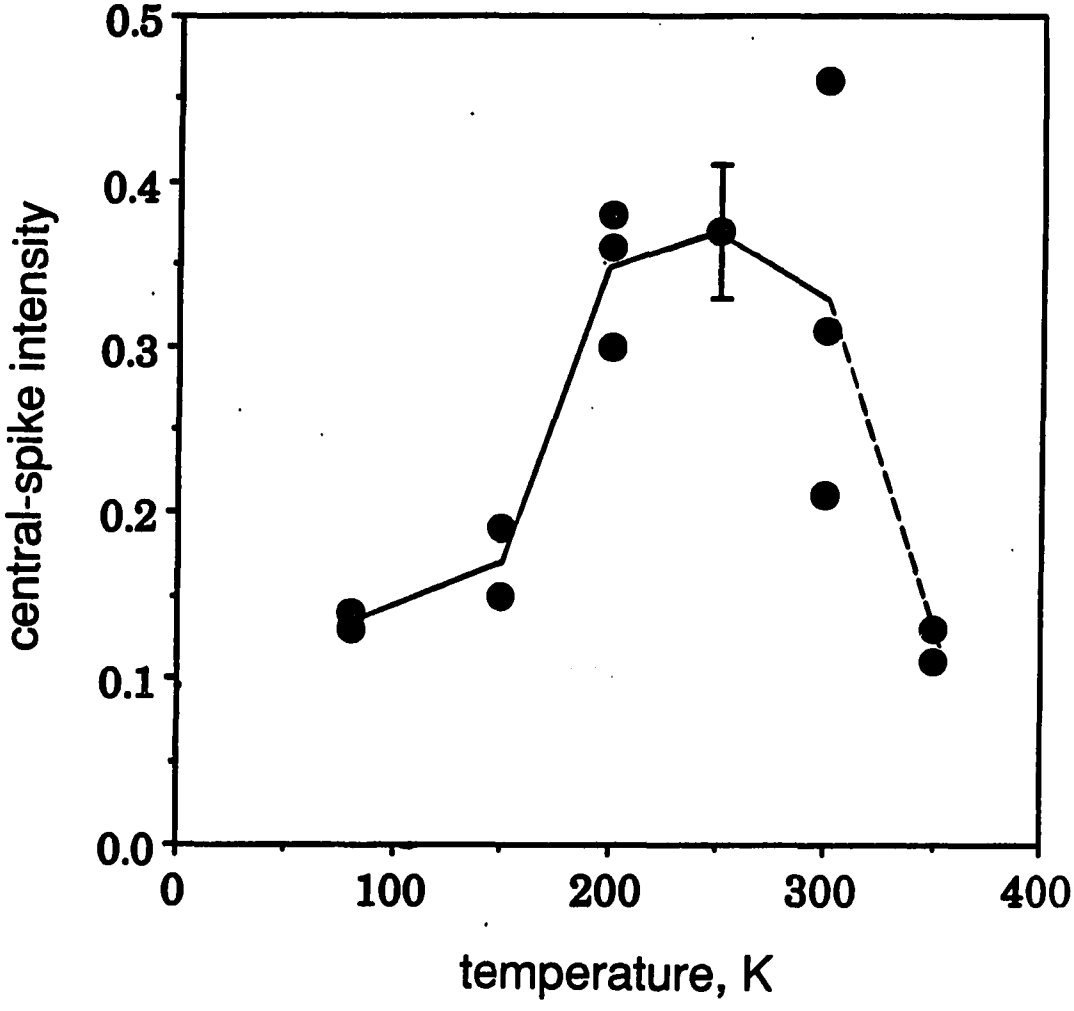

Figure 2. (continued)

(b) Normalized intensity at the first-maximum for Pt/Pd(100) as a function of substrate temperature. Straight lines, connecting the average intensity value at each coverage, are drawn in for clarity.

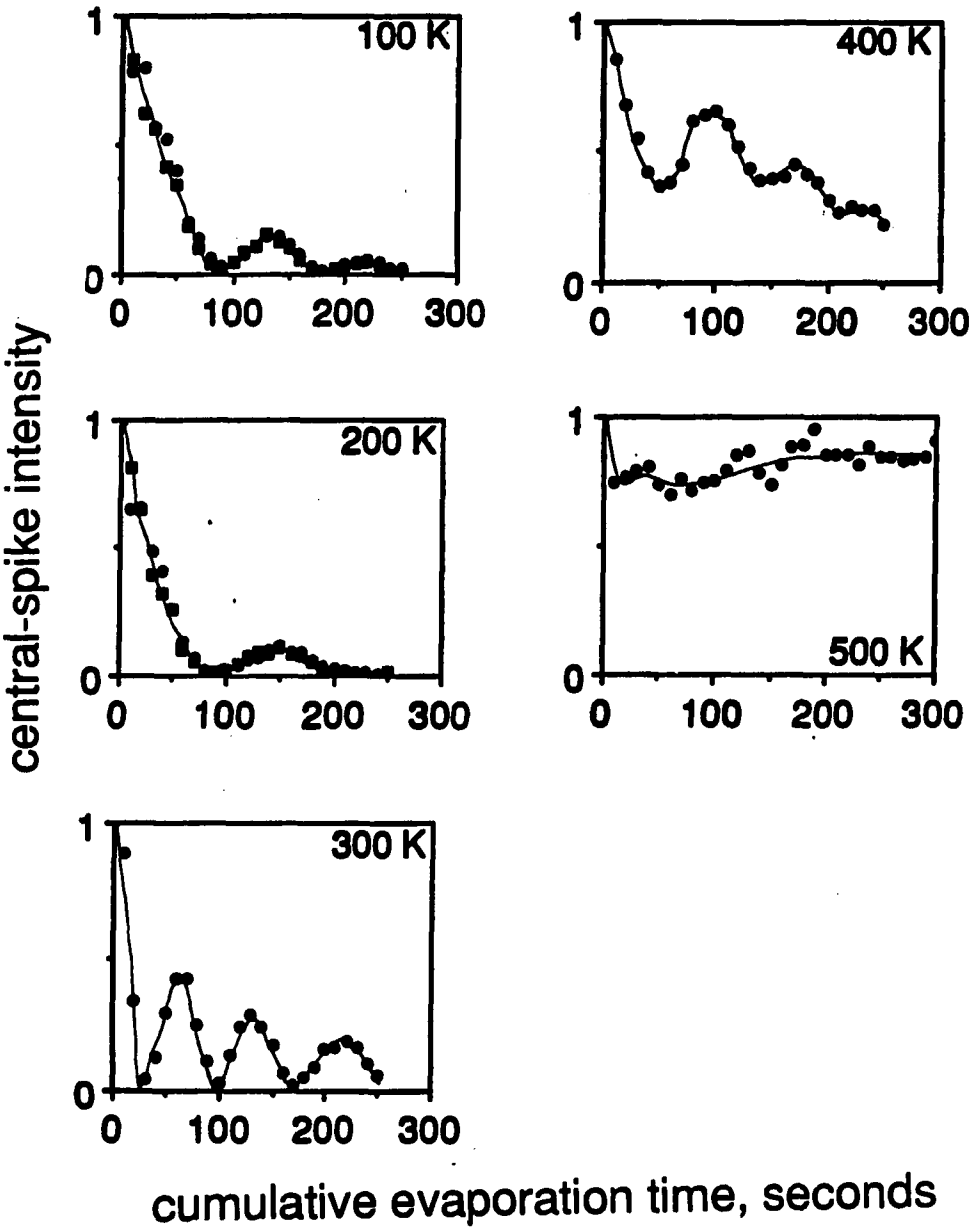

Figure 3. Pd/Pd intensity oscillations

(a) Normalized central-spike intensity of Pd/Pd(100) as a function of cumulative evaporation time, t, for various temperatures. The beam energy is 145 eV. Curves between data points are drawn in to guide the eye.

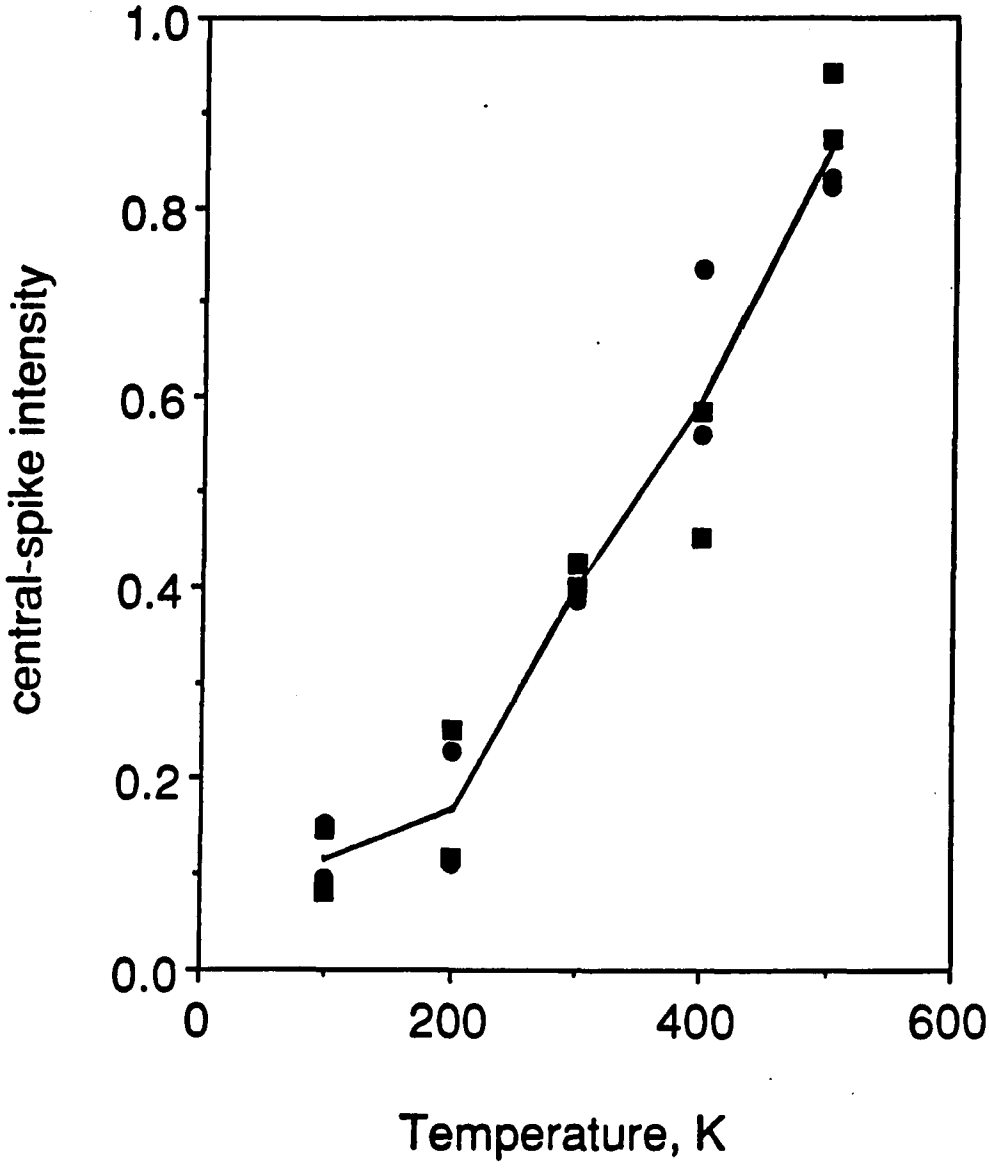

Figure 3. (continued)

(b) Normalized central-spike intensity at the first-maximum for Pd/Pd(100) as a function of substrate temperature. Straight lines, connecting the average intensity value at each coverage, are drawn in for clarity.

persistent, high-amplitude oscillations observed; rather damped oscillations, if any, occur. For Pt/Pd(100) the number and amplitude of oscillations is peaked at ca. 250 K. Above this temperature, further damping occurs, although the general shape of the curve is preserved throughout the temperature range studied. For Pd/Pd(100), oscillations are evident up to ca. 400 K, but a slow change in the shape of the curve begins above ca. 300 K. At 500 K, periodic behavior of the central-spike intensity is no longer apparent.

A composite view of the temperature-dependence of initial growth is presented in Figures 2b and 3b. Here, central-spike intensity at the first-maximum of the oscillation curve is plotted as a function of temperature. Since no oscillations are observed at 500 K for Pd/Pd, the intensity shown is measured at the average cumulative evaporation time required to reach the first-maximum in the lower-temperature data. The initial temperature-dependence of the diffracted intensity is the same for both systems - a low temperature plateau followed by a rapid rise beginning at ca. 150 K for Pt, ca. 200 K for Pd. The high temperature behavior for the two systems is quite different. For Pd, the intensity nearly regains its full initial value, whereas a plateau between 200 to 300 K is followed by a rapid decrease for Pt.

This same temperature-dependence is demonstrated by the annealing experiments. Results are shown in Figures 4 and 5 for Pt and Pd overlayers, respectively. Little temperature-dependence is observed at low temperatures. A clear increase in the central-spike intensity begins at ca. 150 K for Pt, ca. 200 K for Pd.

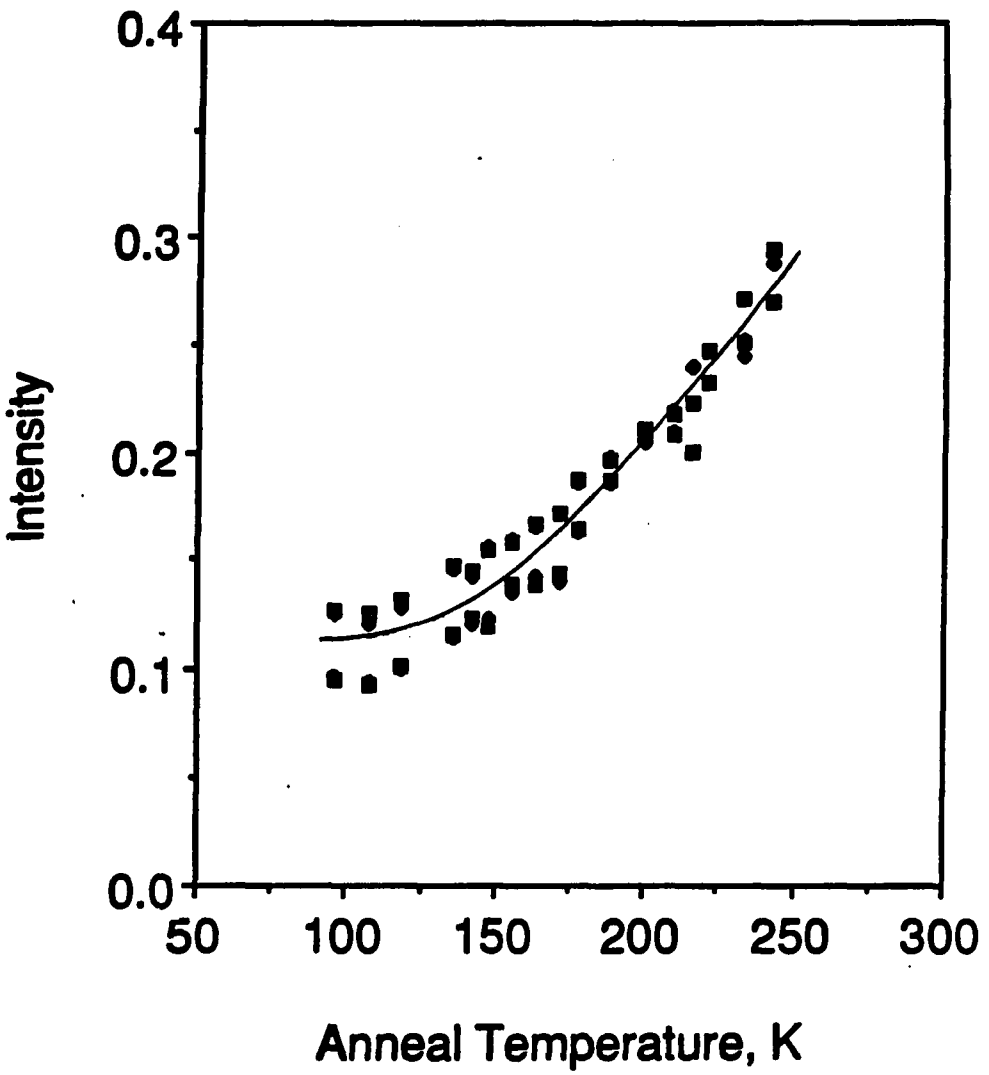

Figure 4. Pt/Pd anneals

Normalized central-spike intensity for ca. 1 ML Pt deposited on Pd(100) at ca. 90 K, and heated to successively higher temperatures. The (1,-1) and (-1,-1) beams at 145 eV are shown. A smooth line between average values is drawn to guide the eye. Note the limited temperature range here. High temperatures were avoided to deter dissolution of the Pt overlayer.

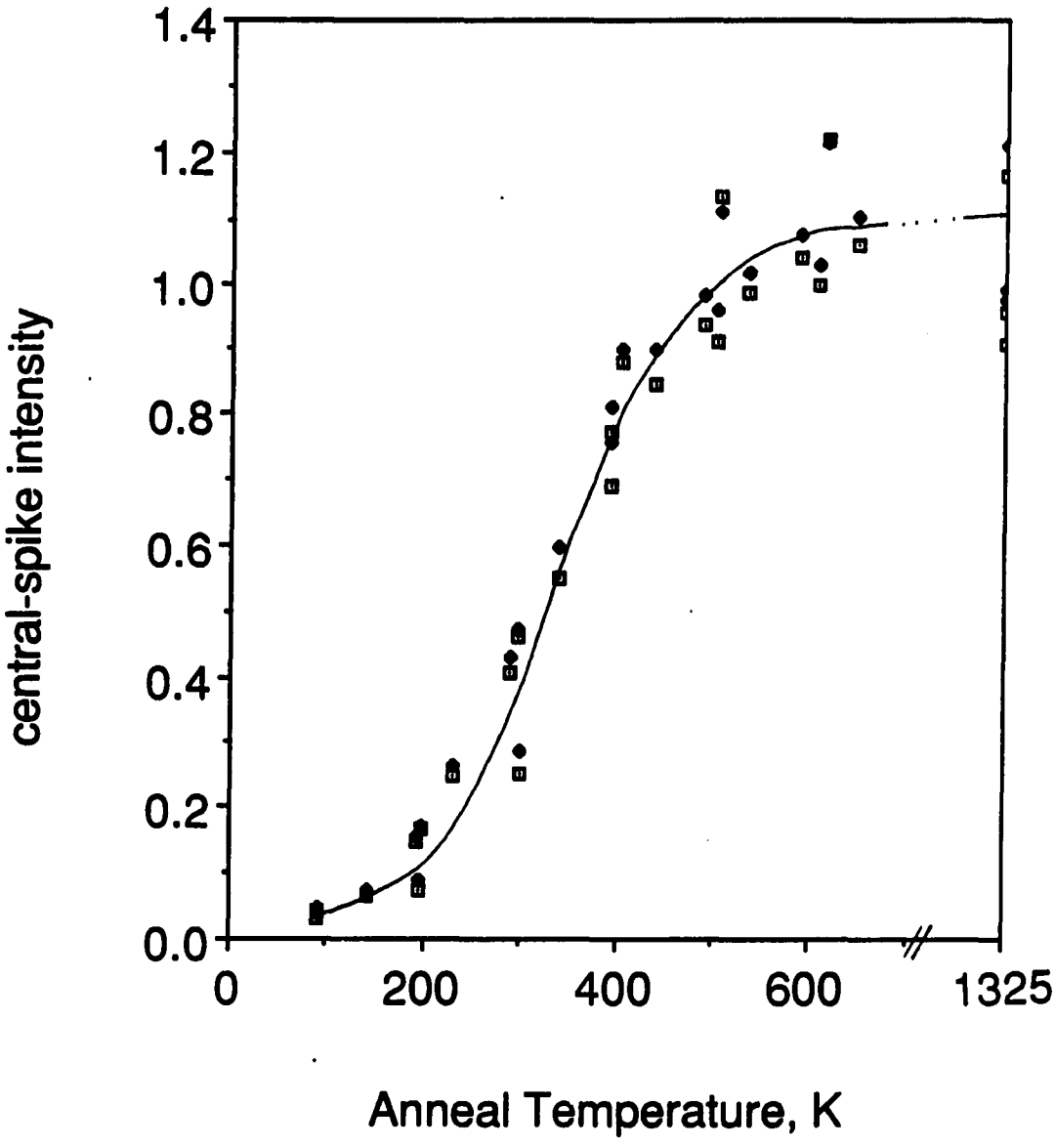

Figure 5. Pd/Pd anneals

Normalized central-spike intensity for ca. 1 ML Pd deposited on Pd(100) at ca. 90 K, and heated to successively higher temperatures. The (1,-1) and (-1,-1) beams at 145 eV are shown. Note the expanded temperature range. A smooth line between the average values is drawn in to guide the eye.

B. Discussion

The initial plateau and subsequent rise of the central-spike intensity indicates thermally-activated diffusion begins to play a key role in the growth process at a transition temperature. At sufficiently low temperatures, deposited atoms are not able to surmount the activation barrier to diffusion, so the growth process and resulting film structure are temperature-independent. However, the distinct oscillations observed in this diffusionless regime reflect some layer-by-layer character of initial film growth even *in the absence of surface diffusion*. This assertion may seem surprising since a diffusional mechanism is typically associated with layer-by-layer growth (8). We previously reported that intensity oscillations are predicted from random deposition in the diffusionless regime, when adsorption is restricted to fourfold-hollow adsorption sites (11,15,25). For epitaxial growth of Pd(100), fourfold-sites are the physically-required adsorption sites. Our fourfold-site random deposition model predicts an intensity value of 0.09 for the first oscillation maximum in the diffusionless regime, in reasonable agreement with experiment.

Deviations from perfect layer-by-layer growth are not as high as one would expect from the low intensity amplitudes of Figures 2 and 3. Within the kinematic approximation, intensity at the out-of-phase condition is calculated as

$$I = (N_0 - N_1 + N_2 - N_3 + \ldots)^2 \left(\sum_i N_i\right)^{-2}, \qquad (1)$$

where N_i is the effective number of atoms exposed in layer i, and i=0 corresponds to the topmost substrate layer. If one assumes an equal penetration depth of the normally-incident beam at all exposed layers, then each atom blocks scattering from a net of one atom in the layer below. N_i is then calculated as the difference in coverages between layer i and i+1. We now compare the intensities predicted from a perfectly-filled and imperfectly-filled layer (at equal total coverage), as depicted in Figures 6a and 6b. For simplicity, we depict atop rather than fourfold-hollow site filling, but any configuration will give the same result with the above assumption. We calculate the fractional intensity for Figure 6b according to equation (1):

$$\frac{I^{imp}}{I^{per}} = \frac{\left(N_0^{imp} - N_1^{imp} + N_2^{imp}\right)^2}{\left(N_0^{imp} + N_1^{imp} + N_2^{imp}\right)^2} = \frac{\left(2N_2^{imp} - N_1^{imp}\right)^2}{\left(2N_2^{imp} + N_1^{imp}\right)^2} \qquad (2)$$

since $N_0 = N_2$ and $I^{per} = 1$. (The superscript "per" stands for perfect; "imp" stands for imperfect.) Rearranging,

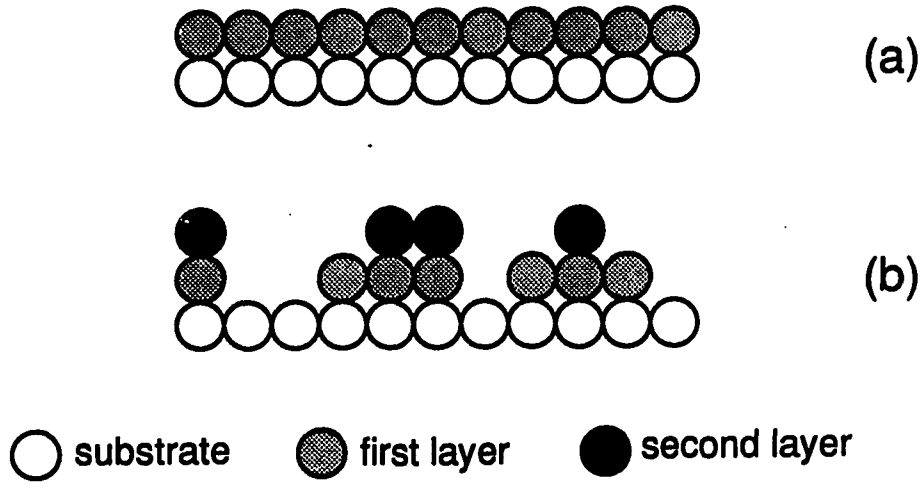

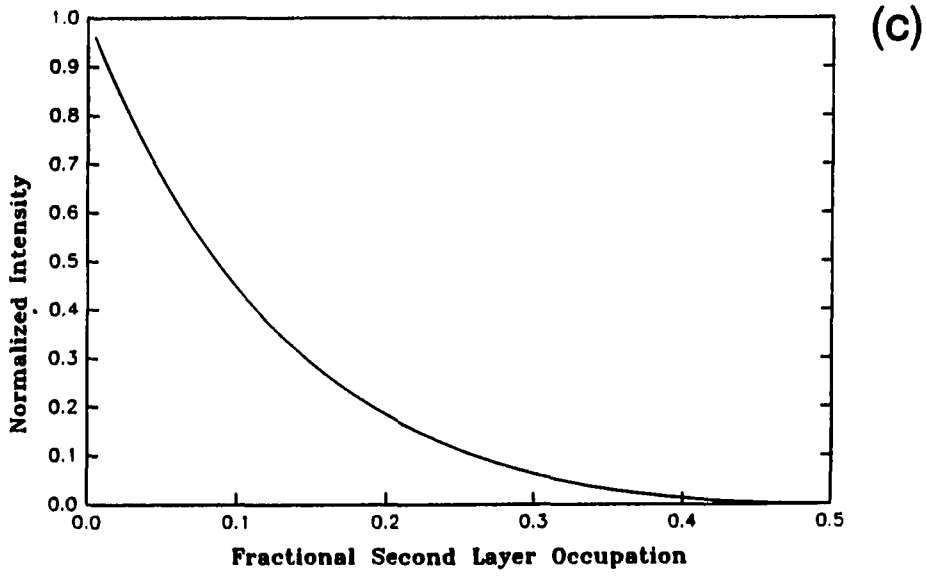

Figure 6. Central-spike intensity for imperfect growth

(a) Perfectly filled layer, θ=1 ML.

(b) "Imperfect layer", θ=1 ML. Adatoms fill second layer before first layer is complete.

(c) Intensity as a function of fractional second layer coverage (θ_2/θ_1, θ = 1 ML), according to equation (3).

$$\frac{I^{imp}}{I^{per}} = \left(1 - \frac{1}{x + \frac{1}{2}}\right)^2 \qquad (3)$$

where $x = N_2^{imp}(1 - N_2^{imp})^{-1}$. We plot the intensity ratio as a function of fractional second layer coverage in Figure 6c. It is evident that small deviations from perfect layer-by-layer growth severely affect the central-spike intensity. Based on this model we estimate second layer coverages at the first oscillation maximum to be at most ca. 25 % in the diffusionless regime, and even less than this at higher temperatures. Thus the damped oscillations in Figures 2a and 3a indicate a fair degree of layer-by-layer quality at the lowest substrate temperatures.

Absolutely matching the intensity is not the primary goal of this study, since experiments have shown that normalized intensities at the first maximum from beams of different out-of-phase energies or beams of different symmetry vary, sometimes as much as 40 % (16). We are more interested in predicting the trends in the intensity as a function of temperature and understanding the influence of diffusion on the intensity and associated film structure.

It is expected that increased surface mobility will enhance the quality of the growing film. We associate the experimentally-observed intensity increase at ca. 150 and 200 K for Pt and Pd on Pd(100) with the onset of adatom diffusion. Assuming a prefactor of ca. 10^{13} s^{-1}, this implies an activation barrier to surface diffusion of ca. 10 kcal/mol for Pt and ca. 13 kcal/mol for Pd, in good agreement with previously reported values for other unreconstructed fcc(100) metals: 11 kcal/mol for

Cu/Cu(100) (12), 14.6 kcal/mol for Ni/Ni(100) (26). The onset temperature also agrees well with field-ion microscopy (FIM) studies of Pd on Ta(110), where single atoms were observed to begin diffusing at 180 K (27). The effects of limited diffusion on the resulting film structure during epitaxial growth is discussed further in section IV.

The experimental, high-temperature intensity behavior for Pt and Pd differ dramatically. Whereas for Pt, the coverage-dependent oscillation amplitude peaks at ca. 250 K and decreases with increasing temperature (Figure 2a), the intensity during Pd growth loses its oscillatory nature as temperature increases above 300 K (Figure 3a). By 500 K, the intensity is nearly constant as a function of coverage. For the fixed-coverage annealing experiments on Pd, the initial central-spike intensity is nearly completely recovered with increasing temperature (Figure 5).

We attribute the experimental high-temperature plateau and subsequent decrease in I_{m1} for Pt deposition (Figure 2) to interference from overlayer reconstruction (28) and/or interlayer mixing (29), reducing the tendency to form large, ordered, (1x1) overlayer terraces. The effect on the integral-order spot intensities is evident well before superstructure spots of the Pt reconstruction are visible. The "turnaround" temperature of the Pt intensity at ca. 250 K corresponds well with the FIM study of Kellogg, in which metastable (1x1) islands of Pt on Pt(100) formed in the field were stable up to 270 K and reconstructed above this temperature (30).

The high-temperature results of Pd are attributed to surface diffusion which is essentially unlimited on the timescale of these

experiments. The relatively constant intensity at 500 K indicates the initial surface condition is approximately maintained throughout growth; i.e., all deposited atoms reach existing step edges between deposits. For growth at 400 K, remnants of oscillations are clearly visible, indicating that at this temperature, diffusion is not completely unlimited relative to the timescale of deposition.

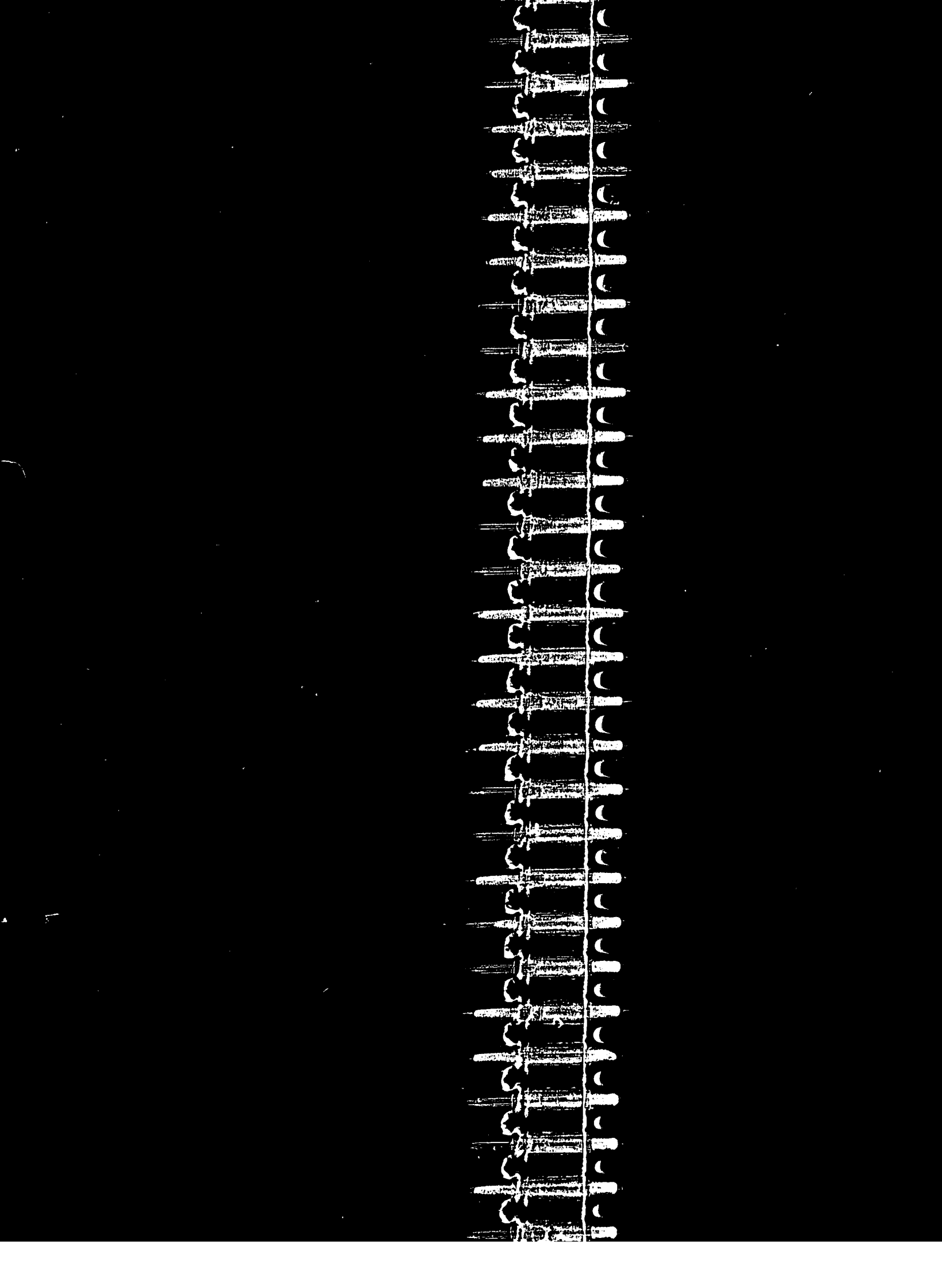

IV. EFFECTS OF SURFACE DIFFUSION IN THE ONSET REGIME

In this section, we consider effects of thermally-activated diffusion on the growth morphology. In particular, we are interested in temperatures surrounding the onset of diffusion, which our experiments show to be ca. 150-200 K for these systems.

One would first expect the onset of adatom diffusion to enhance the quality of layer-by-layer growth. Some thought reveals that the effect of limited surface diffusion is actually quite complex. Assume atoms of the growing layer occupy equilibrium positions, fourfold-hollow sites for the case of fcc(100) epitaxial growth. Layer-by-layer growth is obviously promoted by interlayer diffusion, where atoms can diffuse off terraces to incomplete layers below. There is also a small, but competing effect that reduces layer-by-layer growth. Consider an atom that just diffused off a terrace (i.e., across a step) into a lower layer. If the atom binds adjacent to this terrace at a kink-site, it may create an additional site for growth of the next (upper) layer. If the newly-created site is immediately filled, the coverage of the upper layer is sustained. The diffusing atom may even fill a "hole" in the lower layer creating *more than one* adsorption site for growth of an upper layer, leading to the possibility of a net *increase* in the coverage of the upper layer. (This process is particularly relevant at near complete-layer coverages.) Similarly, lateral diffusion leads to intralayer clustering, again creating adsorption sites for the growth of the next layer. Not surprisingly, our calculations show that the net

effect of clustering is to *reduce* the layer-by-layer quality of the growing film.

V. RATE EQUATION ANALYSIS OF A SPECIFIC MICROSCOPIC DEPOSITION MODEL

We present a microscopic model describing adsorption and diffusion processes applicable to epitaxial growth on fcc(100) surfaces in the temperature regime surrounding the onset of diffusion. We analyze the rate equations during growth in the context of this specific model.

A. The Model

The competition between random deposition and thermally-activated diffusion plays a key role in determining the quality of the growing film. Isolated atoms diffusing laterally between nearest-neighbor sites (17) can become involved in two-dimensional clustering. Additionally, diffusion *between* layers (across island edges at steps) also has an important influence on the resultant film structure. We consider a simple, microscopic deposition model for epitaxial fcc(100) growth, incorporating the essential features of both the adsorption site geometry and diffusion dynamics. We assume random deposition with constant impingement rate at fourfold-hollow sites, on a perfect fcc(100) substrate. Lateral and interlayer single-atom diffusion are explicitly represented in our model. Cluster mobility and rearrangement is neglected.

Specifically, we assume that lateral diffusion of isolated atoms between nearest-neighbor sites in the same layer occurs with rate h, and interlayer diffusion through bridge sites at island edges to lower layers occurs with rate g (see Figure 7). If there is more than one

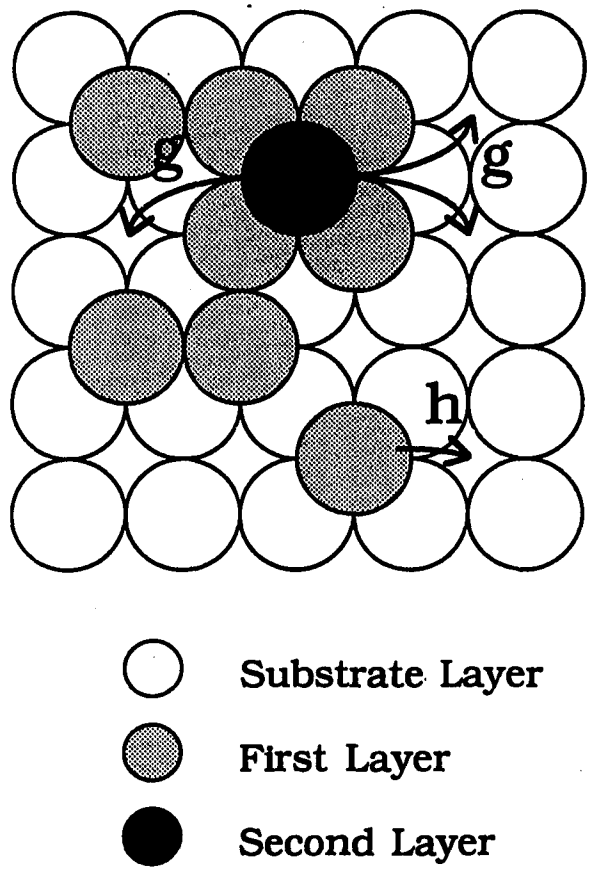

Figure 7. Illustration of types of diffusion used in modelling the data

g: rate of interlayer diffusion

h: rate of lateral (intralayer) diffusion

symmetrically-equivalent, fourfold-hollow site available in the lowest terrace into which an atom can diffuse, one is chosen at random. We neglect diffusion from lower to higher layers in this model since all atoms reaching a step "up" are assumed to attach irreversibly to the island edge.

Since the activation barrier for detachment of atoms from clusters should be higher than for diffusion of isolated atoms, cluster breakup should be negligible at temperatures near the onset of diffusion. Cluster mobility and rearrangement are also forbidden in our model. FIM studies by Schwoebel and Kellogg (27) show Pd clusters on Ta(110) migrate as a single unit between 250 and 325 K, temperatures above those we are interested in. However, unstable island configurations were observed to rearrange as low as 190 K on this surface, a temperature above which single atoms were observed to diffuse (180 K). Our model should provide an adequate account of the microscopic processes operating during epitaxial growth at temperatures up to and just above the onset of diffusion, but the Pd/Ta study demonstrates that our assumptions are certainly inadequate at higher temperatures.

B. Comparison to Existing Models

In existing growth models, rate equations for the layer coverages or cluster densities are developed in terms of the deposition and diffusion rates, but the details of the adsorption site are assumed unimportant (31-33). At low temperatures (temperatures at which surface diffusion is inoperative) these models predict no oscillations in the diffracted

intensity (31). Ignoring the details of the adsorption site is strictly valid only in the case of atop adsorption, which stipulates simple-cubic growth.

In earlier publications, we demonstrated the necessity of incorporating the adsorption site geometry into the growth model (when adsorption is *not* limited to the atop site) for correct predictions of low-temperature, diffusionless intensity behavior (11,18,25,34). It is clear that for adsorption at atop sites, there is essentially no site "requirement", i.e., every deposited atom can serve as the starting point for the next layer. However, as soon as a more complicated adsorption site is specified, severe restraints are placed on initiation of upper layers. For example, adsorption onto bridge sites requires a pair of atoms in a lower layer *before* the next layer can fill, threefold-hollow adsorption sites requires a triangle of atoms, fourfold-hollow sites requires a square arrangement of four atoms, etc. (34). The necessity of *creating the adsorption site* in the lower layer before initiating an upper severely limits the growth of upper layers. This imposes an inherent layer-by-layer quality to the growing film *even in the absence of diffusion*. Our model explains the experimentally observed oscillations for fcc(100) growth at low temperatures (1,11,14,35), which are not predicted by the phenomenological models.

The failure of the atop, diffusionless model to correctly predict experimental observations of quasi-layer-by-layer growth on fcc(100) metals in the diffusionless temperature regime encourages us to extend our master equation analysis for random adsorption at fourfold-hollow

sites into the realm of operative diffusion. We start from a hierarchial form of the exact master equations for a microscopic model which incorporates the adsorption site geometry as well as the desired diffusional processes. Exact solution of such equations is not possible. However, approximations explicitly treating short-range spatial correlations may be invoked. The short-range correlations directly result from the specification of the adsorption site geometry and are particularly important even in the diffusionless, low-temperature regime.

Besides giving correct low-temperature predictions, an advantage of our model over the phenomenological models is that we need not make assumptions about island size, shape or distribution to calculate diffusional (stepping) probabilities. For example, islands are assumed to grow via incorporation of diffusing adatoms at a rate proportional to the island circumference in reference (33), which implies circular islands; or interlayer diffusional rates are assumed to be proportional to the product of available space in the lower layer and uncovered space in the upper layer in reference (31), which implies atoms anywhere on a terrace have an equal probability of stepping down (even if they are not at an island edge). Despite these shortcomings, these models work fairly well at intermediate and higher temperatures, the regime at which our model is invalid. We feel our model fills a unique niche in the description of growth in the critical regime surrounding the onset of diffusion.

C. Rate Equation Analysis

Our analysis is based on rate equations corresponding to the hierarchial form of the exact master equations for the model described in subsection A. A direct result of specifying an adsorption site geometry comprised of more than one atom is positive spatial correlations, which induce short-range order. We adapt dynamic versions of cluster approximations to treat short-range order, and appraise the reliability of these approximations by comparing different levels of approximation with each other, with Monte Carlo simulations and with experiment.

In this model, rate equations for the probability of a filled site (θ_j), a filled nearest neighbor (NN) pair (θ_{jj}), etc., in layer j, etc., are:

$$\frac{\partial}{\partial t}\theta_j = dP_{\bar{j}} + g[G_{j,j+1} + G_{j,j+2} + \ldots - L_j] \tag{4}$$

$$\frac{\partial}{\partial t}\theta_{jj} = 2dP_{j\bar{j}} + g[\tilde{G}_{j,j+1} + \tilde{G}_{j,j+2} + \ldots] + hH_j \tag{5}$$

The parameter d represents the deposition rate. $P_{\bar{j}}$ denotes the probability of a fourfold-hollow adsorption site in layer j (composed of a square arrangement of four atoms in layer j-1). $P_{j\bar{j}}$ denotes the probability of a layer j atom adjacent an empty fourfold-hollow site. The first term in equation 4 (5) represents the probability of creating filled sites (NN pairs) by direct deposition into empty sites (filled-empty pairs). The second term in equation 4 (5) describes the creation and depletion of filled sites (NN pairs) via interlayer diffusion.

Proceeding with rate g, $G_{j,k}$ ($\tilde{G}_{j,k}$) describes the creation of filled sites (NN pairs) in layer j by interlayer diffusion from above, i.e., downward diffusion from layers k>j. The loss of a j^{th}-layer-atom by diffusion downward to "lower" layers is described by L_j, where

$$L_j = \sum_{k=j}^{j-1} G_{k,j}. \tag{6}$$

Note there is no loss term associated with the downward diffusion of NN pairs from layer j, since all clusters are assumed to be "frozen". NN pairs may also be formed by the lateral diffusion of isolated atoms. Once a site next to a filled site is reached, we assume a cluster is irreversibly formed. The intralayer diffusion rate is represented by h, and the probability of pair formation within layer j by H_j.

Next we invoke constraints to ensure that a filled site in layer j implies the four supporting sites are filled in layer j-1, etc. These restrictions are absent in the traditional cluster approximations (36). The lowest-order, single-site approximation (in which all configurations are completely factorized in terms of their constituent atoms) is inappropriate here since all interlayer spatial correlations are neglected. Thus, we consider only higher-order approximations, in particular, the pair- and square-approximations. In the pair-approximation, all configurational probabilities are factorized in terms of NN pair-probabilities, which provide a closed set of equations for $d\theta_j/dt$ and $d\theta_{jj}/dt$ (37). Modifying the standard pair-factorization

slightly, we more accurately account for multilayer, geometric constraints. This modification is explained in the Appendix.

We also utilize the more sophisticated square-approximation, which explicitly treats the statistics of a square configuration of four sites (38). We retain equations for the probability of a filled site, NN pair, diagonal NN pair, bent triple, and square arrangement for each layer in which the approximation is applied, and factorize probabilities of more complex configurations in these terms. Again, slight modification is necessary to account for geometric constraints (see Appendix). Note that for the epitaxial growth of a fcc(100) face, it is especially important to adequately describe the statistics of a square arrangement since it constitutes the adsorption site. Thus, this level of approximation is particularly appropriate for epitaxial growth on Pd(100).

D. Results

Consider first the low-temperature, diffusionless regime. Both the pair and square-approximation effectively reproduce previous exact results for the first four layer-coverages and diffracted intensity (up to three monolayers) (34). In Figure 8, square-approximation results for the first dozen layer-coverages in the fourfold-hollow, random-deposition model are contrasted with results for the atop model. The much narrower width of the growth front (number of incomplete layers) for the fourfold-hollow model relative to the atop model, demonstrates the enhanced layer-by-layer tendency in this model, *even in the absence of diffusion.*

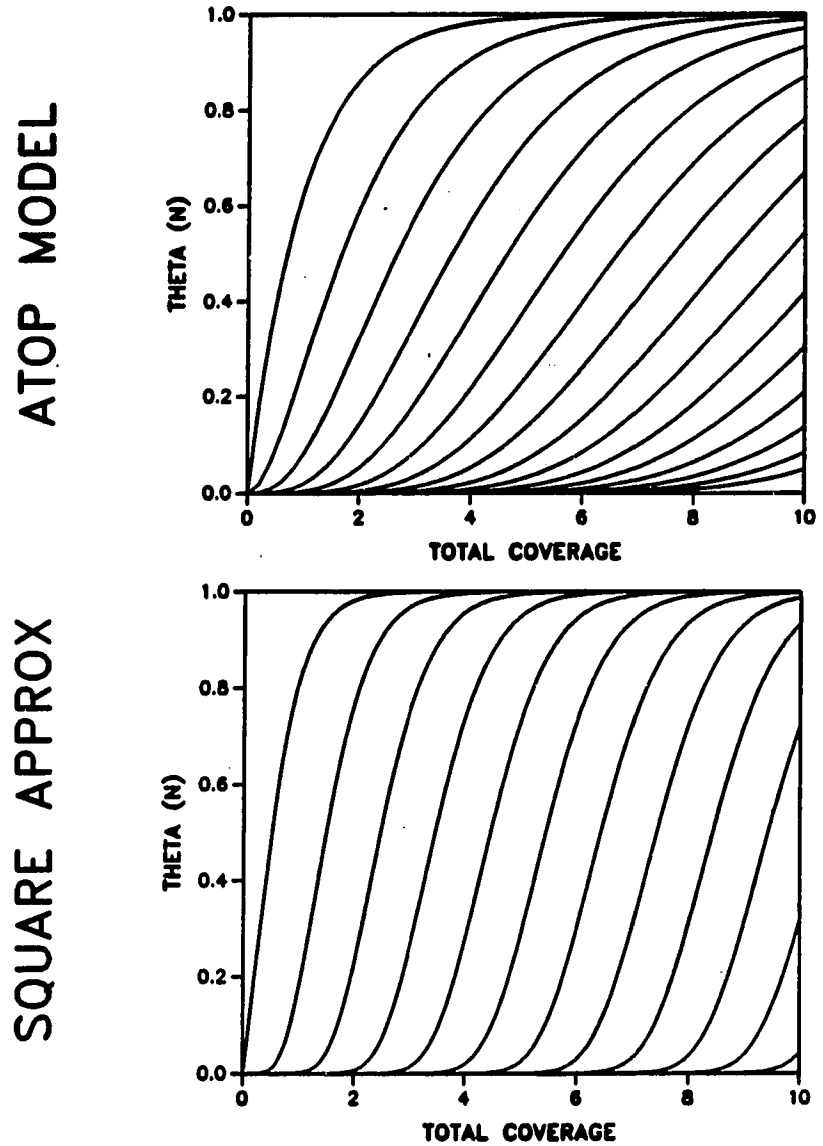

Figure 8. Layer-coverage curves calculated from the rate equations with no diffusion

Each solid curve represents the coverage of a given layer. The number of solid curves intersecting any given vertical line (defining a total coverage) yields the total number of growing layers at that coverage. The incomplete layers make up the "growth front". The atop model leads to "rougher" growth (larger growth front) than the fourfold-hollow model.

Next we quantitatively illustrate the competition between lateral and interlayer diffusion during growth. Figure 9 displays the predicted behavior of the first-maximum of the central-spike intensity (I_{m1}) for varying interlayer and lateral diffusion rates. Results from both the pair- and square-approximation are shown. In the absence of lateral diffusion, I_{m1} increases with increasing interlayer diffusion, indicating an enhanced tendency toward layer-by-layer growth, as expected (curve a). Increasing lateral diffusion, in the absence of interlayer diffusion, decreases I_{m1} (curve b), demonstrating the diminished layer-by-layer quality as intralayer clustering begins to occur. When both diffusion mechanisms operate with equal rates (curve c), there is some cancellation of opposing effects, with net trend toward layer-by-layer growth.

Figure 9 also reveals consistency between the pair and square-approximations used in the derived rate equations. To check the validity of these equations we compare our results to Monte Carlo simulations of these processes, shown as filled symbols in Figure 9 (39). In general there is good agreement between the rate equation and Monte Carlo results, except at high rates in curve a. This region represents a situation where lateral diffusion is forbidden, but interlayer diffusion proceeds with very high rate. This is a physically-unreasonable scenario. The breakdown of our rate equations in this regime is of no consequence to their applicability to the physical processes operative during thin film growth near the onset of diffusion.

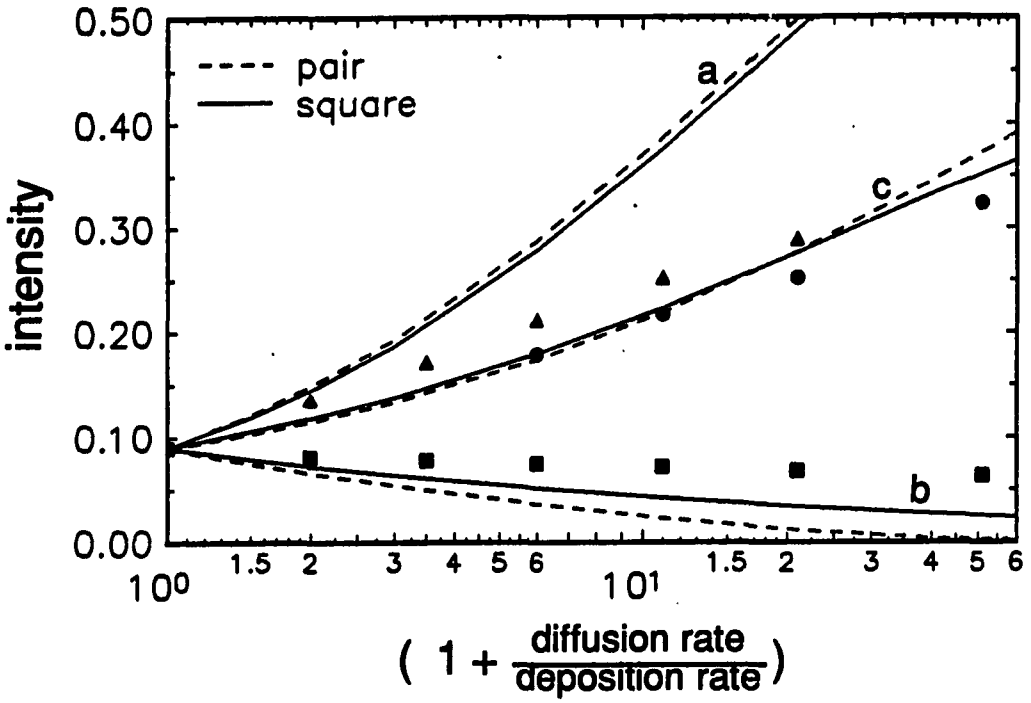

Figure 9. Competition between diffusional processes

Dependence of the first-maximum in the central-spike intensity on the diffusional processes, g (interlayer diffusion rate) and h (lateral or intralayer diffusion rate). Discrete points are Monte Carlo simulation results obtained from reference (39). ▲: curve a, h = 0; ■: curve b, g = 0; ●: curve c, h = g.

We now apply our model to describe the temperature-dependence of the experimental data for the first-maximum in the intensity oscillation curve, using the square-approximation for first-layer statistics, pair-approximation for the second layer, and neglecting higher-layer populations. We note that for random deposition at T=0, third-layer coverage is 3×10^{-4} ML (34) at the first intensity maximum. We expect third-layer occupations to decrease as temperature increases, justifying the neglect of higher layers in this calculation. We assume Arrhenius forms for the lateral and interlayer microscopic diffusion rates:

$$h = \nu_h \exp\left(-\frac{E_h}{kT}\right) \tag{7}$$

$$g = \nu_g \exp\left(-\frac{E_g}{kT}\right) \tag{8}$$

k is the Boltzmann constant and T the substrate temperature. The prefactors, ν, should be on the order of kT/h or 10^{12}-10^{13} attempts per second. Activation energies, E_h and E_g, with values of about 10 kcal/mole are required to match the experimentally observed "onset" of diffusion for Pt at about 150 K. For Pd, the experiment "onset" temperature of ca. 200 K requires activation energies of ca. 13 kcal/mol. Our rate equations show the first intensity maximum increase at the onset temperature as experimentally observed, but much more steeply, as shown in Figures 10a and b. Reducing interlayer diffusion relative to lateral

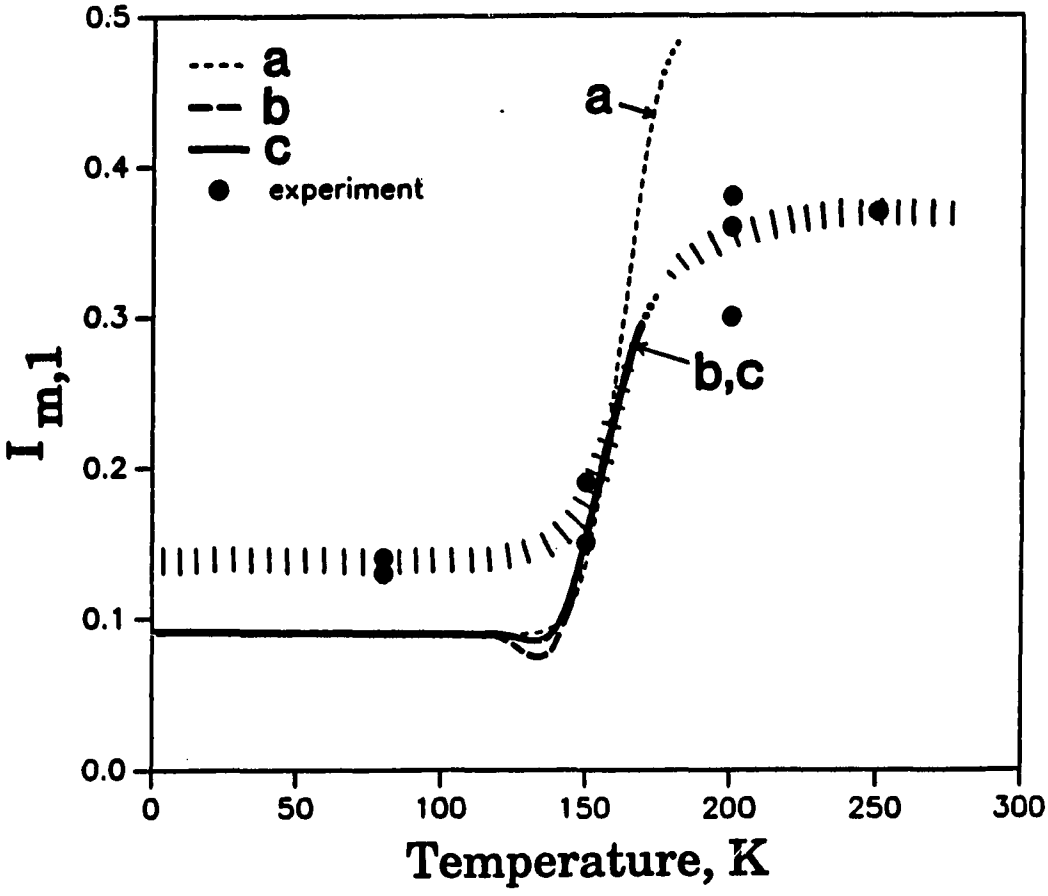

Figure 10. Temperature-dependence of first-maximum intensity (I_{m1})

(a) Pt: The data, represented by the solid circles, are from Figure 2b. The hatched line is included as a qualitative guide to the eye. Other lines represent modelling results using the following parameters: (a) $E_h=E_g=10.0$ kcal/mol, $\nu_g=\nu_h=10^{13}$ s^{-1}; (b) $E_g=9.2$ kcal/mol, $E_h=8.7$ kcal/mol, $\nu_g=\nu_h=10^{13}$ s^{-1}; (c) $E_g=E_h=9.0$ kcal/mol, $\nu_g=10^{12.5}$ s^{-1}, $\nu_h=10^{13.1}$ s^{-1}.

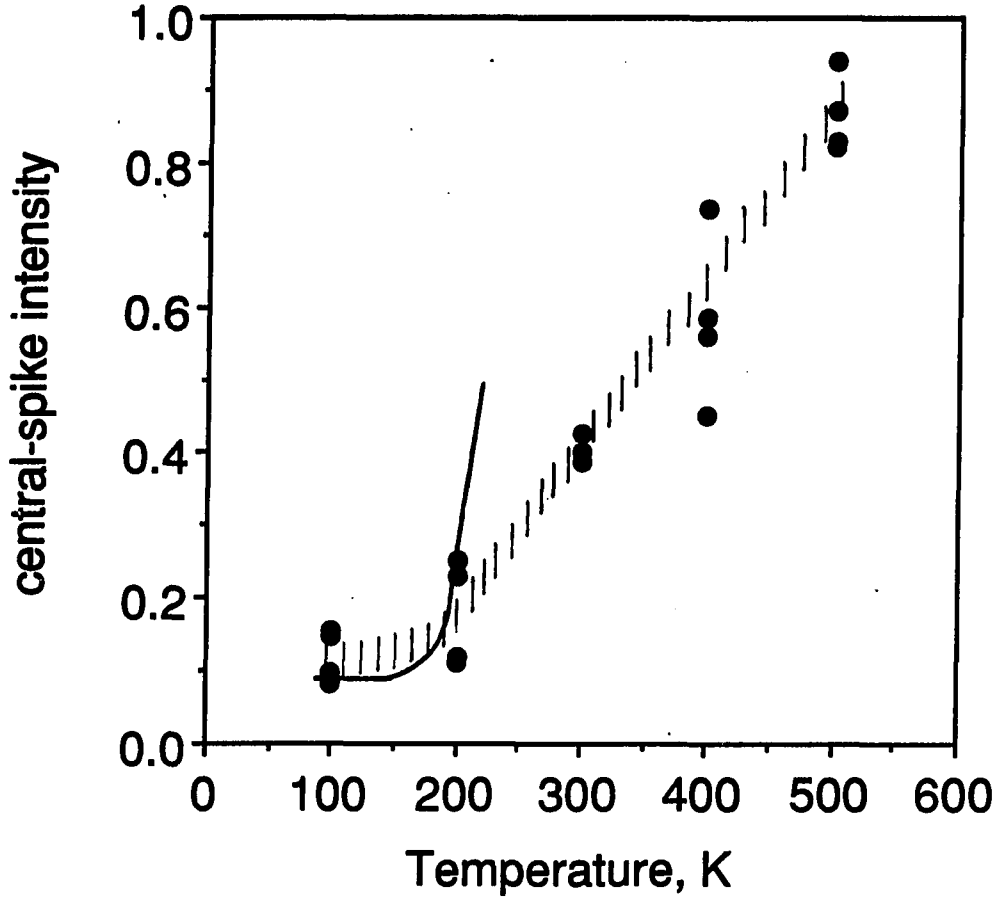

Figure 10. (continued)

(b) Pd: The data, represented by the solid circles, are from Figure 3b. The hatched line is included as a qualitative guide to the eye. Solid line represent modelling results using the following parameters: $E_h=E_g=12.7$ kcal/mol, $\nu_g=\nu_h=10^{13}$ s^{-1}

diffusion improves the fit to the experimental data. (The slower increase observed in experiment is probably associated with a small concentration of defects on our initial substrate, resulting in a variety of activation energies. Our modelling assumes an ideal surface.) We note that this fitting procedure does not allow a unique determination of rate parameters. Several choices with the same approximate fit to the data are shown in Figure 10a.

The high-temperature, experimental results for Pt and Pd show contrasting behavior (see Figures 2 and 3). Whereas Pd shows nearly complete recovery of the central-spike intensity, Pt shows a plateau followed by a rapid decrease. The high-temperature behavior of Pt films is dominated by processes other than simple adatom diffusion, as explained in section III, and shall not be considered further. The rate equations developed here and Monte Carlo simulation results of reference (39) predict full recovery of the central-spike intensity, as is experimentally observed for Pd (Figure 3). However, the rate equations predict a rather slow approach to unity with increasing temperature. Cluster mobility and rearrangement are certainly operative at high-temperatures, and since we neglect all cluster processes our model is suspect in this regime. The breakdown of our physical assumptions at high-temperatures limits the use of our model to temperatures up to and just above the onset of diffusion. Within this range, our analysis shows favorable agreement both with Monte Carlo simulations and experiment.

VI. NOVEL REPRESENTATION OF THE LAYER-COVERAGE DISTRIBUTION

Standard representations of the layer-coverage distribution relate the layer-coverages as functions of time or total coverage. We introduce a new representation based on the relationship of consecutive layer coverages, i.e., $\theta_{j+1} = f_j(\theta_j)$. For perfect layer-by-layer (Frank-van der Merwe) growth a very simple relationship exists between the layer coverages: $f_j^{FVM}(x) = 0$ for $x < 1$, and $f_j^{FVM}(1) = \theta_{j+1}$, taking all values between zero and unity. In the absence of overhangs, it is also true that the coverage in layer j+1 is always less than or equal to the coverage in layer j, in other words, $0 \leq f_j(x) \leq x$ (for $\theta_j = x$). Thus a clear quantification of deviations from ideal layer-by-layer growth is provided by this representation: the less layer-by-layer the growth, the larger $f_j(x)$.

Natural limits are placed on the range of $f_j(x)$ for epitaxial growth on a fcc(100) face, as illustrated in Figure 11a. The darkened axes show the relationship, $\theta_2 = f_1(\theta_1)$, for perfect layer-by-layer growth. The solid curve shows the relationship derived from the diffusionless (T=0), fourfold-hollow site, random deposition model (34). Growth at nonzero temperatures (but with the onset regime) is described by a curve bounded by these extremes - within the area bounded by these curves.

An elegant geometric characterization of intensity oscillations behavior exists in this representation. At the first-maximum of the

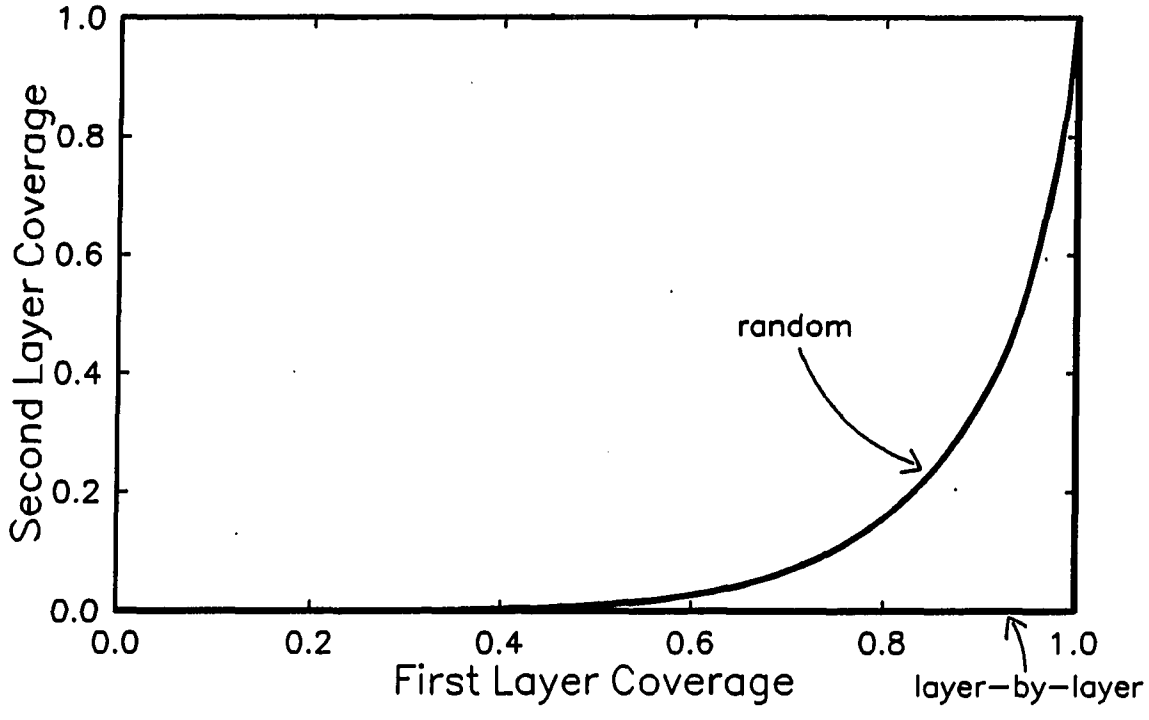

Figure 11. Characteristics of f_1

(a) Natural limits of f_1-curve
The darkened axes show the relationship between θ_2 and θ_1 for perfect layer-by-layer growth. The solid curve shows the exact, diffusionless (T=0) results calculated from the fourfold-hollow, random deposition model. The area between defines the bounds of f_1 for growth at nonzero temperatures, within the onset regime.

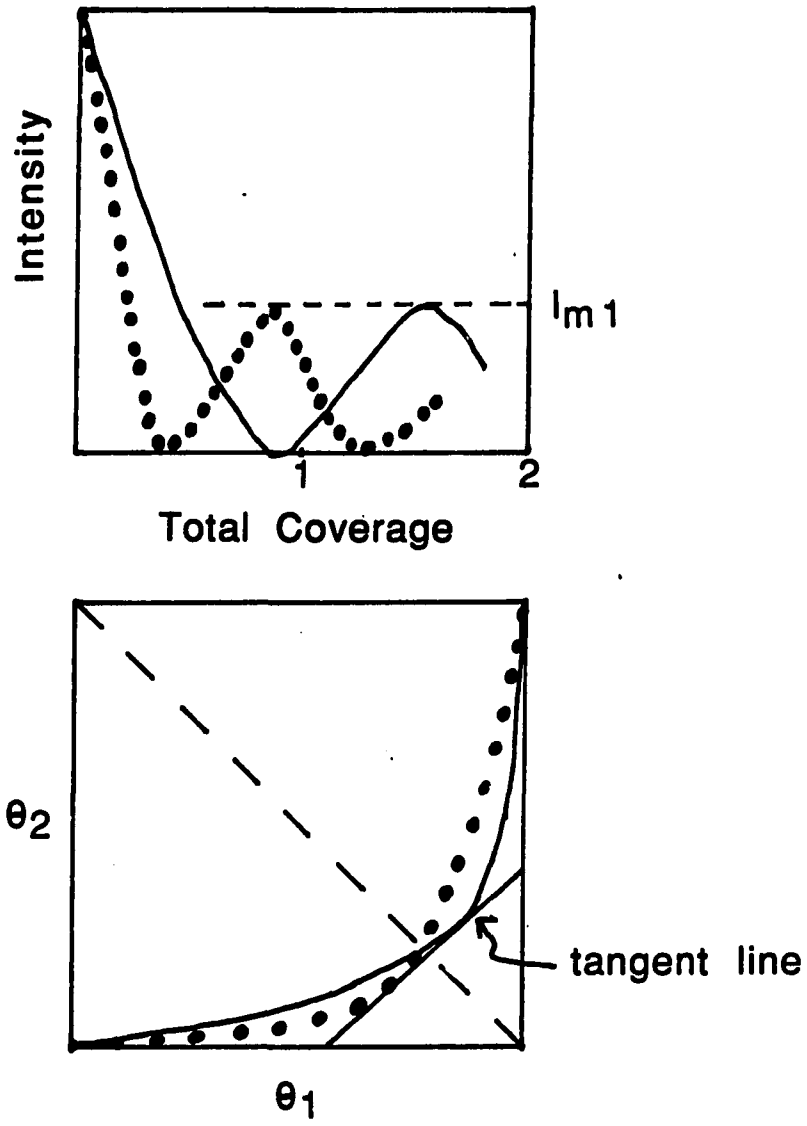

Figure 11. (continued)

(b) Relationship between total coverage at I_{m1} and f_1-curve The total coverage at the first-maximum of the central-spike intensity (I_{m1}) (top) determines the intersection of the f_1-curve and tangent line (bottom). Dotted curves: $\theta_{total}(I_{m1}) < 1$ ML; solid curves: $\theta_{total}(I_{m1}) > 1$ ML.

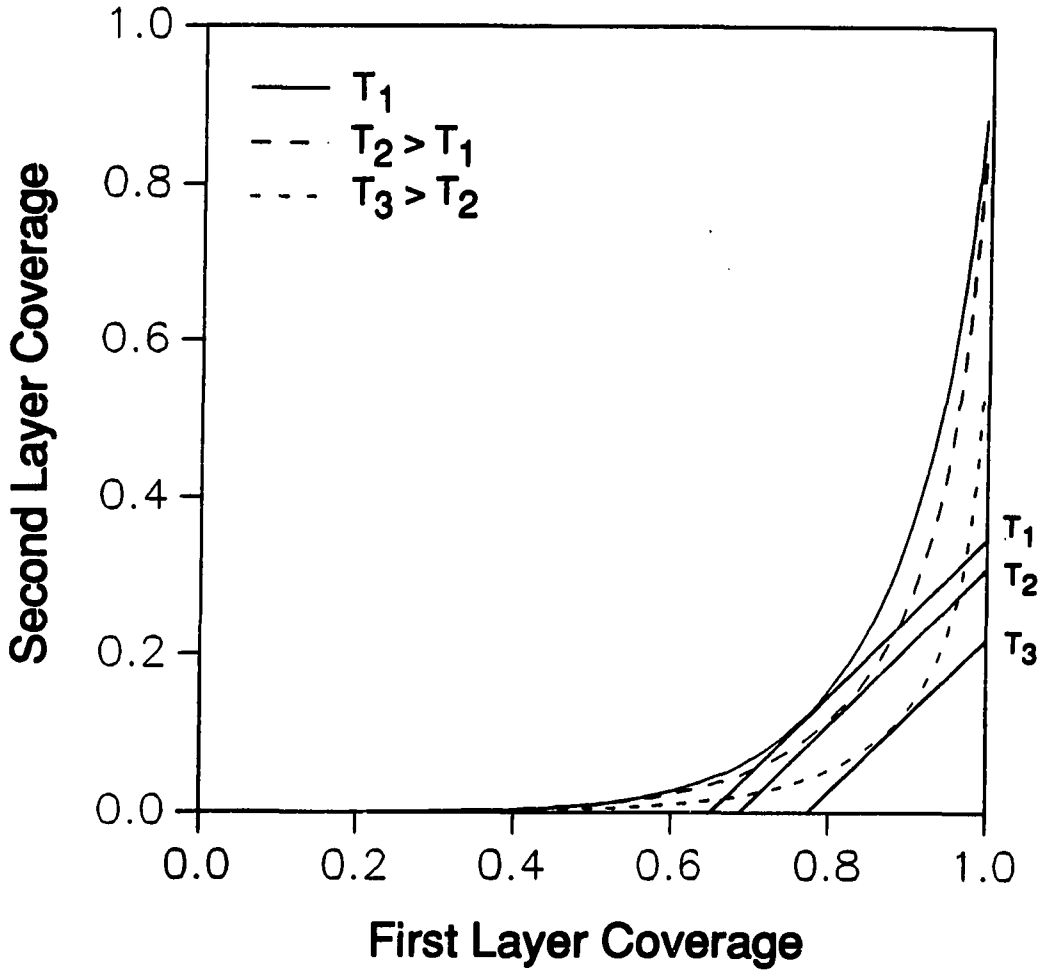

Figure 11. (continued)

(c) Temperature-dependence of f_1
Schematic depiction of the shifting of the tangent line as substrate temperature increases.

oscillation curve, third- and higher-layer occupations are negligible. Noting $N_0 = (1-\theta_1)$, $N_1=(\theta_1-\theta_2)$ and $N_2=\theta_2$, the intensity according to equation (1) is

$$I_{m1} \propto \left(1 - 2\theta_1^* + 2\theta_2^*\right)^2 \tag{9}$$

where θ_1^* and θ_2^* are the normalized occupations of the first- and second-layers at the first-maximum. At the first intensity maximum,

$$\frac{\partial I_{m1}}{\partial t} = 2\left(1 - 2\theta_1 + 2\theta_2\right)\left(-2\frac{\partial \theta_1}{\partial t} + 2\frac{\partial \theta_2}{\partial t}\right) = 0 \tag{10}$$

which is fulfilled when

$$\frac{\partial \theta_2}{\partial \theta_1} = 1 \tag{11}$$

Thus the rate of filling the first and second layers is equal at the first-maximum of the oscillation curve. Equation (11) also indicates that the slope of the f_1 curve $(\partial f_1/\partial \theta_1)$ is unity at the first-maximum. Described geometrically, this means that the first-maximum corresponds to the point where f_1 is *tangent* to the line

$$\theta_2^* = \theta_1^* - \left(\frac{1 + I_{m1}}{2}\right) \tag{12}$$

(The intercept in equation (12) is derived from equation (9).) As the tangent point traverses this line-segment the total coverage at the first-maximum ($\theta_{m1} = \theta_1^* + \theta_2^*$) changes from a minimum of $1 - \frac{1}{2}[1 - \sqrt{I_{m1}}]$

for $\theta_2^* = 0$, to a maximum of $1 + \frac{1}{2}[1 - \sqrt{I_{m1}}]$ for $\theta_1 = 1$. The general relationship between θ_1, θ_2 and the tangent line is shown in Figure 11b. If the first-maximum corresponds to a total coverage of exactly 1 ML, the f_1 curve would intercept the tangent line at the dashed line of Figure 11b (i.e., the most "symmetric" choice). The temperature-dependence of the f-curves is shown in Figure 11c. As temperature increases, the f curves generally flatten out, shifting the tangent line to lower y-intercept values as depicted in Figure 11c.

Using the rate equations developed in section V, we directly calculate the layer-occupations and evaluate the relationships between them, the diffracted intensity and the onset of diffusion within the $\theta_{j+1} = f(\theta_j)$ representation. Figure 12 shows the temperature-dependence of f_1-curves derived from the rate equations with various choices of ν_h, ν_g, E_h and E_g. A clear change in the general shape of the f-curve is evident at the temperature which diffusion begins. Table 1 gives the central-spike intensity and the first two layer coverages associated with associated the first-maximum.

Previous attempts to derive analytic forms of the f_j at nonzero temperatures are based on perturbation of the exact T=0 random fourfold site model (11). We assume $f_1^T = f_1^{T=0} + \partial f$, where ∂f is varied to match experimental first, second and third intensity maxima at each temperature. Higher-order f-functions are generated according to a scaling relation chosen to reproduce exact T=0 short time behavior. This analysis proved very sensitive to the form of the scaling relation and relied too heavily on the exact, T=0 form to generate f-curves for higher

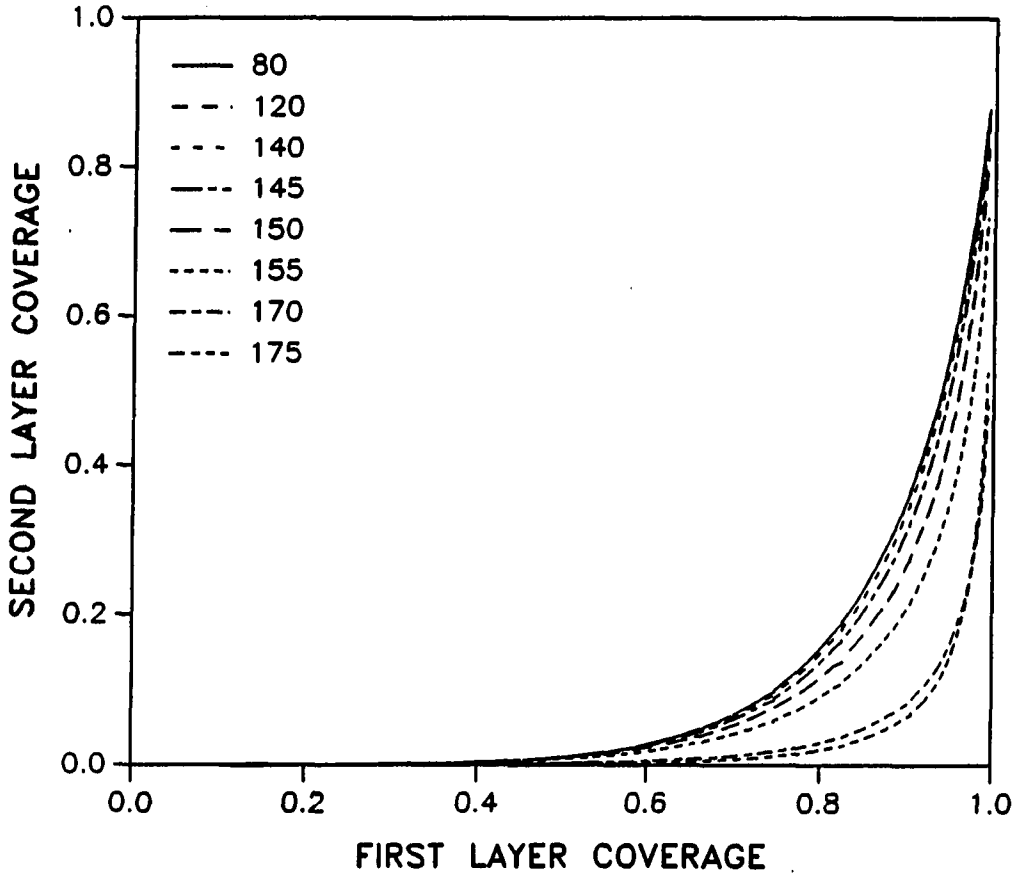

Figure 12. Calculated f_1 curves at various substrate temperatures (K)

The onset of diffusion is evident as a change in the curve shape as temperature increases.

(a) $E_g=E_h=10$ kcal/mol, $\nu_g=\nu_h=10^{13}$ s^{-1}

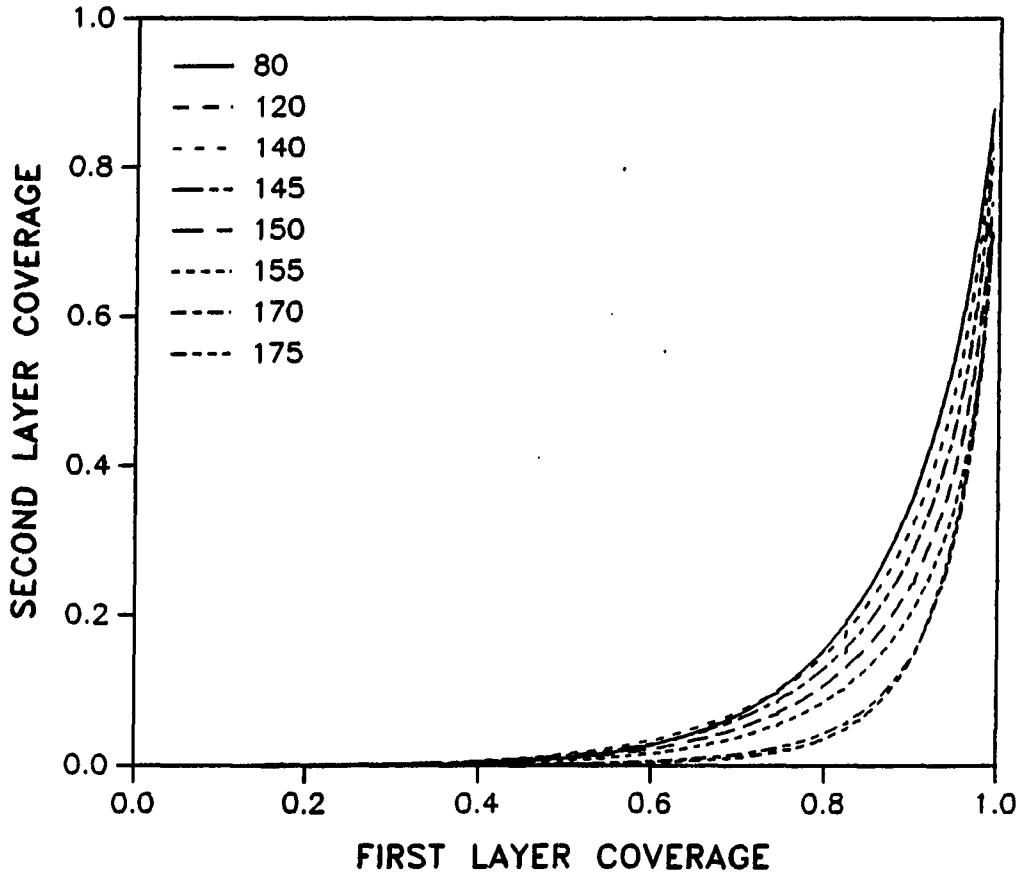

Figure 12. (continued)

(b) $E_g=E_h=9$ kcal/mol, $\nu_g=12.5\ s^{-1}$, $\nu_h=10^{13.1}\ s^{-1}$

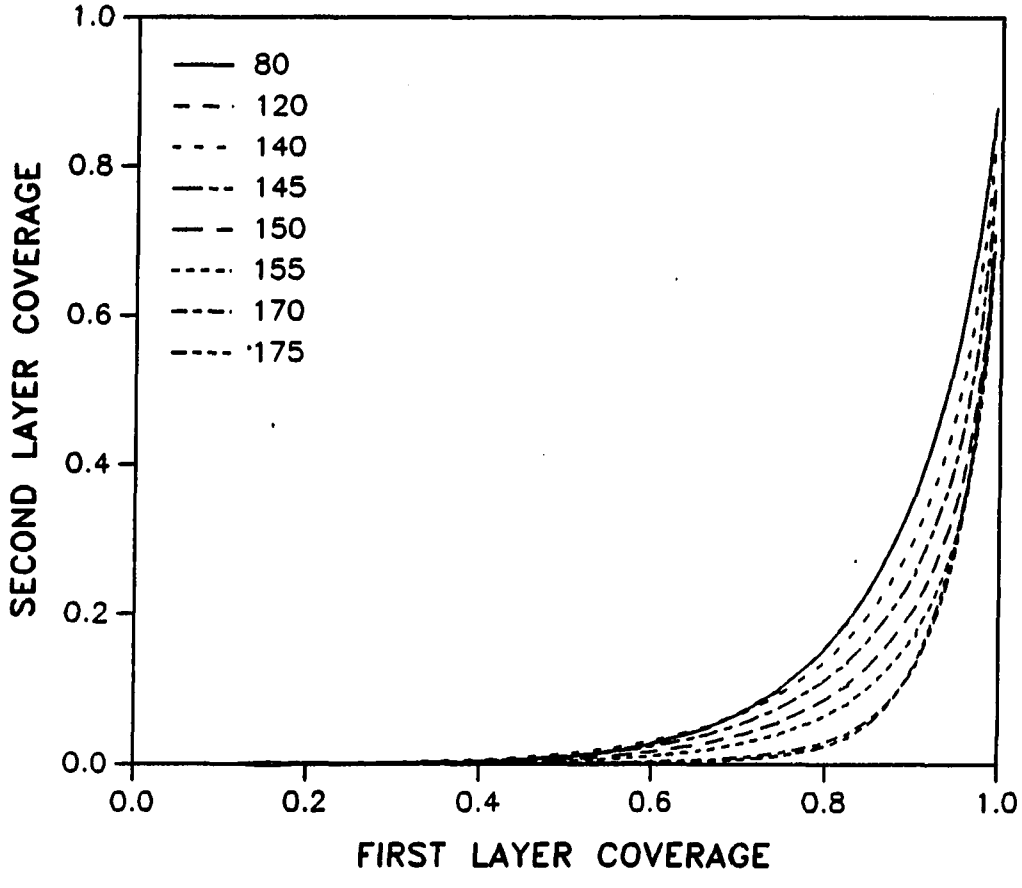

Figure 12. (continued)

(c) E_g=9.1 kcal/mol, E_h=8.7 kcal/mol, $\nu_g=\nu_h=10^{13}$ s^{-1}

Table 1. Central-spike intensity and first two layer occupations at the first maximum of the oscillation curve (I_{m1})

Temperature, T, is given in degrees Kelvin. $\theta_{1(2)}$ is the coverage in the first (second) layer.

a: $E_g=E_h=10$ kcal/mol, $\nu_g=\nu_h=10^{13}s^{-1}$

b: $E_g=E_h=9$ kcal/mol, $\nu_g=12.5s^{-1}$, $\nu_h=10^{1.13}s^{-1}$

c: $E_g=9.1$ kcal/mol, $E_h=8.7$ kcal/mol, $\nu_g=\nu_h=10^{13}s^{-1}$

	a			b			c		
T	I_{m1}	θ_1	θ_2	I_{m1}	θ_1	θ_2	I_{m1}	θ_1	θ_2
80	0.09	0.77	0.12	0.09	0.77	0.12	0.09	0.77	0.12
120	0.09	0.77	0.12	0.09	0.77	0.12	0.09	0.77	0.12
140	0.10	0.78	0.12	0.09	0.79	0.13	0.11	0.80	0.13
145	0.11	0.79	0.12	0.12	0.81	0.14	0.14	0.82	0.13
150	0.14	0.81	0.12	0.15	0.83	0.13	0.19	0.84	0.12
155	0.19	0.84	0.12	0.20	0.84	0.11	0.24	0.86	0.11
170	0.40	0.91	0.08	0.30	0.86	0.08	0.34	0.85	0.06
175	0.45	0.91	0.07	0.32	0.86	0.07	0.35	0.86	0.06

temperatures. We do not further pursue analytic derivation of f-functions.

To summarize this section, we have shown that to a first approximation, the first maximum in the intensity oscillation curve corresponds to equal rates of filling the first and second layers. In a graphical $\theta_2 = f(\theta_1)$ representation, this corresponds to the point of tangent with unit slope. This novel, yet simple, graphical representation provides insight on the temperature-dependence of the layer-coverages during growth. The onset of diffusion is demarked by a change in the general shape of the f-curves. This graphical view is a general representation and not restricted to fcc(100) epitaxial growth.

VII. TRANSIENT MOBILITY

A potential limitation of the growth model described in section V is the neglect of any "transient mobility", i.e., the possibility that energy accommodation between a deposited atom and the substrate occurs via surface mobility, even at temperatures below which thermally-activation diffusion is operative. The energy-source for this mobility is considered to be the heat released upon adsorption with the formation of the adatom-surface bond, which is typically on the order of 70 kcal/mol for metal systems (1). Transient mobility was predicted in molecular-dynamic simulations of low-temperature epitaxial growth by Schneider and coworkers (40). Egelhoff and Jacob extended this prediction to explain low-temperature RHEED oscillations during the epitaxy of metal films (1). Based on analysis of LEED profile lineshapes, a ballistic (directed) motion on the order of 10 unit spacings was necessary to explain the RHEED oscillations within this proposal (1).

The postulate of transient mobility at low temperatures is in direct contradiction of FIM measurements in which W atoms evaporated onto a W tip at 80 K did not migrate from the initial contact site, not even by a single lattice constant (41). Recent molecular-dynamic simulations for Pt/Pd(100) and Cu/Cu(100) by Sanders and DePristo showed that transient mobility is limited to *at most* one lattice spacing, but rarely even that (2,42). These authors noted that the prediction of transient mobility by Schneider and coworkers cannot be extended to metal

systems since their simulation inadequately treats energy-dissipation through a metal substrate. In particular, the active zone set up in this study was simply "too rigid" to properly model a metal surface. Heats of adsorption are effectively localized at the deposited atom, enhancing the conversion to kinetic energy, which results in an overestimation of the metal adatom mobility. In fact, the results of Schneider, et. al. were imitated when the active zone was reduced (surface made "more rigid"); but with proper treatment of the surface, effectively no transient mobility was observed (42). It was concluded that transient mobility is *not* a principal mechanism for the development and sustainment of layer-by-layer growth in metal systems.

If transient mobility is operative at low temperatures in our study, one might expect more restricted mobility in the Pt/Pd(100) system than for Pd/Pd(100) because the relatively heavy mass of Pt optimizes energy transfer to the substrate on impact. This should result in an increased amplitude, and perhaps more persistent oscillations for Pd than for Pt. Analysis of the classical equations for energy transfer within the hard-cube approximation (43) show that under conditions of conserved energy and momentum, after initial impact (and transfer of some of the bond energy to the substrate) a deposited Pd atom retains ca. 34 kcal/mol. A deposited Pt atom retains ca. half this energy, 16 kcal/mol. The energies calculated here are significantly less than that presumed by Egelhoff and Jacob, since we assume that some of the energy released upon adsorption is dissipated to the substrate. Additionally, the substrate is modelled as a hard-cube as opposed to a single atom, which is a

somewhat more physically reasonable model. (We note that both the hard-cube calculation and the calculation used in reference (1) are crude, and both should overestimate the energy released.) For an adatom to begin to migrate, it must have an energy at least equal to the diffusional barrier, ca. 10-15 kcal/mol. If we assume there is energy transferred with each impact during transport, the Pd atom may have sufficient energy to move at most 2 to 3 lattice spacings upon adsorption (within the hard-cube approximation), but Pt diffusion should be limited to at most 1 hop. These distances are significantly less than the directed motion along 10 lattice spacings which is required in the explanation of the low temperature oscillations in the RHEED study on the basis of transient mobility (1).

Our data do not show a very significant difference in the low temperature Pt and Pd intensity oscillation behavior, and it is important to note that *low temperature oscillations are observed for both Pt and Pd*. Transient mobility is not a sufficient explanation for these observations. Low-temperature intensity oscillations are fully explained within the fourfold-hollow site, random deposition model, *without* the need of invoking transient mobility. The fourfold-hollow adsorption site and general lack of transient mobility is also supported by molecular dynamics simulations which show that the deposited atom "settles" into the fourfold-hollow site, independent of where it first impacts inside the unit cell (2,42).

VIII. CONCLUSIONS

Epitaxial growth of Pt and Pd on Pd(100) is studied via LEED as a function of coverage and temperature. At low and moderate temperatures, both systems exhibit distinct oscillations and similar growth behavior. Growth is nearly temperature-independent at low-temperatures ($\lesssim$ ca. 150-200 K), where thermally-activated diffusion is negligible. A dramatic change is observed in the diffracted intensity at ca. 150 K for Pt, and ca. 200 K for Pd, and is associated with the onset of diffusion. Reconstruction and/or interlayer mixing interferes with the growth of Pt overlayers at temperatures greater than ca. 250 K. For Pd, the resulting film morphology is determined by the extent of surface diffusion at temperatures greater than ca. 200 K.

We present a model which describes growth in the temperature regime where single-atom diffusion begins. The role of diffusion in changing film structure is nontrivial. Interlayer diffusion (from "higher" to "lower" layers) makes growth more layer-by-layer like. Lateral (intralayer) diffusion, although providing the means for atoms to migrate to step edges from where they can step down (enhancing layer-by-layer growth), also adds to two-dimensional clustering within a layer, making growth *less* layer-by-layer like for two reasons. First, at temperatures where the breakup or migration of clusters is negligible, atoms clustering in "upper" layers are permanently trapped, thwarting diffusion to "lower" layers. Second, clustering produces more adsorption sites (at fixed coverage) for the birth of upper layers, easing the spread of

the growth front. For similar reasons, enhanced lateral diffusion during growth also reduces the layer-by-layer quality. These effects are predicted by the presented microscopic growth model, which incorporates fcc(100) adsorption-site geometry and explicit rates for interlayer and lateral diffusional processes. This model explains experimental observations of intensity oscillations at low temperatures without invoking transient mobility. It is used to predict the layer-coverages and diffracted intensity during growth at temperatures within the onset regime. We also present a novel representation of the layer-coverages which provides insight to the relationships among the layer-coverages, the diffracted intensity and the onset of diffusion.

IX. APPENDIX: FCC MULTILAYER PAIR- AND SQUARE-APPROXIMATIONS

Pair- or square-approximations are used in calculating the configurational probabilities P, G, L, $\tilde{G}$ and H in equations (5) and (6). Consider $P_{\bar{j}}$, the probability of an empty fourfold-hollow adsorption-site in layer j. This is defined as the difference between the probability of a square arrangement of four layer j-1 atoms (empty *or* filled in layer j) and the probability of filled site in layer j:

$$P_{\bar{j}} = \begin{pmatrix} j-1 & & j-1 \\ & \bar{j} & \\ j-1 & & j-1 \end{pmatrix} = \begin{pmatrix} j-1 & j-1 \\ j-1 & j-1 \end{pmatrix} - (j) \equiv S_{j-1} - (j) \qquad (13)$$

where $\bar{j}$ indicates the layer j site is empty. The conventional pair-approximation (37) would factor S_k as $(kk)^4\ (k)^{-4}$. For fcc(100) geometry S_k, (kk) and (k) implies 9, 6, and 4 filled (k - 1)th layer supporting sites, respectively (see Figure 13). However, the number of supporting sites implied from the factorized form of S_k is {4 x 6 (from the $(kk)^4$ term) - 4 x 4 (from the $(k)^4$ term) = 8. Physically we know there must be 9 atoms in the k-1 layer to support the square arrangement of four atoms (see Figure 13). Thus we modify the conventional, pair-approximation factorized form of S_k to include an additional factor of (k-1). This correctly accounts for the necessary number of supporting atoms.

The probability of an filled-empty pair in layer j is treated in the same way:

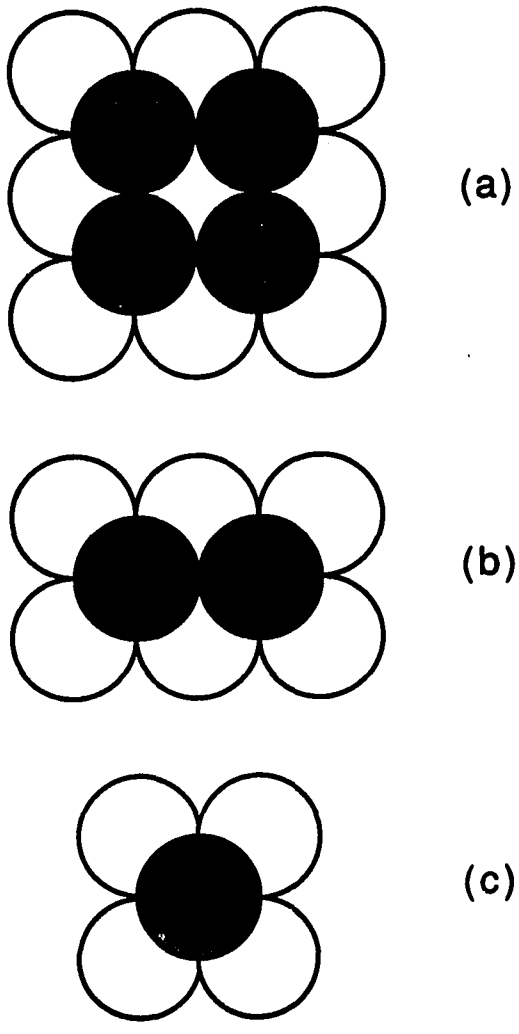

Figure 13. Supporting atoms required for various configurations in the fourfold-hollow model

(a) a square of atoms in layer j requires 9 atoms in layer j-1

(b) a pair of atoms in layer j requires 6 atoms in layer j-1

(c) a single atom in layer j requires 4 atoms in layer j-1

$$P_{jJ} = \begin{pmatrix} j-1 & j-1 & j-1 \\ & j & \overline{J} \\ j-1 & j-1 & j-1 \end{pmatrix} = \begin{pmatrix} j-1 & j-1 & j-1 \\ & j & \\ j-1 & j-1 & j-1 \end{pmatrix} - (jj) \equiv S_{(j)j-1} - (jj) \tag{14}$$

The first term on the right side is factorized as:

$$(j-2)\begin{pmatrix} j-1 & j-1 \\ & j \\ j-1 & j-1 \end{pmatrix} \frac{(j-1\ j-1)^3}{(j-1)^4} = \frac{(j-2)(j)(j-1\ j-1)^3}{(j-1)^4} \tag{15}$$

in modified form. The number of implied lower layer sites are correctly accounted for by the additional (j-2) term. Configurations associated with diffusional gain and loss terms are more complicated, however analogous factorization is implemented.

In the square-approximation, the S_{j-1} term in the factorization of P_J (equation 13) represents a square-arrangement of four atoms and is retained without factorization. The $S_{(j)j-1}$ term in the factorization of P_{jJ} (equation 14) is factorized as:

$$(j)\begin{pmatrix} j-1 & j-1 \\ j-1 & j-1 \end{pmatrix}(j-1\ j-1)^{-1} \tag{16}$$

One can readily check that this factorization correctly accounts for the number of lower-layer filled-sites.

The modification to the standard pair- and square-approximations is necessary to avoid site overcounting in the factorizations. More importantly, this modification ensures the geometric constraints imposed

by the explicit specification of the adsorption-site geometry are maintained throughout the factorization of the rate equations.

X. ACKNOWLEDGEMENTS

We are grateful for experimental assistance from W.-D. Wang, W.-Y. Leung, N.-J. Wu, and O. L. Warren. Additionally, we thank D. E. Sanders for discussions of unpublished work. The experimental component of this work is supported by a Presidential Young Investigator Award of the National Science Foundation, Grant No. CHE-8451317, Camille and Henry Dreyfus Teacher-Scholarship (P.A.T.) and the Ford Motor Company. The theroretical component is supported by the Division of Chemical Sciences, Office of Basic Energy Sciences. One of us (J.W.E.) is supported by the Ames Laboratory. Also, some experimental equipment and all facilities are provided by this Laboratory, which is operated for the US Department of Energy by Iowa State University under Contract No. W-7405-ENG-82.

REFERENCES

1. W. F. Egelhoff, Jr. and I. Jacob, Phys. Rev. Lett. 62 (1989) 921.
2. J. W. Evans, D. E. Sanders, P. A. Thiel and A. E. DePristo, Phys. Rev. B 41 (1990) 5410.
3. E. Bauer, Z. Kristallographie 110 (1958) 372 and 395; also Appl. Surface Sci. (1982) 479.
4. J. A. Venables, G. D. T. Spiller, M. Handbüchen Rep. Prog. Phys. 47 (1984) 399.
5. R. Kern, G. Lelay, J. J. Metois, in Current Topics in Materials Science, Volume 3, edited by E. Kaldis (North-Holland, Amsterdam, 1979).
6. E. Bauer and J. H. van der Merwe, Phys. Rev. B 33 (1986) 3657.
7. D. A. Steigerwald and W. F. Egelhoff, Jr., Surface Sci. 192 (1987) L887.
8. S. T. Purcell, B. Heinrich and A. S. Arrott, Phys. Rev. B 35 (1987) 6458.
9. M. Doyana, R. Yamamoto, T. Kaneko, M. Imafuku, C. Kokubu, T. Izumya and T. Hanamure, Vacuum 36 (1986) 909.
10. D. K. Flynn, W. Wang, S.-L. Chang, M. C. Tringides and P. A. Thiel, Langmuir 4 (1988) 1096.
11. D. K. Flynn, J. W. Evans and P. A. Thiel, J. Vac. Sci. and Technol. A 7 (1989) 2162.
12. J. J. DeMiguel, A. Cebollada, J. M. Gallege, J. Ferrón and S. Ferrar, J. Crystal Growth 88, 442 (1988).

13. J. J. DeMiguel, A. Sánchez, A. Cebollada, J. M. Gallego, J. Ferrón and S. Ferrar, Surface Sci. 189/190 (1987) 1062.

14. M. Jałochowski and E. Bauer, Phys. Rev. B 37 (1988) 8622.

15. J. W. Evans, D. K. Flynn and P. A. Thiel, Ultramicroscopy 31 (1989) 80.

16. D. K. Flynn-Sanders and P. A. Thiel, Chemistry Department, Iowa State University (1990), manuscript in preparation.

17. G. Ehrlich in, Chemistry and Physics of Solid Surfaces V, Chapter 12, edited by R. Vanselow and R. Howe (Springer-Verlag, Berlin, 1984).

18. J. W. Anderegg and P. A. Thiel, J. Vac. Sci. and Technol. A 4 (1986) 1367.

19. P. A. Thiel and J. W. Anderegg, Rev. Sci. Instrum. 55 (1984) 1669.

20. H. Herz, H. Conrad and J. Küppers, J. Phys. E 12 (1979) 369.

21. B. C. DeCooman and R. W. Vook, J. Vac. Sci. and Technol. A 21 (1982) 899.

22. M. Henzler, Surface Sci. 22 (1970) 12.

23. C. S. Lent and P. I. Cohen, Surface Sci., 139 (1984) 121.

24. J. M. Pimbley and T.-M. Lu, J. Appl. Phys. 57 (1985) 1121.

25. J. W. Evans, Vacuum (1990) in press.

26. R. T. Tung and W. R. Graham, Surface Sci. 97 (1980) 73.

27. P. R. Schwoebel and G. L. Kellogg, Phys. Rev. B 38 (1988) 5326.

28. S. Hagstrom, H. B. Lyon and G. A. Somorjai, Phys. Rev. Lett. 15 (1965) 491.

29. G. L. Kellogg and P. R. Schwoebel, Surface Sci. 224 (1989) 489.

30. G. L. Kellogg, Surface Sci. 177 (1986) L1021.

31. P. I. Cohen, G. S. Petrich, P. R. Pukite, G. J. Whaley and A. S. Arrott, Surface Sci. 216 (1989) 222.

32. D. Kashiev, J. Crystal Growth 40 (1977) 29.

33. R. Kariotis and M. G. Lagally, J. Vac. Sci. Technol. B 7 (1989) 269.

34. J. W. Evans, Phys. Rev. B 39 (1989) 5655.

35. G. Lilienkamp, C. Kozoil and E. Bauer, in Reflection High-Energy Electron Diffraction and Reflection Imaging of Surfaces, edited by P. K. Larsen and P. J. Dobson (Plenum Press, New York, 1988).

36. W. Haubenreisser and H. Pfeiffer, in Modern Theory of Crystal Growth I. Crystals: Growth, Properties and Applications (#9), edited by A. A. Chernov and H. Müller-Krumbharr (Springer-Verlag, Berlin, 1983).

37. G. H. Gilmer, H. J. Leamy, K. A. Jackson and H. Reiss, J. Crystal Growth 24/25 (1974) 495.

38. R. Dickman, Phys. Rev. A 34 (1986) 4246; 38 (1988) 2588; Phys. Lett. A 122 (1987) 463.

39. J. W. Evans, Chemistry Department, Iowa State University, manuscript in preparation (1990).

40. M. Schneider, A. Rahman and I. K. Schuller, Phys. Rev. Lett. 55 (1985) 604; Phys. Rev. B 34 (1986) 1802.

41. R. D. Young and D. C. Schubert, J. Chem. Phys. 90 (1965) 3943.

42. D. E. Sanders and A. E. DePristo, Chemistry Department, Iowa State University, manuscript in preparation (1990).

43. F. O. Goodman and H. Y. Wachman, Dynamics of Gas-Surface Scattering, Chapter 6, (Academic Press, New York) 1976. For our calculation, the mass of the cube (substrate) is taken as 4 times the mass of a Pd atom. The initial energy of the depositing atom is set equal to the binding energy of that atom (Pt or Pd) with a Pd(100) surface. Binding energies are 66.56 kcal/mol for Pd/Pd(100) and 75.78 kcal/mol for Pt/Pd(100), provided by D. E. Sanders, Iowa State University, private communication.

PAPER V:

PRACTICAL DETERMINATION OF THE OUT-OF-PHASE ENERGY FOR MONITORING INTENSITY OSCILLATIONS DURING THIN FILM GROWTH

Practical Determination of the Out-of-Phase Energy for Monitoring Intensity Oscillations during Thin Film Growth

D. K. Flynn-Sanders and P. A. Thiel

Department of Chemistry and Ames Laboratory - US DOE
Iowa State University
Ames, Iowa 50011

ABSTRACT

We compare methods for experimental determination of the out-of-phase energy, used to monitor intensity oscillations during thin film growth. Often, a maximum in the energy-dependence of the full-width at half-maximum (FWHM) is used as a convenient measurement of the out-of-phase energy. We comment on possible inconsistencies in extracting the width from the inhomogeneously-broadened profiles normally associated with epitaxial growth. Out-of-phase scattering conditions are not the only criteria to be considered when choosing viable energies to monitor intensity oscillations during thin film growth. We present a new method to experimentally determine the out-of-phase energy based on the energy-dependence of the central-spike intensity, and compare with alternative methods. We discuss the criteria for selecting the most suitable beam energy at which intensity oscillations can be monitored during thin film growth.

I. INTRODUCTION

The properties of thin films are often remarkably different from the bulk. One striking example is the chemical reactivity of gold films on platinum. Cyclohexene dehydrogenation over platinum is accelerated when a layer of gold is present, whereas this reaction does not proceed on gold itself (1-3). A completely different example stems from the rate of electron transport via quantum tunneling. This mechanism is not viable in bulk-like layers, but has appreciable rate when film thickness is comparable to the extension of electronic wavefunctions (10 - 100 Å) (4).

The exact origin of properties unique to thin films is often not known, but is undoubtedly associated with the quasi-two-dimensional nature of the film, and the strong influence of the substrate throughout the film. Since these properties often vary with thickness, uniformly thick films are desirable. This has stimulated voluminous research into epitaxial thin film growth (5-7). Films that exhibit layer-by-layer growth are preferred, since thickness is relatively controllable.

Diffraction techniques such as reflection high-energy electron diffraction (RHEED) (8,9), low-energy electron diffraction (LEED) (10-12), and thermal-energy atom scattering (TEAS) (13) have been used to study films that grow in a layer-by-layer fashion. These techniques rely on the oscillatory nature of the diffracted intensity with coverage, which reflects the successive filling of layers. The behavior for ideal layer-by-layer growth at an out-of-phase condition is

depicted in Figure 1. At out-of-phase energies, optimal destructive interference occurs between scattering from consecutive layers (14,15), resulting in maximum oscillation amplitude. Thus determination of the out-of-phase energies is the starting point for many epitaxial growth experiments.

Henzler has given a general formula to calculate characteristic voltages, V_{hk}, for in-phase and out-of-phase scattering, which rests upon the kinematic approximation (15):

$$V_{hk} = \frac{150}{4d^2}\left\{S - (hx + ky) + \frac{(h\underline{a}^* + k\underline{b}^*)^2 d^2}{4\pi^2\,[S - (hx + ky)]}\right\}^2 \qquad (1)$$

Here, (hk) are the Miller indices of the reflection of interest, and $\underline{a}^*$, $\underline{b}^*$ are the reciprocal lattice vectors of the surface plane described by lattice vectors a, b. Letting $\underline{c}$ denote a unit vector perpendicular to the surface plane and d the step height, the vector, $\underline{g} = x\underline{a}+y\underline{b}+d\underline{c}$, represents the displacement between scattering centers in successive planes, as depicted in Figure 2a. S is integral for in-phase scattering, where the Bragg conditions for the three dimensional crystal are satisfied; and half-integral for out-of-phase scattering, where scattering from successive planes interferes destructively. The dependence of the energy, V_{hk}, on S is shown in Figure 2b for the (0,-1) and (1,1) beams.

As discussed extensively by Henzler (16,17) a periodic variation in the diffracted spot shape with energy is generally observed when steps are present on the surface. Some form of splitting or spot broadening is

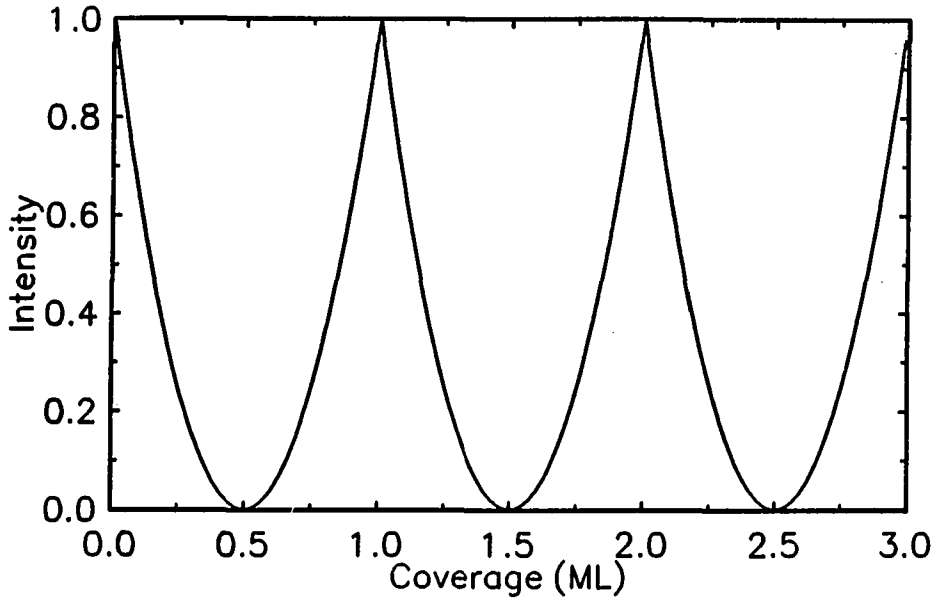

Figure 1. Idealized intensity oscillations

Kinematically diffracted intensity at an out-of-phase condition ($S_1 = 0$, $S_2 = \pi/d$) as a function of coverage, based on the equation $I = (2\theta\text{-}1)^2$.

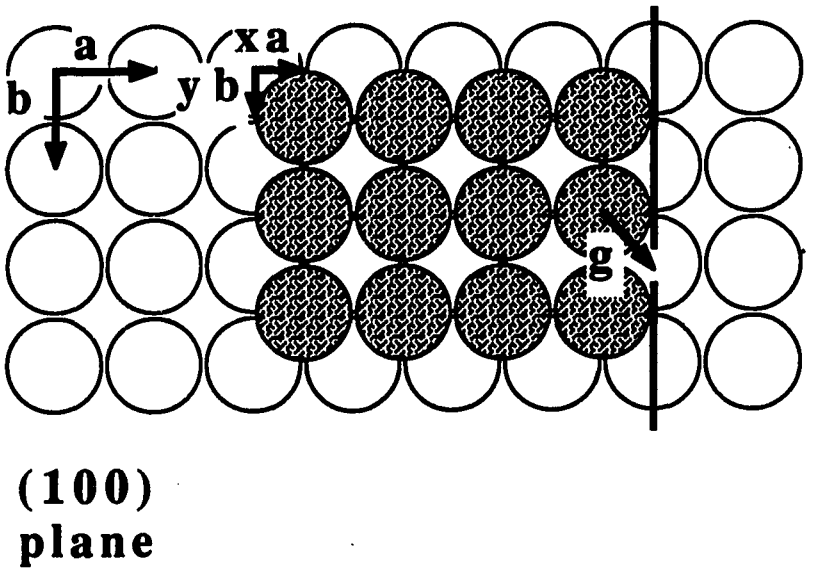

Figure 2a. Schematic depiction of an fcc(100) surface (open circles) with an island of atoms in a top layer (shaded circles)

The real-space vectors are defined in the text.

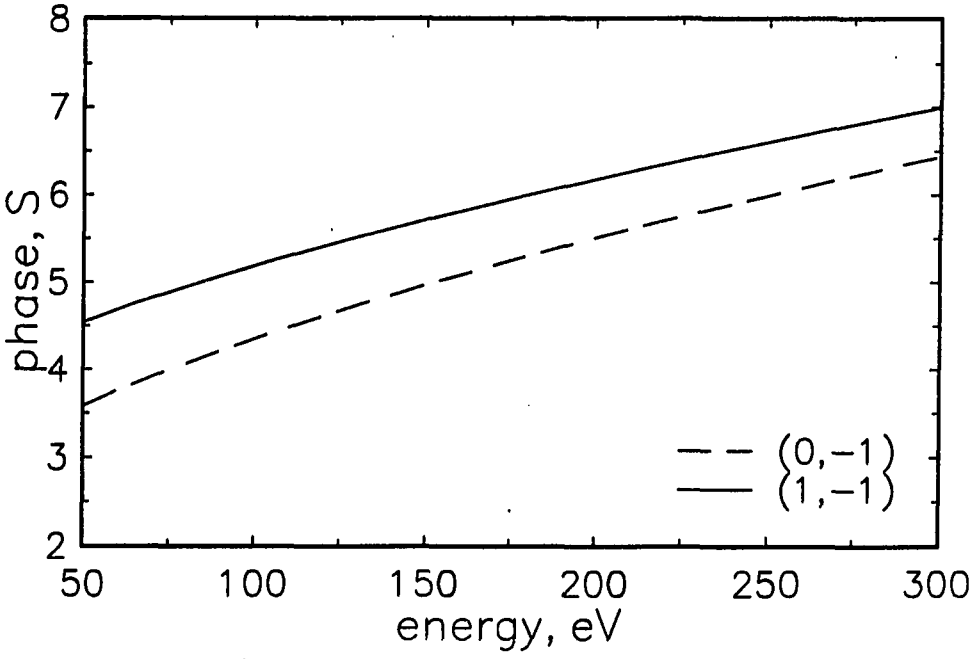

Figure 2b. Phase, S, as a function of energy, V_{hk}, according to equation 1, for the (0,-1) and (1,-1) beams

present at out-of-phase energies [half-integral S in equation (1)], whereas characteristically sharp diffraction spots are observed at the in-phase conditions. Thus out-of-phase conditions should be experimentally determinable from maxima in the energy-dependence of the FWHM. This procedure has in fact been used in a study of Pt film growth on Pd(100) (10).

However, experimental measurement of the FWHM is not always appropriate. For example, sometimes during thin film growth, profiles exhibit ring-structure, (10,18,19), and the straightforward analysis of the FWHM is not possible. Or, low instrument resolving power may obscure the energy-dependent variations of the FWHM. Additionally, since equation (1) is based on a kinematic derivation, multiple-scattering effects may lead to a shift in the experimentally-observed characteristic voltages. Or, a shift may simply be due to an unsuspected voltage offset in the instrument. Therefore, simply "dialing in" the calculated voltage does not guarantee an out-of-phase condition suitable for monitoring intenisty oscillations during thin film growth.

We exemplify some of these difficulties in the experimental determination of the out-of-phase condition for Pd/Pd(100). Note that this is a homoepitaxial system, so layer-by-layer growth is thermodynamically required (20). This is an ideal system for study, since potential complications in film growth due to alloying or agglomerization do not enter. Profiles are acquired with a conventional LEED apparatus. We consider the abstraction of physically meaningful measurements from the type of profile lineshapes commonly observed during

epitaxial growth, and discuss alternative methods to determine out-of-phase conditions. The criteria for the most suitable energy for monitoring intensity oscillations are presented.

II. EXPERIMENTAL DETAILS

The experimental details, including descriptions of the ultrahigh vacuum apparatus, film deposition procedures, sample cleaning procedures, and data acquisition system, are available elsewhere (10,21). The most salient features of the apparatus are a standard, four-grid Varian LEED optics and a computer-interfaced video camera (22). Pd is deposited by thermal evaporation from a resistively heated source (23). Normal incidence LEED spot profiles are acquired as a function of energy. Since energy control and window centering are not automated, an experiment spanning 50 to 300 eV takes 1.5 to 2 hours. To minimize errors associated with residual gas effects, the energy range is scanned in 10 eV increments several times, such that the resultant increments are only 2 to 3 eV. As in previous studies (10,11,19,24) a constant background, associated with point defects (16,25), is set equal to the minimum intensity value of each profile and subtracted. There is no compensation for "grid structure" from the LEED optics and the profiles are not smoothed.

III. EXPERIMENTAL RESULTS

Representative profiles for ca. 1/2 ML (monolayer) Pd deposited on Pd(100) at 100 and 300 K are shown as a function of energy in Figures 3 and 4. Kinematically determined values of the phase, S, (calculated according to equation (1)) are also shown. These profiles are inhomogeneously-broadened, consisting of two components. At some energies, profiles for Pd deposition at 300 K exhibit definitive ring-structure, as demonstrated by the end profiles in each figure. Theoretically, energies exhibiting ring-structure should coincide with those predicted by equation (1) for half-integral S. Ring-structure is not apparent in profiles obtained by depositing at 100 K. Instead, a homogeneously-broadened component of very low amplitude is superimposed on the central-spike.

We define the reciprocal-space characteristic distance of each profile according to Figure 5. For sharp profiles it is simply the FWHM. For profiles exhibiting ring-structure, the FWHM is clearly not applicable, since more than two crossing points at the half-maximum are possible. In these cases, the ring diameter is a better measure of the reciprocal-space characteristic distance. For profiles consisting of a superposition of a central-spike and homogeneously-broadened component (as in the 100 K profiles) the FWHM of the broadened portion is used as the reciprocal-space characteristic distance. The characteristic distance is normalized to the Brillioun zone length (i.e., spot separation) at each energy. In cases where the peak intensity goes to

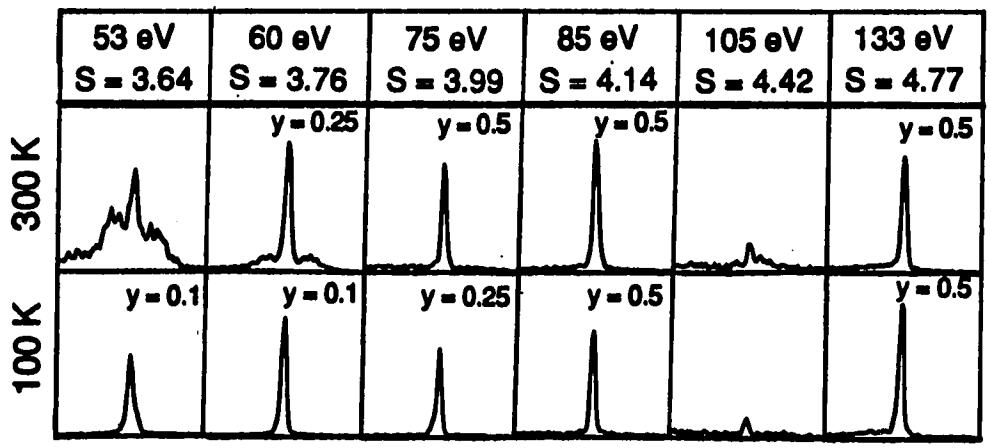

Figure 3. (0,-1) Spot profiles as a function of energy at 100 and 300 K The phase, S, is calculated according to equation (1).

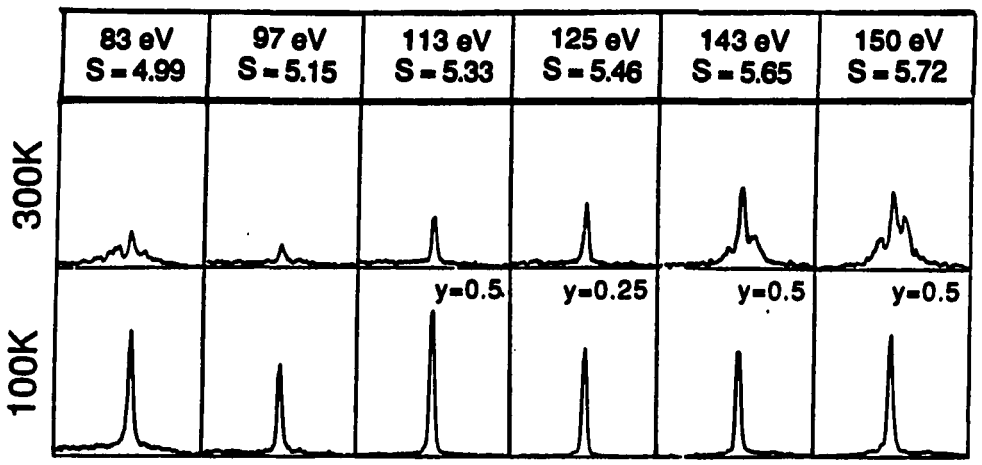

Figure 4. (1,-1) Spot profiles as a function of energy at 100 and 300 K The phase, S, is calculated according to equation (1).

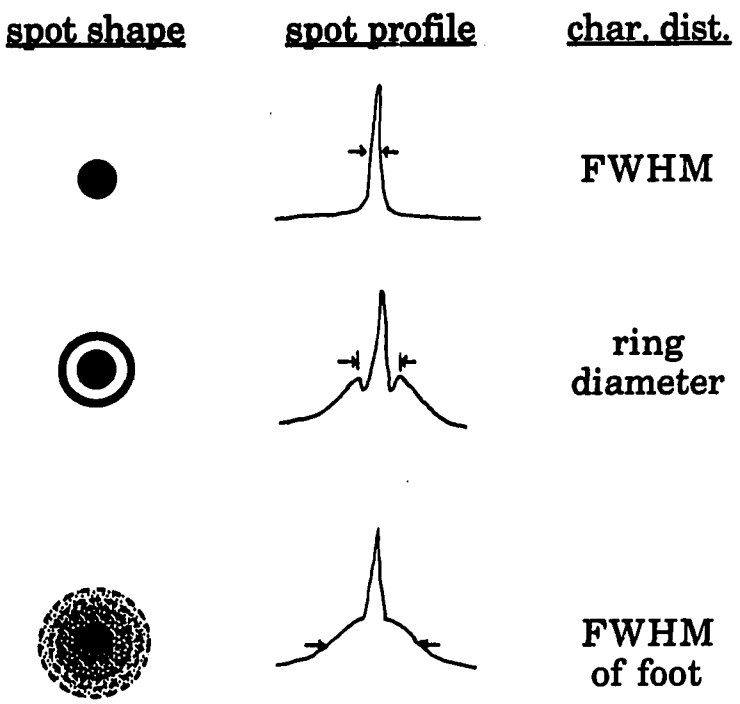

Figure 5. Reciprocal-space characteristic distance

Schematic depiction of LEED spot shapes and profiles associated with different surface structures, and the corresponding reciprocal-space characteristic distance.
(a) flat surface
(b) islands of regular size or separation
(c) islands of random size and separation

zero, the reciprocal-space characteristic distance has ambiguous meaning, and is not measured.

Each reciprocal-space characteristic distance in Figure 5 is representative of a periodic surface dimension in real-space. The FWHM of a sharp profile is related to the average terrace width. The larger the terraces, the sharper the spot. Two island-distribution models can successfully reproduce ring-structured profiles, like those we observe at intermediate temperatures during epitaxial growth: (1) islands of constant size and random separation or (2) islands of random size and constant separation (18,26). The ring diameter is related to either the island size (case 1) or separation (case 2). For the homogeneously-broadened component of the two-component profiles (typical of growth at low temperatures) the FWHM of the broadened component gives information on the average island size (27).

Figures 6 and 7 show the energy-dependence of the reciprocal-space characteristic distance of the (0,-1) and (1,-1) spots for ca. 1/2 ML Pd deposited on Pd(100) surface at 100 and 300 K. The dashed line in each figure is a measure of the instrument limit, determined by the FWHM of clean surface profiles. The open circles represent energies at which the profile does *not* show distinct broadening, and is simply the FWHM of the whole profile. At energies where the broadened component is distinguishable from the central-spike, a filled circle represents the ring diameter or FWHM of the homogeneously-broadened componet (whichever is appropriate to the profile under consideration). Filled (empty) arrows indicate out-of-phase (in-phase) energies, as predicted from

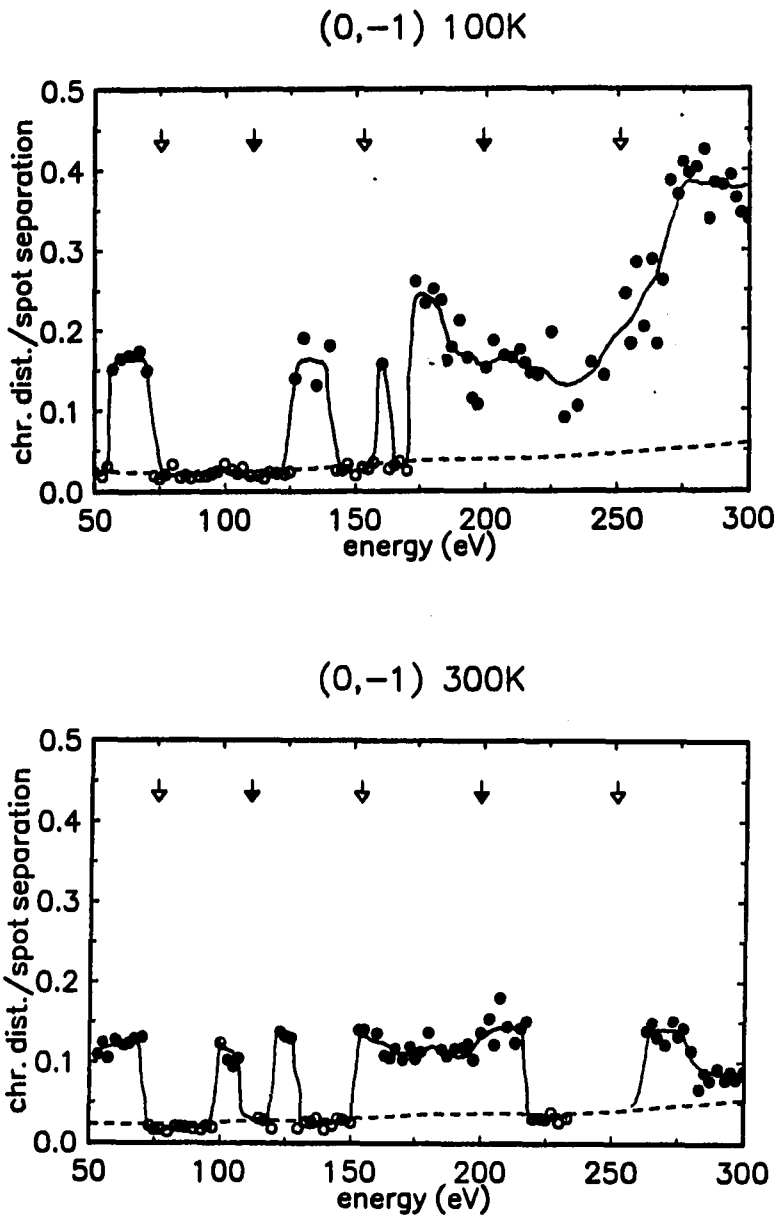

Figure 6. (0,-1) Reciprocal-space characteristic distance as a function of energy at 100 and 300 K for ca. 1/2 ML Pd on Pd(100)

The symbols are defined in the text. The line through the data reflects the energy-dependence of the profile shape.

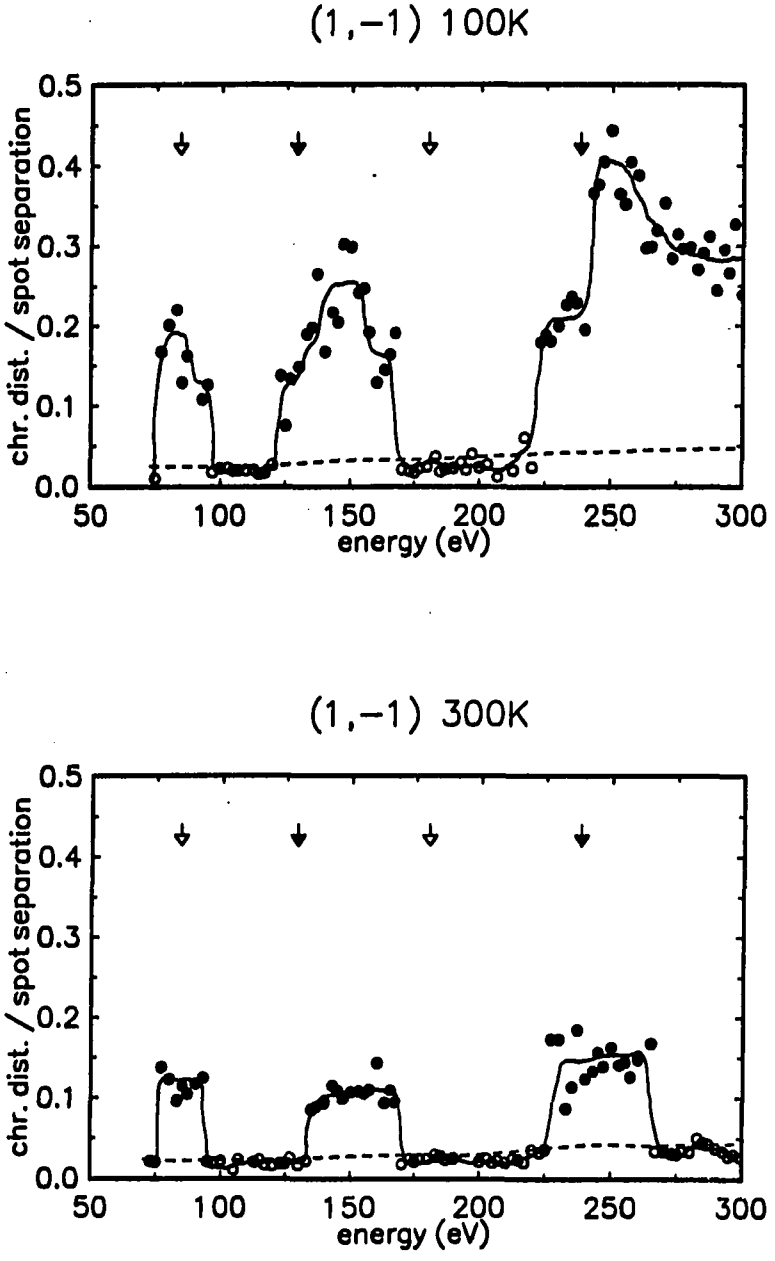

Figure 7. (1,-1) Reciprocal-space characteristic distance as a function of energy at 100 and 300 K for ca. 1/2 ML Pd on Pd(100)

The symbols are defined in the text. The line through the data reflects the energy-dependence of the profile shape.

equation (1). As a visual aid, a line through both filled and empty circles demonstrates how the basic profile shape changes as a function of energy. We see from these figures that the structure in the profiles is energy-dependent, but the maxima of Figures 6 and 7 do not necessarily correspond with out-of-phase energies predicted by equation (1). The experimentally observed out-of-phase energies (determined from the maxima) are summarized in Table 1.

Table 1. Comparison of three methods for experimental determination of out-of-phase energies

(a) (0,-1): Each column represents an out-of-phase energy, calculated according to equation (1). Values entered in each row are evaluated from our data and reported in eV.

(0,-1)		S = 3.5 45 eV	S = 4.5 111 eV	S = 5.5 199 eV	S = 6.5 307 eV
FWHM	100 K	63	??	174	262
	300 K	≤ 61	102	184	272
A/A_0*	100 K	??	(87,115) 101	(150,201) 175	(236,274) 255
	300 K	≤ 50	113	(172,201) 187	(242,292) 267
S-D**	100 K	55	100	180	280
	300 K	53	100	189	282

* Numbers in parentheses are maxima of A/A_0 curve, assuming a symmetrically-split peak. The reported value is the average.

** S-D = spike-difference

?? cannot be determined from data

Table 1. . (continued)

(b) (1,-1): Each column represents an out-of-phase energy, calculated according to equation (1). Values entered in each row are evaluated from our data and reported in eV.

(1,-1)		S = 4.5 47 eV	S = 5.5 129 eV	S = 6.5 238 eV
FWHM	100 K	83	147	236
	300 K	85	151	237
A/A_0^*	100 K	(73,108) 91	(120,166) 143	(211,286) 249
	300 K	(87,103) 95	(113,151) 144	(195,235) 215
S-D**	100 K	83	149	241
	300 K	84	156	251

IV. DISCUSSION

The out-of-phase diffraction profiles of Figures 3 and 4 consist of a summation of two components, a sharp-component (central-spike), and a ring-like or low intensity broadened-component (foot). Such diffraction features are typical during epitaxial growth (14,26). The broadened-component is the resultant of scattering from a distribution of islands of various sizes and separations which develop during growth, and reflects pair-correlations within a layer. Two-component lineshapes have been experimentally obtained for epitaxial growth of W/W(110) (18), Si/Si(111) (12,27,28) Pt/Pd(100) (10,11) and Pd/Pd (19).

It is fortuitous that in our previous study of Pt thin film growth on Pd(100) (10,11), between 300 and 350 K the island distribution was narrow enough to show appreciable foot intensity, yet broad enough to prevent ring structure. Without ring-structure, the FWHM of the total profile (i.e., without component separation) was always straightforwardly determinable, and was used as a measure of the reciprocal-space characteristic distance. The energy-dependence mimicked the expected trend: near the out-of-phase energy the central-spike intensity decreased such that the half-maximum probed some portion of the foot; near the in-phase energy the sharp-component regained intensity such that the FWHM fell somewhere on the central-spike. The variation of the FWHM with energy allowed the experimental determination of the out-of-phase energy. We stress that this determination via simple FWHM measurement was possible only because the coverage distribution was such that both

components of the profile were probed as a function of energy. However, it is important to realize that the data of reference 10 propose a misleading representation of the system, inasmuch as the reported FWHM is not a measure of a characteristic surface dimension. The FWHM of these "composite" profiles is determined solely by the relative heights of each separate component, and does not necessarily reflect information on correlations on the surface or a "characteristic" distance; rather it is a convoluted measurement strongly dominated by the complex energy-dependence of the intensity of each component of the profile.

The data of the present study show that, besides being an unphysical parameter for describing two-component profiles, the FWHM of the total profile is not rigorously determinable when the profiles exhibit ring-structure. Profiles should be separated, *then* ring diameters or FWHMs of broadened-components measured. However, our instrument does not have sufficient sensitivity to always allow unambiguous separation of the low-amplitude, foot from the constant background, particularly at low temperatures, where islands are very small and widely distributed. The distinction between a one-component and two-component lineshape is not always obvious. Therefore a rather large error is associated with the reciprocal-space characteristic distance measurement in these cases.

An alternative measurement of the out-of-phase energy is derived from the energy-dependence of A/A_0, the ratio of the broadened-component to total profile intensity. Closed forms for the energy- and coverage-dependence of A/A_0 have been derived (14,26). At half-monolayer coverage, A/A_0 should oscillate with energy between zero and unity, for

in-phase and out-of-phase scattering, respectively. At the out-of-phase energy, A/A_0 is predicted to oscillate with coverage between 1 and 0 for half-layer and full-layer coverages. Experimentally, Gronwald and Henzler did observe oscillations in the energy- and coverage-dependence of A/A_0 for epitaxial growth of Si on Si(111), but the amplitude of these oscillations did not reach the predicted extremes (27). Disagreement between theory and experiment was attributed to experimental uncertainties in obtaining exact half-monolayer coverage (26). (In fact, the extreme sensitivity of A/A_0 to the layer-coverages for two- and three-level systems was evaluated by Lent and Cohen (14). As the third-level coverage increases, the maxima of A/A_0 decrease, but remain peaked at the out-of-phase energies. With third-level scattering greater than ca. 20%, the A/A_0 maxima are split symmetrically about the out-of-phase condition.) Nonetheless, out-of-phase energies should be available experimentally via inspection of the energy-dependence of A/A_0.

Figures 8 and 9 show the energy-dependence of A/A_0, for the (0,-1) and (1,-1) beams, for ca. 1/2 ML Pd deposited at 100 and 300 K. The abstraction of A is ambiguous when the profiles exhibit ring-structure. We choose A to be the height of the profile under the central-spike, which in some cases is less than the overall height of the ring. Distinct maxima are observed in Figures 8 and 9 for deposition at 300 K. At 100 K the maxima are not as distinct. Whether or not these data show the splitting predicted by Lent and Cohen for appreciable third-level occupation (14), outside of experimental fluctuation, is debatable. Assuming that the split is statistically significantly, we determine the

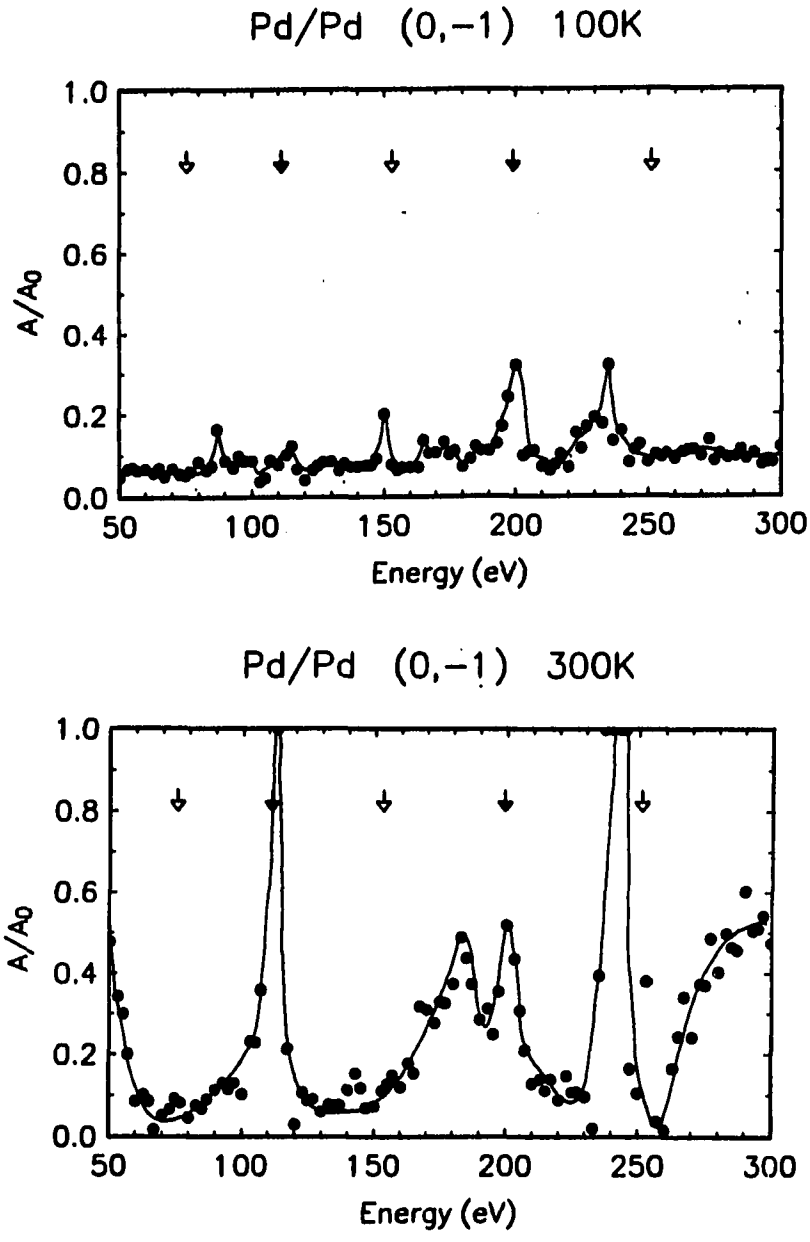

Figure 8. (0,-1) A/A_0 for ca. 1/2 ML Pd deposited on Pd(100) at 100 and 300 K as a function of energy

The solid line, added as a visual aid, assumes the A/A_0 maxima are split, as predicted by reference (14). The arrows are defined previously in the text.

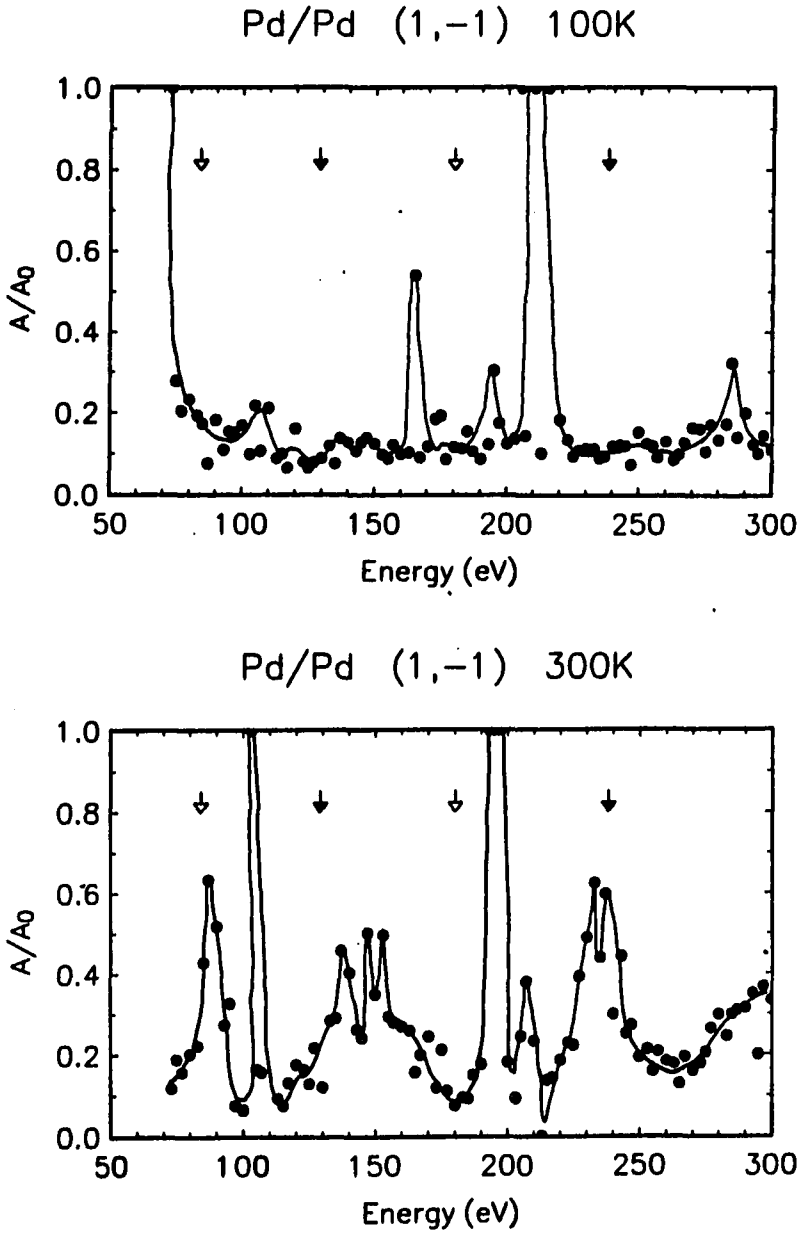

Figure 9. (1,-1) A/A_0 for ca. 1/2 ML Pd deposited on Pd(100) at 100 and 300 K as a function of energy

The solid line, added as a visual aid, assumes the A/A_0 maxima are split, as predicted by reference (14). Arrows are defined previously in the text.

out-of-phase voltages shown in Table 1.

Clearly, the energy-dependence of the FWHM and A/A_0 both show an inadequacy in determining out-of-phase energies in these experiments. Some of the values derived for Table 1 are based on judgement calls that perhaps others would make differently. For example, one may question whether the chosen A/A_0 maxima in the 100 K data of Figures 8 and 9 are actually physically significant. Some structure in the energy-dependences in Figures 6 through 9 are knowingly ignored. And, we have already mentioned the large uncertainties associated with abstracting the broadened-component from the base of the profiles, particularly when it is of very low intensity. We now present an alternative view of the energy-dependence of the profile data, useful for determining conditions under which appreciable intensity oscillations during thin film growth may be monitored. This procedure is based on variations in the central-spike intensity, and is complementary to the methods already discussed.

The energy-dependence of the intensity, I(V), diffracted from a surface is quite complex (29-31). There are peaks at incident wavelengths that satisfy Bragg's law of diffraction due to the fact that electrons can penetrate several layers into the crystal. These are the so-called kinematic, or single-scattering, peaks. In this picture, the out-of-phase condition should always coincide with a minimum in the I(V) curve. Secondary peaks arise from multiple-scattering events, which are not represented in the kinematic approximation.

Changes in the I(V) due to the presence of steps on the surface are superimposed on this already-complicated energy-dependence. Laramore and

coworkers modelled the effect on the I(V) resulting from a Gaussian distribution of step heights (32), which was successfully applied in a study of Al(110) (33). Laramore showed that the main effect of a distribtuion of steps is to shift the principal (Bragg) peaks toward higher energies (with respect to the flat surface), by reducing the low-energy portion and augmenting the high-energy portion of each peak.

Figures 10 and 11 show the profile maximum (proportional to the total intensity at $S_{\parallel} = 0$) as a function of energy for the (0,-1) and (1,-1) beams of the clean and 1/2 ML-covered surfaces at 100 and 300 K. [Due to the long times required for data acquisition, the intensities are undoubtedly affected by residual gas adsorption, particularly at 100 K, and should not be compared to I(V) curves. However, since the clean and 1/2 ML experiments were done in identical fashion, the data are directly comparable to each other.] The diminution of the low-energy side of each principal peak is evident. The high-energy side of each peak for the clean and covered surfaces usually overlap. Secondary peaks associated with residual gases or multiple-scattering, for the most part, are not affected.

The two-component lineshape of these profiles compels us to consider the changes in the energy-dependence of the central-spike intensity upon deposition. Plotted in Figures 12 and 13 is the height of the sharp-component [i.e., $(A_0 - A)$] of the (0,-1) and (1,-1) beams for the clean and covered surfaces at 100 and 300 K. These curves have an energy-dependence similar to the total intensity (Figures 12 and 13), demonstrating the dominance of the sharp-component in the overall energy-

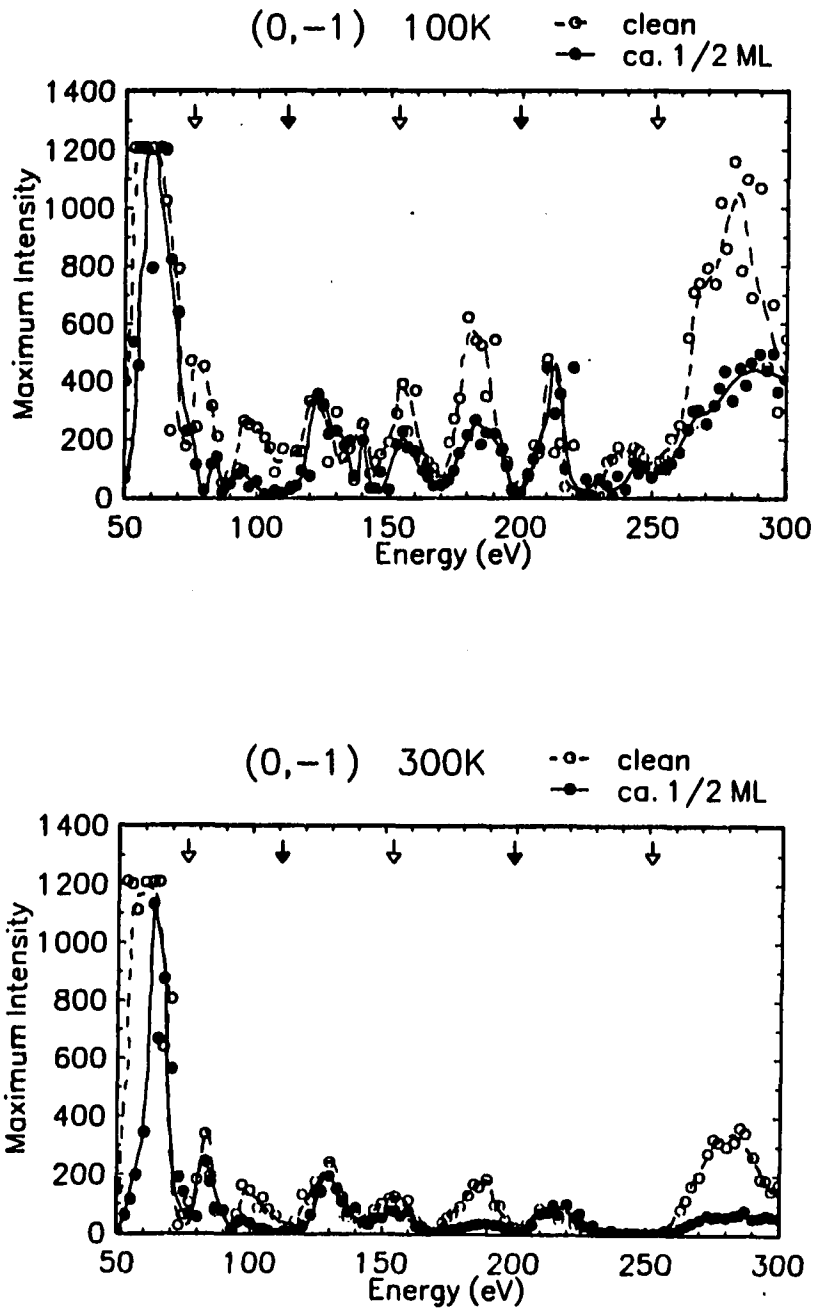

Figure 10. (0,-1) Maximum intensity (S_1 = 0) at 100 and 300 K as a function of energy

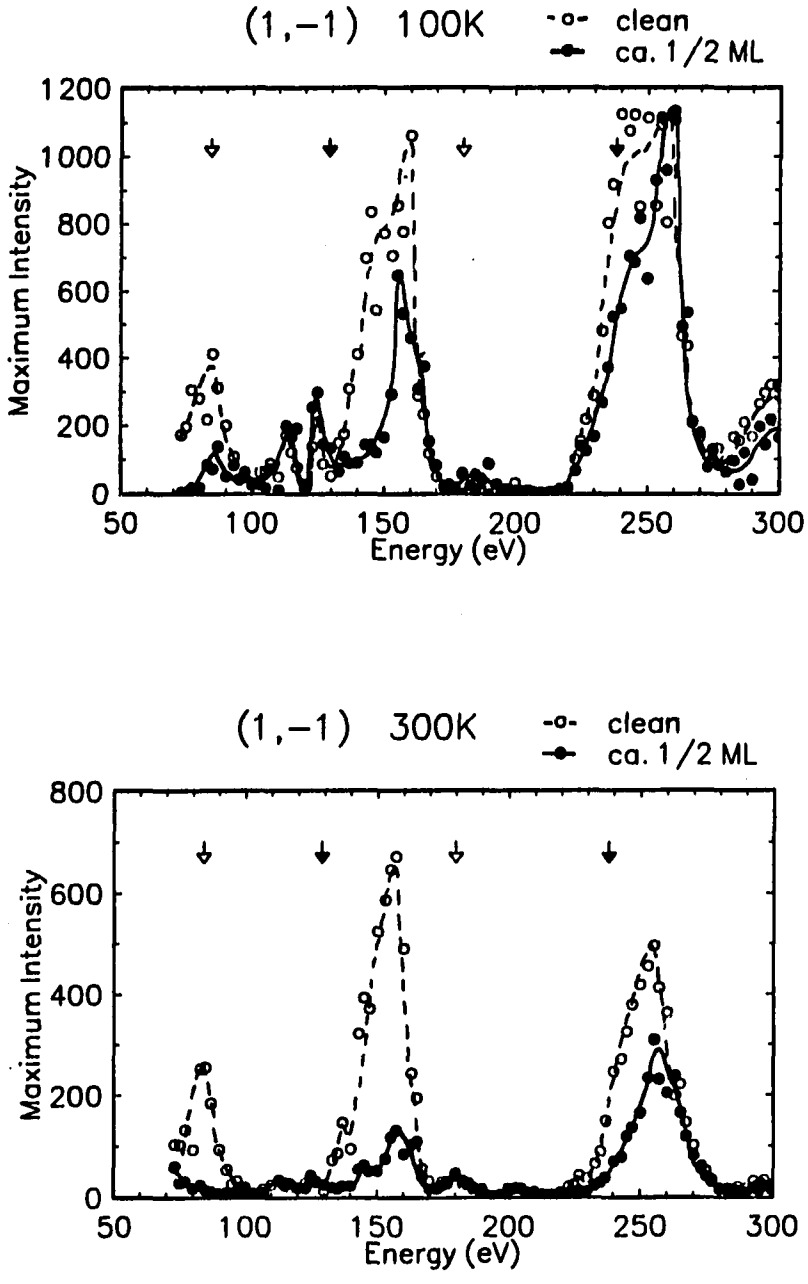

Figure 11. (1,-1) Maximum intensity (S_j = 0) at 100 and 300 K as a function of energy

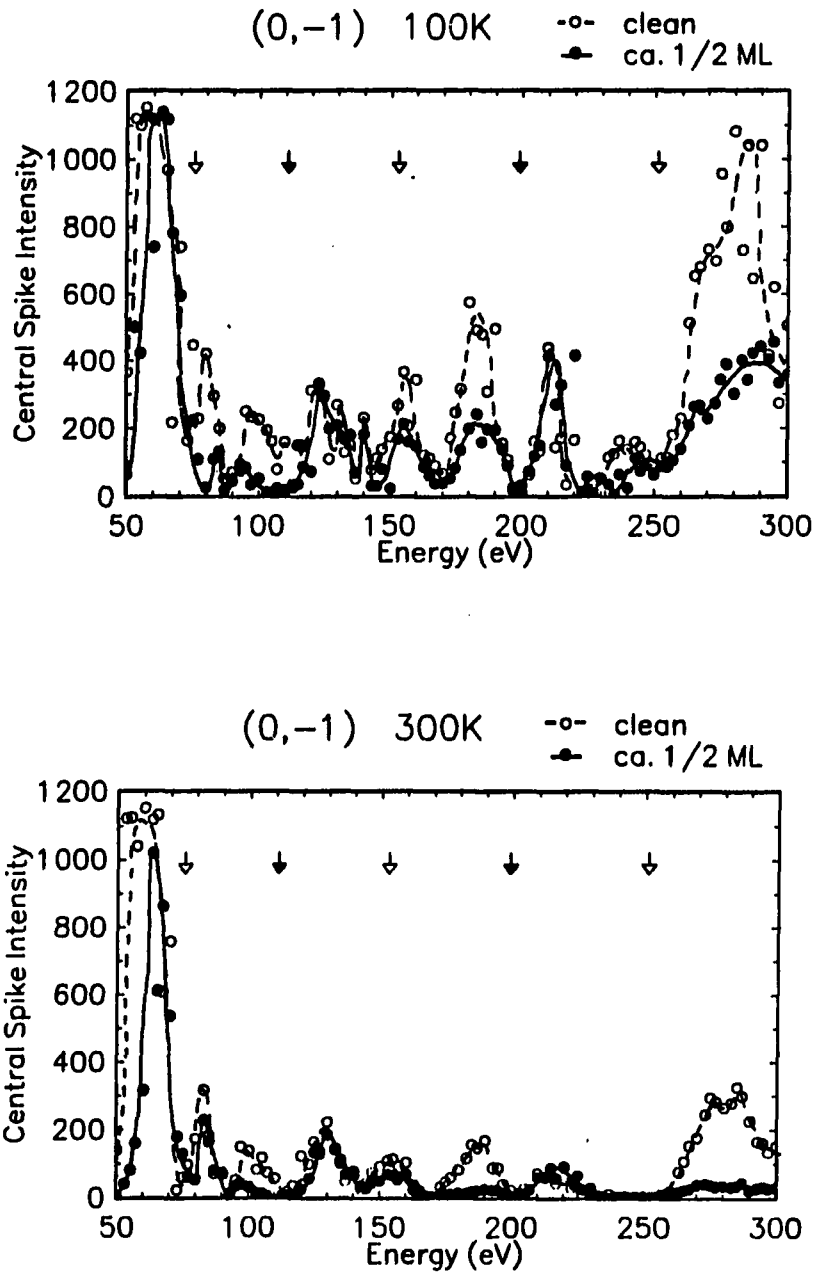

Figure 12. Energy-dependence of the (0,-1) sharp-component intensity, as defined in the text (S_I = 0), at 100 and 300 K

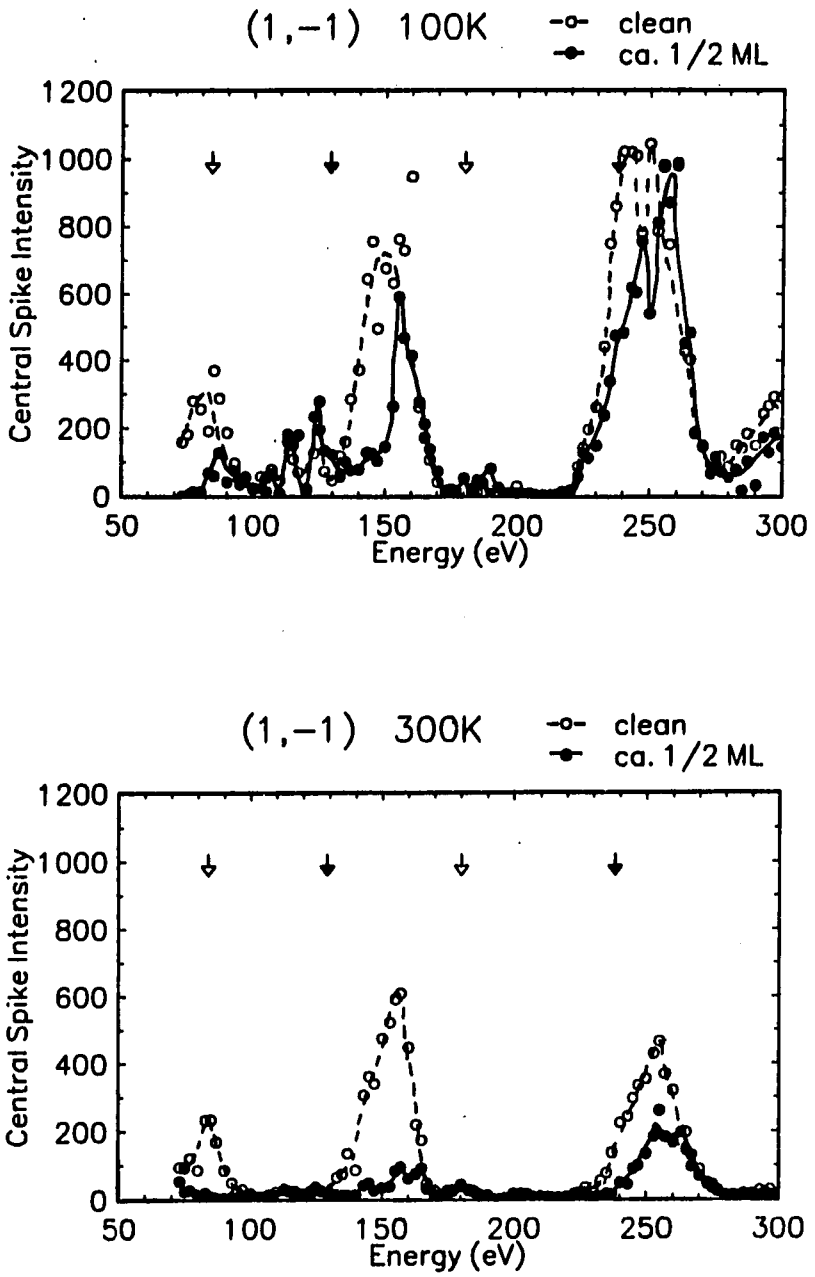

Figure 13. Energy-dependence of the (1,-1) sharp-component intensity, as defined in the text (S_I = 0), at 100 and 300 K

dependence.

We define the spike-difference at any energy as the absolute difference in central-spike intensity between the clean surface and that from a surface covered with about half-monolayer deposit. Coverage should be near half-monolayer, but exactly half-monolayer is not required. Since the spike-difference is not normalized, as is the FWHM (via the spot separation) or A/A_0 (via A_0), and especially since it is derived from two separate experiments, the spike-difference is more subject to experimental fluctuations than either of those methods. We also note that in the evaluation of A/A_0, the impact of multiple-scattering effects on the data is minimized by the division by A_0, whereas the spike-difference would seemingly enhance the observation of multiple-scattering effects. However, as we now demonstrate, the energy-dependence of the spike-difference provides an alternate measurement of viable out-of-phase conditions.

Figures 14 and 15 show the spike-difference as calculated from Figures 12 and 13. Distinct maxima are observed despite indications exact half-monolayer coverage is missed in the 100 K experiment. For Pd/Pd(100), out-of-phase energies determined via the spike-difference at 100 and 300 K are summarized in Table 1.

One criticism of this procedure is that by the nature of the spike-difference evaluation (i.e., simple substraction), the strongest peaks tend to dominate the result. However, out-of-phase energies best suited to monitoring intensity oscillations during thin film growth are those with *maximized* differences between the clean and covered surfaces,

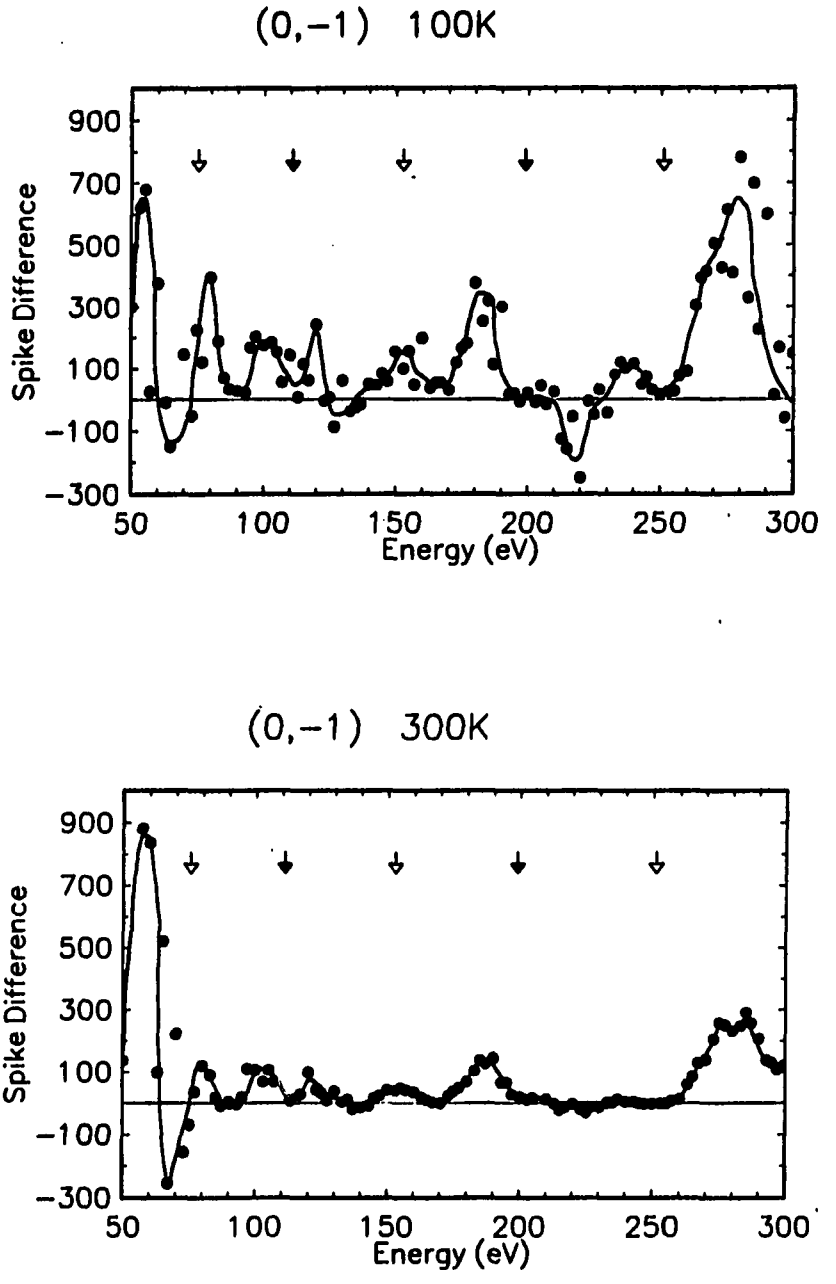

Figure 14. Spike-difference (as defined in the text, (S_1 = 0)) of the (0,-1) as a function of energy, at 100 and 300 K

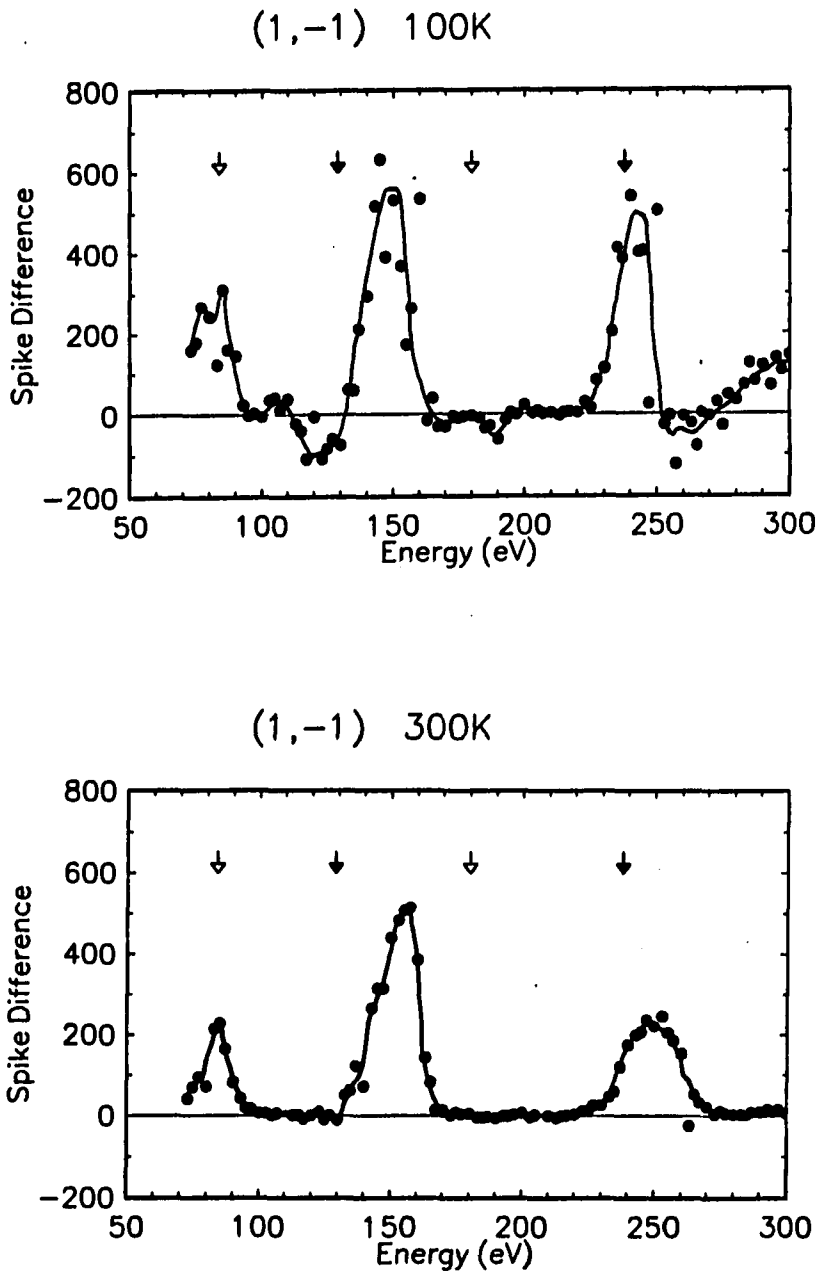

Figure 15. Spike-difference (as defined in the text, (S_l = 0)) of the (1,-1) as a function of energy, at 100 and 300 K

balanced by the highest initial intensity. The maximum difference ensures a high sensitivity to the presence of steps. A high initial intensity is required since intensity is usually damped as growth proceeds. Lastly, one might consider the energy itself. Since multiple-scattering effects are minimized at lower energies (34), low energies are preferred if data are to be interpreted within the kinematic approximation.

V. CONCLUSIONS

We demonstrate the usefulness of representing diffraction data in terms of the spike-difference when experimentally determining out-of-phase energies suitable for monitoring intensity oscillations during thin film growth. One simply calculates the difference in the sharp-component of a diffraction profile, between the clean and approximately half-monolayer covered surfaces. The best suited out-of-phase energies are those of maximized difference. This evaluation is particularly suitable for homoepitaxial studies. It is less applicable for hetereoepitaxy, except in those cases where scattering factors of the substrate and overlayer are well matched.

Out-of-phase energies obtained in this representation for Pd on Pd(100) at both 100 and 300 K are presented in Table 1. We have shown that consistent out-of-phase determinations are obtained with the spike-difference even where irregular beam shapes or very short-ranged correlations obscure straightforward evaluation via other methods. The *experimental* determination of out-of-phase conditions is necessary for intensity oscillation studies of thin film growth, since theoretical predictions (15) do not always provide workable results. The spike-difference determination may be used as a complement to, or in place of, FWHM or A/A_0 out-of-phase determinations.

REFERENCES

1. J. W. A. Sachtler, M. A. Van Hove, J. P. Biberian and G. A. Somorjai, Phys. Rev. Lett. 45 (1980) 1601; also Surface Sci. 110 (1981) 19.
2. J. W. A. Sachtler, J. P. Biberian and G. A. Somorjai, Surface Sci. 110 (1981) 43.
3. J. W. A. Sachtler and G. A. Somorjai, J. Catalysis 81 (1983) 77.
4. Research Briefings 1986 (National Academy Press, Washington, DC, 1986).
5. Thin Film Growth Techniques for Low-Dimensional Structures, edited by R. F. C. Farrow, S. S. P. Parkin, P. J. Dobson, J. H. Neave and A. S. Arrott (Plenum Press, New York, 1987).
6. R. Kern, G. Lelay and J. J. Métois in Current Topics in Materials Science, Volume 3, edited by E. Kaldis (North-Holland, Amsterdam, 1979).
7. G. Honjo and K. Yagi, in Current Topics in Materials Science, Volume 6, edited by E. Kaldis (North-Holland, Amsterdam, 1980).
8. Reflection High Energy Electron Diffraction and Reflection Imaging of Surfaces, edited by P. K. Larson and P. J. Dobson (Plenum Press, New York, 1988).
9. J. H. Neave, B. A. Joyce, P. J. Dobson and N. Norton, Appl. Phys. A 31 (1983) 1.
10. D. K. Flynn, W.-D. Wang, S.-L. Chang, M. C. Tringides and P. A. Thiel, Langmuir 4 (1988) 1096.

11. D. K. Flynn, J. W. Evans and P. A. Thiel, J. Vacuum Sci. Technol. A 7 (1989) 2162.

12. R. Altsinger, H. Busch, M. Horn and M. Henzler, Surface Sci. 200 (1988) 235.

13. J. J. De Miguel, A. Cebollada, J. M. Gallego, J. Ferrón and S. Ferrar, J. Crystal Growth 88 (1988) 442.

14. C. S. Lent and P. I. Cohen, Surface Sci. 139 (1984) 121.

15. M. Henzler, Surface Sci. 22 (1970) 12.

16. M. Henzler, Appl. Phys. A 34 (1984) 205.

17. M. Henzler, in Electron Spectroscopy for Surface Analysis Topics in Current Physics, Volume 4, edited by H. Ibach (Springer-Verlag, Berlin, 1977).

18. P. Hahn, J. Clabes and M. Henzler, J. Appl. Phys. 51 (1980) 2079.

19. D. K. Flynn-Sanders and P. A. Thiel, Chemistry Dept., Iowa State University, manuscript in preparation (1990).

20. E. Bauer and J. H. van der Merwe, Phys. Rev. B 33 (1986) 3657.

21. S. L. Beauvais, R. J. Behm, S.-L. Chang, T. S. King, C. G. Olson, P. R. Rape and P. A. Thiel, Surface Sci. 189/190 (1987) 1069.

22. J. W. Anderegg and P. A. Thiel, J. Vacuum Sci. and Technol. A 4 (1986) 1367.

23. B. C. DeCooman and R. W. Vook, J. Vacuum Sci. Technol. 21 (1982) 899.

24. see, for example, Figure 2 of M. Henzler, Surface Sci. 168 (1986)

744; also, Figure 1 of G. Schulze and M. Henzler Surface Sci. 73 (1978) 553.

25. M. Henzler, Appl. Surface Sci. 11/12 (1982) 450.
26. J. M. Pimbley and T.-M. Lu, J. Appl. Phys. 57 (1985) 1121; 57 (1985) 4587; 59 (1986) 2439.
27. K. D. Gronwald and M. Henzler, Surface Science 117 (1982) 180.
28. M. Henzler, Surface Sci. 168 (1986) 744.
29. L. J. Clarke, Surface Crystallography: An Introduction to Low Energy Electron Diffraction (John Wiley and Sons, New York, 1985).
30. J. B. Pendry, Low Energy Electron Diffraction (Academic Press, London, 1974).
31. J. J. Lander, in Progress in Solid State CHemistry, Volume 2, edited by H. Reiss (Pergamon Press, Oxford, 1965).
32. G. E. Laramore, J. E. Houston and R. L. Park, J. Vac. Sci. Technol. 10 (1973) 196.
33. D. Aberdam, R. Baudoing, Y. Gauthier, Surface Sci. 62 (1977) 567.
34. L. D. Roelofs, A. R. Kortan, T. L. Einstein, R. L. Park, Phys. Rev. Lett. 46 (1981) 1465.

APPENDIX: RECOATING LEED OPTICS

The phosphor coating on a LEED screen is very fragile and may become damaged, either by insulating inclusions, metal overlayers, cracks in the phosphor coating or the development of "dark spots". All of these problems can be remedied by coating the screen with a fresh surface of phosphor. Described below is a recoating technique based on sedimentation of a suspension onto the screen. Extreme care must be taken in the preparation of the solution to minimize the number of aggregated particles. The phosphor simply settles on the LEED screen and then the solution is gradually drained out. Lastly, the screen is slowly dried to remove residual water.

Pretreatment

The LEED screen is made of either aluminum or stainless steel. The Varian 981-0129 is made of stainless steel. Determine which you have and follow the prescribed pretreatment.

Stainless Steel: Degrease with methanol. A pickle is necessary only when removing a previous coating. One of two pickles may be used. Pickle 1: 30 volume % HNO_3, 3 volume % HF. Warming the solution will quicken its action. See note below concerning HF safety. Pickle 2: 100 ml HNO_3, 20 ml HF, 20 ml HCl, 800 ml warm deionized, distilled water. See note below concerning HF safety.

(We used the second pickle for about 5 minutes in the ultrasonic bath.)

Aluminum: Degrease with methanol. Dip for 20 seconds in a 6 volume % HF solution. Rinse carefully with deionized, distilled water. Dip for 60 seconds in a 32 volume % solution of HCl. Do not dip for longer than these times. If the aluminum turns black in the HCl solution, repeat the HF and HCl dips. See note below concerning HF safety.

HF Safety: HF is an extremely hazardous acid which may cause severe burns very deep into the tissue. Use of HF requires the utmost care, and special safety precautions must be taken. Protective clothing is essential. In our laboratories, a face shield, neoprene gloves (mid arm length) and neoprene apron are stored under the sink in room 220. Special nalgene labware, including beakers and graduated cylinders are also stored in this room, on the west wall shelves. HF is used only in the hood (room 217) and only when at least one other person is available in our laboratory area. In case of exposure to HF, immediately wash the exposed area of your body with plenty of water. This is very important, since often a burning sensation does not occur until several hours after the exposure. For this reason it is a good practice to wash well after using HF whether you are aware of an exposure or not. If you are aware of an exposure, contact Occupational Medicine and explicitly specify that

the exposure was to HF (not just acid), since the treatment for HF is different than that for other acids. Calcium gluconate gel is available in the first-aid closets for HF burns (EXCEPT in eyes). To use this gel, after washing with water (ca. 20 minutes) shake gel, apply, rub vigorously. You must still report to Occupational Medicine.

Solution Preparation

Prepare two solutions as described in detail below. Adjust ingredients proportionately to meet your requirements of total volume. The recipe below makes 3 l, which is an adequate volume for the Varian 981-0129 LEED screen. Assemble the following ingredients:

Solution 1: 2.5 l deionized, distilled water
1.8 g $Ba(NO_3)_2$

Solution 2: 0.5 l deionized, distilled water
0.18 g silica gel
3.18 g phosphor

A note about the phosphor. We have used RCA-33-Z-151M, a zinc sulphide phosphor activated with Ag, which contains no Cd. This phosphor is commonly used for black and white television screens. It gives bluish LEED spots, to which the camera is sensitive, but not your eyes. The particles of this phosphor are rounded polyhedra, i.e., somewhat

crystalline, that range from 1.5 to 6 microns in diameter. There are, however, quite a number of clustered particles that are approximately 15 to 30 microns. A better phosphor to use is Lumilox® Yellow-Green B20-1B. It is available from Riedel-DeHaan AG, Seelze Hannover, Federal Republic of Germany. This phosphor has a yellow-green emission to which both your eye and the camera are sensitive. However, this phosphor contains beryllium, which is absorbed through the skin and is toxic (especially in this powdered form), and, thus OSHA regulated. This phosphor is made up of highly spherical particles, more uniform in size, 2-3 microns. Again, clusters of 15-30 microns are common. Because of high toxicity, extreme care must be taken to avoid contact with this phosphor. Always wear gloves and avoid breathing the dust.

The object of the following procedure is to get a homogeneous solution of small, fine phosphor particles. A large ultrasonic bath is necessary. A sonic disruptor (also called an ultrasonicator, but not to be confused with an ultrasonic bath) may also be used, and is recommended for preparation of the RCA phosphor. Adjust the procedure to fit whatever equipment is on hand to achieve the final goal: homogeneous solution of small, fine particles. At Ames Laboratory, there was a sonic disruptor in the group of Dr. Burkhart, once located in Metals Development (it may take a bit of searching to find that equipment now). A few words of caution. All water, including rinse water, should be deionized, distilled water. Make sure <u>all</u> of the glassware used is clean and free of dust. Unless specified, do not let the phosphor solution stand. Continue immediately with the next step to prevent settling.

Always cover the solutions to protect from dust. Never put a volumetric flask *with* a stopcock in the ultrasonic bath. The stopcock will get wedged down by the action of vibration and become nearly impossible to remove.

Solution 1:

Add the $Ba(NO_3)_2$ to a convenient amount of water in an Erlenmeyer or volumetric flask (300-500 ml). Shake vigorously by hand for 2 minutes. Put in the ultrasonic bath until ready to use, anywhere from 10 minutes (minimum) to 2+ hours. The solutions will get hot after some time in the ultrasonic bath, so be sure to periodically (ca. every 10-30 minutes) check the bath temperature and replace the bath water with cool water as necessary. Also, periodically shake the solution vigorously by hand. Shake vigorously before using.

Solution 2:

Because aggregated particles are prevalent in the RCA phosphor, we use a sonic disruptor to prepare this solution. In a beaker, make a solution of the silica gel and phosphor with 150 to 175 ml of water. Use the sonic disruptor at 30 % duty cycle on a setting of 4, while stirring vigorously with a magnetic stirbar. Continue for about 5 minutes. Stop to let the solution cool if necessary. Continue for about another 6 minutes. Use immediately. If using the Lumilox® phosphor, combine water, phosphor + silica gel in a volumetric or Erlenmeyer. Shake vigorously by hand for ca. 2 minutes. Put in

ultrasonic bath for ca. 5 minutes. Repeat the hand-shaking and ultrasonic steps. Use immediately.

Transfer the phosphor solution into a large Erlenmeyer (≥ 1 l) using the rest of the 500 ml total of water in a squirt bottle to completely transfer the solution from the beaker. Add the $Ba(NO_3)_2$ solution, using water to rinse and make a final volume of ca. 1 l. Shake vigorously by hand 1-2 minutes. Put in ultrasonic bath for 10 minutes. Shake vigorously again by hand for 1-2 minutes. Pour into a 3 or 4 l beaker (a 4 l beaker is available from Dr. Gerstein's group). Rinse the flask several times with deionized, distilled water adding the wash to the beaker. Fill to 3 l with deionized, distilled water to make 3 l. Using a large stirbar (ca. 3 inch), stir on highest setting of stirplate for 5-10 minutes. When the vortex disappears, let the solution settle for 10 minutes. This allows for the sedimentation of large particles. (Be sure that the solution is covered to prevent dust contamination.) Time the settling period. If this period is too long, the desired, finer particles will settle. Carefully decant the solution into another beaker. Do not stir up the bottom of the solution while pouring, and leave enough solution behind to avoid pouring out larger particles. Cover the decanted solution and let settle for 7 minutes. Using a funnel, and directing the solution away from the screen, carefully decant this solution into the sedimentation beaker (in which the LEED screen is already suspended, as described below). It is important to pour evenly

and continuously, to avoid introducing air into the solution. Trapped air may form bubbles which adhere to the LEED screen.

Sedimentation Process

The sedimentation beaker is a 3 l beaker with a stopcock glassblown in the center of the bottom. Set the beaker on a ringstand, or other appropriate holder, as level as possible. Use an area that is as free of vibration as possible, perhaps in an unused room on a thick neoprene mat. Suspend the LEED screen about 3/4 (or slightly more) the distance to the bottom of the beaker using 3 hooks made from stiff wire. Attach the hooks to the screen through the holes near the perimeter of the screen, and bending them around the sides of the beaker (see Figure 1). Do not support the screen in any other way, and do not let the screen hang too low. The goal is that nothing will disrupt the flow of the solution past the LEED screen while draining. Take care to level the screen. The hole in the screen for the electron gun invariably leaves a lingering drop which depletes/disrupts the coating around the hole. A level screen will leave this area is as small and symmetric as possible. Cover the beaker to prevent dust from settling.

Let the solution stand at least 5 hours, until it is very clear (we have used ~ 11 hours). After this time, carefully adjust the stopcock until the solution just begins to slowly drip out. Do not disturb the solution in any way which might disrupt the settled coating. This coating is very fragile, *especially* when it is wet. Set a flow rate to

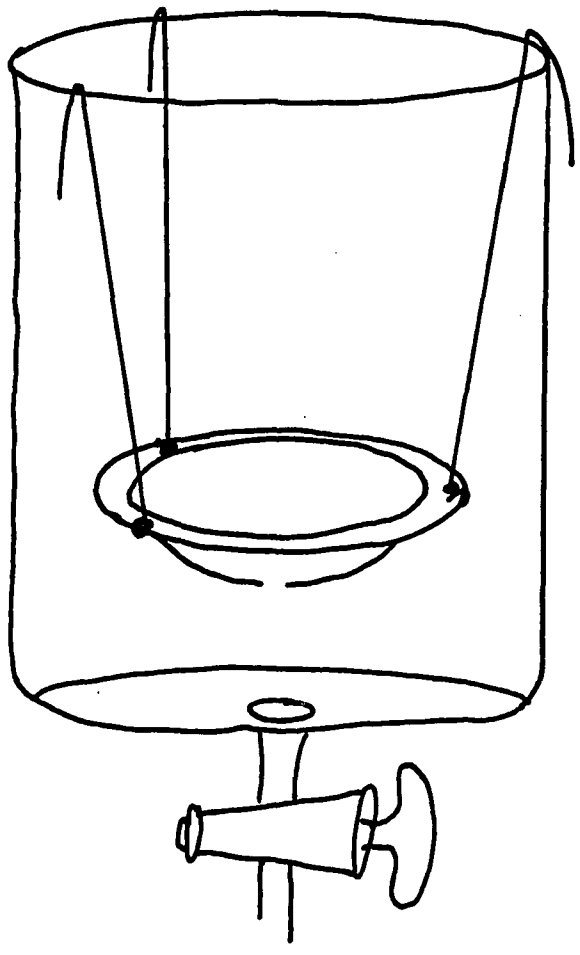

Figure 1. Beaker setup

3 l beaker adapted with a straight-through valve for draining. LEED screen is suspended in the beaker by three stiff wires shaped into hooks.

drain the entire solution in 3 or more hours. We have used ca. 1 drop per second to drain a 3 l solution.

Drying

After draining is complete, let the screen stand (covered) several hours, or overnight. When the screen appears dry, carefully lift it out of the sedimentation beaker and bake for half an hour at 80 C. Keep the screen covered to prevent dust from settling on it. Store the screen in a dust-free desiccator if necessary.

Results

The screen should look homogeneous, with no large particles, dust, bare or thin patches. The sedimentation process may be repeated up to 4 times, if necessary, to get a sufficiently thick coat. However, each time the process is repeated, there is a risk of "lifting" the previous coating, especially when filling the sedimentation beaker. It may be better to restart the procedure with more solution (i.e., in a taller beaker) and/or a more concentrated solution.

We have successfully used this technique to recoat the Varian 981-0129 LEED screen. We prepared the solutions in one day. Sedimentation proceeded overnight. The next day was devoted to draining, followed by room-temperature drying overnight. The third morning the screen was baked. Organization is important, since it is imperative the solutions are used immediately upon preparation. It is helpful if two people work together if time is essential. One person should prepare the solutions,

the other should prepare the screen and set up the sedimentation beaker. If two people are not available, prepare the screen and sedimentation beaker *before* preparing the solutions.

CONCLUSIONS

We examine the epitaxial growth of thin metal films via low-energy electron diffraction (LEED). In particular, we consider Pt and Pd on Pd(100) in an attempt to understand the basic growth processes and the potential of this technique. The main conclusions of this dissertation are summarized below:

(a) We demonstrate the use of a *conventional* LEED apparatus in monitoring diffracted intensity oscillations during the growth of Pt and Pd films on Pd(100). Despite the rather short coherence length of commercial instruments, our LEED profiles are adequately resolved into two separate components at out-of-phase energies. With LEED, we observe intensity oscillations during metal film growth, analogous to those measured with reflection high-energy electron diffraction during the epitaxial growth of semiconductors. The oscillations of the central-spike intensity are damped due to the growth of Pt and Pd/Pd(100) and rather short-lived. We show that only small deviations from perfect layer-by-layer growth severely diminish the central-spike intensity.

(b) The equilibrium growth mode both for Pt and Pd on Pd(100) is layer-by-layer. At low and intermediate temperatures, the system is kinetically limited by the barrier to surface diffusion. From distinct changes in the profile lineshapes with temperature, we estimate the diffusional barrier to be ca. 10 kcal/mol for Pt on Pd(100) and ca. 13 kcal/mol for Pd on Pd(100). At high temperatures, Pt reconstruction interferes with the growth of pseudomorphic layers on Pd(100). For Pd on

Pd(100), growth proceeds via "step propagation" at high temperatures. In this mechanism, nucleation of new layers begins only on very large terraces, thus the initial morphology is more or less maintained throughout growth.

(c) We observe oscillations in the out-of-phase diffracted intensity for the growth of Pt and Pd on Pd(100) at substrate temperatures as low as 95 K. We show intensity oscillations are *predicted* for random deposition at low temperatures, *even in the absence of surface diffusion.* This is in contrast to the assertion by other authors (22) that deposited atoms use their latent heat of condensation (ca. 70 kcal/mol for metal systems) and are transiently mobile, aiding in the development of quasi-layer-by-layer growth. We demonstrate that the *necessity* of creating the fourfold-hollow adsorption site for the birth of an upper layer is sufficient to instill a quasi-layer-by-layer quality to the growth.

(d) Ring-structure in the profile lineshape develops at ca. 200 K for the growth of Pd on Pd(100), and is associated with the onset of diffusion. Indicative of a more uniform growth, ring-structure is evident between ca. 200 and 400 K. Herein is the first report of oscillations in the ring intensity as a function of coverage, demarking the detailed filling of individual layers. Although central-spike intensity oscillations show substantial damping, the *existence* of oscillations in the ring intensity indicates a growth mechanism quite close to perfect layer-by-layer.

(e) Based on the temperature- and coverage-dependence of the in-phase intensity during the epitaxial growth of Pd(100), we propose that in the limit of *very small* islands (one to a few atoms), the interlayer spacing is dependent on the number of atoms in the island. Recent molecular-dynamics simulations, showing that single Pd atoms on Pd(100) are 14 % closer to the Pd substrate than would be predicted from the first Pd(100) interlayer spacing support our postulate (23).

(f) We develop a model to clarify the role diffusion plays in initially enhancing the layer-by-layer quality of thin film growth on fcc(100) surfaces. Interlayer diffusion augments layer-by-layer growth for obvious reasons. Surprisingly, both intralayer and interlayer diffusion result in clustering which *reduces* the layer-by-layer quality. However, the net result of surface diffusion in the onset regime is to enhance the layer-by-layer quality of the growing film, as is observed in our experimental investigation.

(g) We present a novel, graphical representation for the layer-converges during thin film growth. This representation is not restricted to fcc(100) geometry, and can be generally applied to epitaxial growth systems. Deviations from layer-by-layer growth and the onset of diffusion are among the types of information that can be extracted from this new representation.

(h) We present a new procedure to experimentally determine out-of-phase energies suitable for monitoring intensity oscillations during thin film growth. This method, called the Spike-Difference, is based on the energy-dependence of the central-spike intensity, and appears to be less

sensitive to the coverage distribution than the FWHM or A/A_0 methods. The Spike-Difference may be used in conjunction with, or in place of, the FWHM and A/A_0 techniques.

In summary, we show conventional LEED is a useful technique in the investigation of epitaxial growth. A wealth of information is contained in the spot profile, and we are only now learning how to fully evaluate this information. Understanding the growth processes in the simple systems studied here is essential in furthering our knowledge of the creation of interfaces, making possible the development of new materials with novel physical and chemical properties.

REFERENCES

1. A. G. Sault and D. W. Goodman, in Advances in Chemical Physics, edited by K. P. Lawley (John Wiley and Sons, New York, 1989).
2. C. T. Campbell, in Advances in Catalysis, Volume 36, edited by D. D. Eley, H. Pines and P. B. Weisz, (Academic Press, Inc., San Diego, 1989).
3. J. H. Sinfelt, Bimetallic Catalysts (John Wiley and Sons, New York, 1983).
4. J. W. A. Sachtler, M. A. Van Hove, J. P. Biberian and G. A. Somorjai, Phys. Rev. Lett. 45 (1980) 1601.
5. J. W. A. Sachtler, M. A. Van Hove, J. P. Biberian and G. A. Somorjai, Surface Sci. 110 (1981) 19.
6. J. W. A. Sachtler, J. P. Biberian and G. A. Somorjai, Surface Sci. 110 (1981) 43.
7. J. W. A. Sachtler and G. A. Somorjai, J. Catalysis 81 (1983) 77.
8. D. W. Goodman and J. E. Houston, Science 236 (1987) 403.
9. D. W. Goodman and C. H. F. Peden, Ind. Eng. Chem. Fundam. 25 (1986) 58.
10. J. E. Houston, C. H. F. Peden, D. S. Blair, D. W. Goodman, Surface Sci. 167 (1986) 427.
11. C. H. F. Peden and D. W. Goodman, J. Catalysis 100 (1986) 520.
12. J. E. Houston, C. H. F. Peden, P. J. Feibelman, D. R. Hamann, Phys. Rev. Lett. 56 (1986) 375.

13. Magnetic Properties of Low-Dimensional Systems, edited by L. M. Falicov and J. L. Moran-Lopez (Springer-Verlag, Berlin, 1986).

14. J. J. Krebs, B. T. Jonker and G. A. Prinz, in Materials Research Society Proceedings, Volume 151, edited by B. T. Jonker, J. P. Heremans and E. E. Marinero (Materials Research Society, Pittsburgh, 1989) and references therein.

15. B. T. Jonker, K.-H. Walker, E. Kisker, G. A. Prinz, C. Carbone, Phys. Rev. Lett. 57 (1986) 142.

16. J. Gay and R. Richter, Phys. Rev. Lett. 56 (1986) 2728.

17. T. K. Gaylord and K. F. Brennan, Appl. Phys. Lett. 53 (1988) 2047.

18. C. R. O'Dell, Physics Today 43 (1990) 32.

19. E. Bauer and J. H. van der Merwe, Phys. Rev. B 33 (1986) 3657.

20. J. B. Pendry, Low Energy Electron Diffraction (Academic Press, New York, 1974).

21. L. J. Clarke, Surface Crystallography, An Introduction to Low Energy Electron Diffraction (John Wiley and Sons, Chichester, 1985).

22. W. F. Egelhoff, Jr. and I. Jacob, Phys. Rev. Lett. 62 (1989) 921.

23. D. E. Sanders and A. E. DePristo, Iowa State University, Chemistry Department, manuscript in preparation.

ACKNOWLEDGEMENTS

I thank my advisor, Pat Thiel, for her supervision and support throughout this work. She always saw the perspective when I found myself concentrating too much on details. I thank her for her guidance and the many skills she has helped me develop.

I am indebted to Dr. Jim Evans and Dr. Michael Tringides for inspiring discussions of the data and direction in the interpretation. I express gratitude to those who helped with the experiments: Wendi Wang, Dr. Wai Leung, Dr. NaiJuan Wu and Oden Warren. I extend a special appreciation to Oden Warren, who untiringly helped with equipment repairs. I must also mention Dr. Sheng-Liang Chang, a man of exemplary patience and perseverance, whom I'd often think of when frustrated by delicate clean-room tasks. In addition, I thank Jim Anderegg, for consultation over electronic and interfacing problems, and Charlie Burg, for skillful welding.

I thank the past and present members of the Thiel group, who made my work here enjoyable. Assistance was offered whenever requested, and I am most grateful. The comradery among group members made this place more than "just work". Fond memories will be held for the 5:00 "J" meetings. Special thanks to those who made birthdays in the Thiel group deliciously delightful: Mike Columbia, Pam Leavitt, Barb Nielsen, Mary Walczak and to the newest members who will carry on the tradition: Anna Crabtree and the "microwave king" Mark Jensen.

I thank my mother and father, Mary Ann and James, for their encouragement, love and support through all of my endeavors. I especially appreciate the love and patient understanding of my husband, David. His faith in me helped me to strive further.

I am grateful for the opportunity to work in Munich at the Institute of Physical Chemistry in the Spring of 1986. I enjoyed working with Dr. Jürgen Behm and Dr. Keith Jamison. The investigation of K on Ni(110) and Au(110), which is not included in this dissertation, was supported by the Alfred P. Sloan Foundation and the Deutscher Akademischer Austauschdienst.

I thank the Iowa State University Committee for Women in Science and Engineering, Procter and Gamble Company, Association for Women in Science Educational Foundation, American Vacuum Society and Dow Corning Corporation for financial assistance. This work was supported by the Ford Motor Company and the National Science Foundation, Grant No. CHE-8451317 and performed at Ames Laboratory under contract No. 7405-ENG-82 with the U.S. Department of Energy. This dissertation is assigned DOE Report No. IS-T-1415.

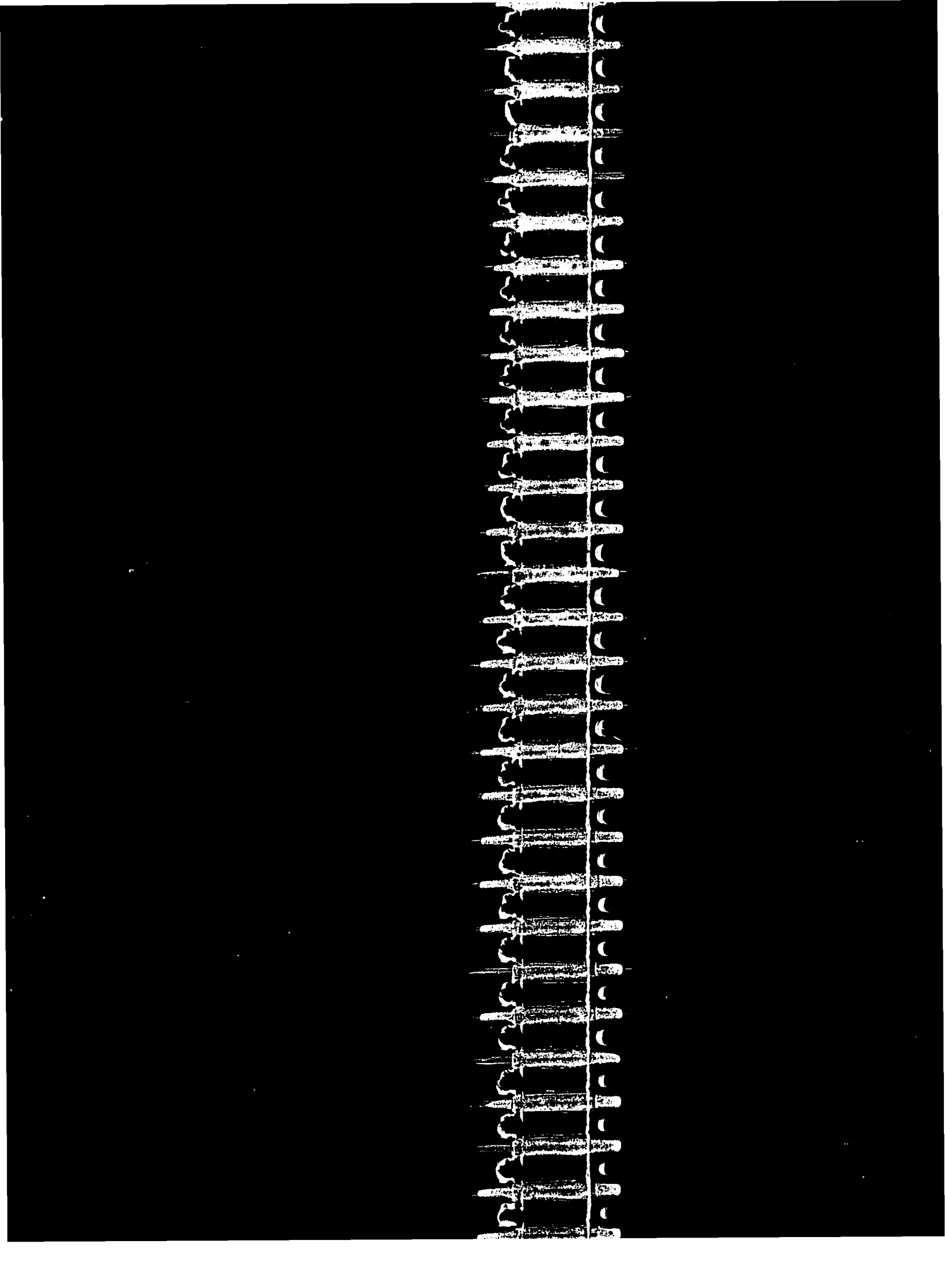

pendence.

We define the spike-difference at any energy as the absolute fference in central-spike intensity between the clean surface and that om a surface covered with about half-monolayer deposit. Coverage ould be near half-monolayer, but exactly half-monolayer is not quired. Since the spike-difference is not normalized, as is the FWHM ia the spot separation) or A/A_0 (via A_0), and especially since it is rived from two separate experiments, the spike-difference is more bject to experimental fluctuations than either of those methods. We so note that in the evaluation of A/A_0, the impact of multiple-attering effects on the data is minimized by the division by A_0, ereas the spike-difference would seemingly enhance the observation of ltiple-scattering effects. However, as we now demonstrate, the energy-pendence of the spike-difference provides an alternate measurement of able out-of-phase conditions.

Figures 14 and 15 show the spike-difference as calculated from gures 12 and 13. Distinct maxima are observed despite indications act half-monolayer coverage is missed in the 100 K experiment. For /Pd(100), out-of-phase energies determined via the spike-difference at 0 and 300 K are summarized in Table 1.

One criticism of this procedure is that by the nature of the spike-fference evaluation (i.e., simple substraction), the strongest peaks nd to dominate the result. However, out-of-phase energies best suited monitoring intensity oscillations during thin film growth are those th *maximized* differences between the clean and covered surfaces,

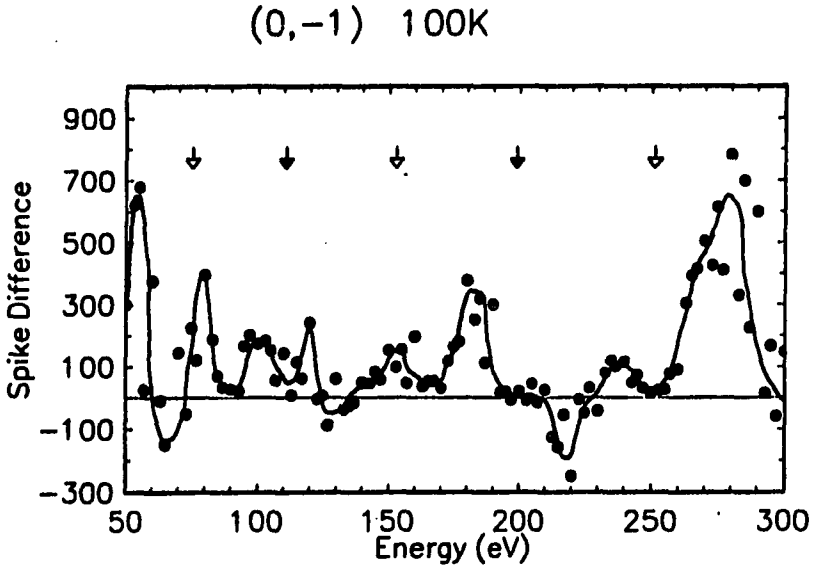

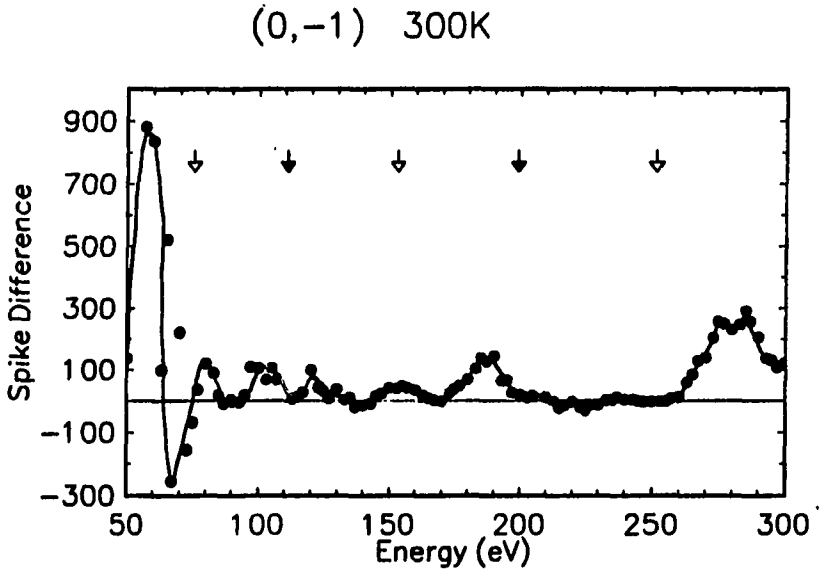

Figure 14. Spike-difference (as defined in the text, (S_1 = 0)) of the (0,-1) as a function of energy, at 100 and 300 K

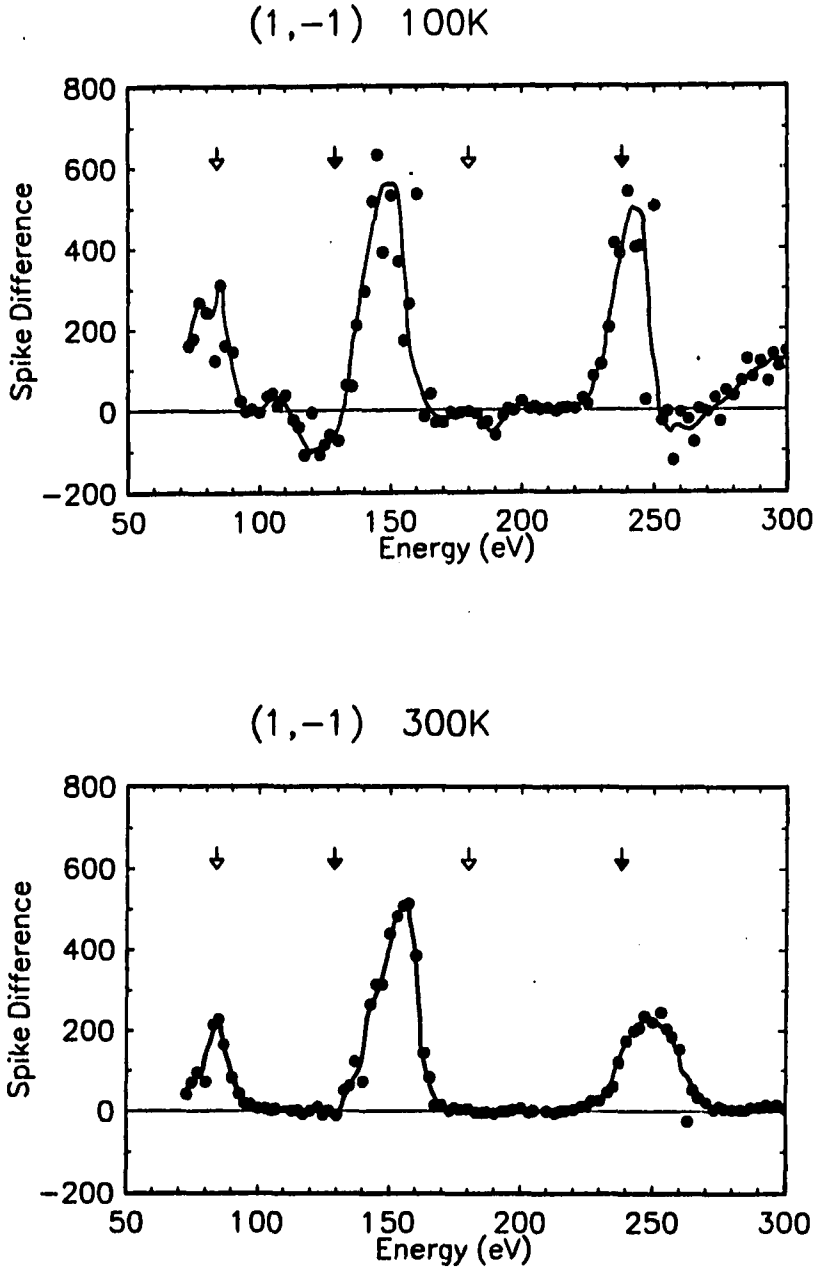

Figure 15. Spike-difference (as defined in the text, (S_1 = 0)) of the (1,-1) as a function of energy, at 100 and 300 K

balanced by the highest initial intensity. The maximum difference ensures a high sensitivity to the presence of steps. A high initial intensity is required since intensity is usually damped as growth proceeds. Lastly, one might consider the energy itself. Since multiple-scattering effects are minimized at lower energies (34), low energies are preferred if data are to be interpreted within the kinematic approximation.

V. CONCLUSIONS

We demonstrate the usefulness of representing diffraction data in terms of the spike-difference when experimentally determining out-of-phase energies suitable for monitoring intensity oscillations during thin film growth. One simply calculates the difference in the sharp-component of a diffraction profile, between the clean and approximately half-monolayer covered surfaces. The best suited out-of-phase energies are those of maximized difference. This evaluation is particularly suitable for homoepitaxial studies. It is less applicable for hetereoepitaxy, except in those cases where scattering factors of the substrate and overlayer are well matched.

Out-of-phase energies obtained in this representation for Pd on Pd(100) at both 100 and 300 K are presented in Table 1. We have shown that consistent out-of-phase determinations are obtained with the spike-difference even where irregular beam shapes or very short-ranged correlations obscure straightforward evaluation via other methods. The *experimental* determination of out-of-phase conditions is necessary for intensity oscillation studies of thin film growth, since theoretical predictions (15) do not always provide workable results. The spike-difference determination may be used as a complement to, or in place of, FWHM or A/A_0 out-of-phase determinations.

REFERENCES

1. J. W. A. Sachtler, M. A. Van Hove, J. P. Biberian and G. A. Somorjai, Phys. Rev. Lett. 45 (1980) 1601; also Surface Sci. 110 (1981) 19.
2. J. W. A. Sachtler, J. P. Biberian and G. A. Somorjai, Surface Sci. 110 (1981) 43.
3. J. W. A. Sachtler and G. A. Somorjai, J. Catalysis 81 (1983) 77.
4. Research Briefings 1986 (National Academy Press, Washington, DC, 1986).
5. Thin Film Growth Techniques for Low-Dimensional Structures, edited by R. F. C. Farrow, S. S. P. Parkin, P. J. Dobson, J. H. Neave and A. S. Arrott (Plenum Press, New York, 1987).
6. R. Kern, G. Lelay and J. J. Métois in Current Topics in Materials Science, Volume 3, edited by E. Kaldis (North-Holland, Amsterdam, 1979).
7. G. Honjo and K. Yagi, in Current Topics in Materials Science, Volume 6, edited by E. Kaldis (North-Holland, Amsterdam, 1980).
8. Reflection High Energy Electron Diffraction and Reflection Imaging of Surfaces, edited by P. K. Larson and P. J. Dobson (Plenum Press, New York, 1988).
9. J. H. Neave, B. A. Joyce, P. J. Dobson and N. Norton, Appl. Phys. A 31 (1983) 1.
10. D. K. Flynn, W.-D. Wang, S.-L. Chang, M. C. Tringides and P. A. Thiel, Langmuir 4 (1988) 1096.

11. D. K. Flynn, J. W. Evans and P. A. Thiel, J. Vacuum Sci. Technol. A 7 (1989) 2162.

12. R. Altsinger, H. Busch, M. Horn and M. Henzler, Surface Sci. 200 (1988) 235.

13. J. J. De Miguel, A. Cebollada, J. M. Gallego, J. Ferrón and S. Ferrar, J. Crystal Growth 88 (1988) 442.

14. C. S. Lent and P. I. Cohen, Surface Sci. 139 (1984) 121.

15. M. Henzler, Surface Sci. 22 (1970) 12.

16. M. Henzler, Appl. Phys. A 34 (1984) 205.

17. M. Henzler, in Electron Spectroscopy for Surface Analysis Topics in Current Physics, Volume 4, edited by H. Ibach (Springer-Verlag, Berlin, 1977).

18. P. Hahn, J. Clabes and M. Henzler, J. Appl. Phys. 51 (1980) 2079.

19. D. K. Flynn-Sanders and P. A. Thiel, Chemistry Dept., Iowa State University, manuscript in preparation (1990).

20. E. Bauer and J. H. van der Merwe, Phys. Rev. B 33 (1986) 3657.

21. S. L. Beauvais, R. J. Behm, S.-L. Chang, T. S. King, C. G. Olson, P. R. Rape and P. A. Thiel, Surface Sci. 189/190 (1987) 1069.

22. J. W. Anderegg and P. A. Thiel, J. Vacuum Sci. and Technol. A 4 (1986) 1367.

23. B. C. DeCooman and R. W. Vook, J. Vacuum Sci. Technol. 21 (1982) 899.

24. see, for example, Figure 2 of M. Henzler, Surface Sci. 168 (1986)

744; also, Figure 1 of G. Schulze and M. Henzler Surface Sci. 73 (1978) 553.

25. M. Henzler, Appl. Surface Sci. 11/12 (1982) 450.
26. J. M. Pimbley and T.-M. Lu, J. Appl. Phys. 57 (1985) 1121; 57 (1985) 4587; 59 (1986) 2439.
27. K. D. Gronwald and M. Henzler, Surface Science 117 (1982) 180.
28. M. Henzler, Surface Sci. 168 (1986) 744.
29. L. J. Clarke, Surface Crystallography: An Introduction to Low Energy Electron Diffraction (John Wiley and Sons, New York, 1985).
30. J. B. Pendry, Low Energy Electron Diffraction (Academic Press, London, 1974).
31. J. J. Lander, in Progress in Solid State CHemistry, Volume 2, edited by H. Reiss (Pergamon Press, Oxford, 1965).
32. G. E. Laramore, J. E. Houston and R. L. Park, J. Vac. Sci. Technol. 10 (1973) 196.
33. D. Aberdam, R. Baudoing, Y. Gauthier, Surface Sci. 62 (1977) 567.
34. L. D. Roelofs, A. R. Kortan, T. L. Einstein, R. L. Park, Phys. Rev. Lett. 46 (1981) 1465.

APPENDIX: RECOATING LEED OPTICS

The phosphor coating on a LEED screen is very fragile and may become damaged, either by insulating inclusions, metal overlayers, cracks in the phosphor coating or the development of "dark spots". All of these problems can be remedied by coating the screen with a fresh surface of phosphor. Described below is a recoating technique based on sedimentation of a suspension onto the screen. Extreme care must be taken in the preparation of the solution to minimize the number of aggregated particles. The phosphor simply settles on the LEED screen and then the solution is gradually drained out. Lastly, the screen is slowly dried to remove residual water.

Pretreatment

The LEED screen is made of either aluminum or stainless steel. The Varian 981-0129 is made of stainless steel. Determine which you have and follow the prescribed pretreatment.

Stainless Steel: Degrease with methanol. A pickle is necessary only when removing a previous coating. One of two pickles may be used. Pickle 1: 30 volume % HNO_3, 3 volume % HF. Warming the solution will quicken its action. See note below concerning HF safety. Pickle 2: 100 ml HNO_3, 20 ml HF, 20 ml HCl, 800 ml warm deionized, distilled water. See note below concerning HF safety.

(We used the second pickle for about 5 minutes in the ultrasonic bath.)

Aluminum: Degrease with methanol. Dip for 20 seconds in a 6 volume % HF solution. Rinse carefully with deionized, distilled water. Dip for 60 seconds in a 32 volume % solution of HCl. Do not dip for longer than these times. If the aluminum turns black in the HCl solution, repeat the HF and HCl dips. See note below concerning HF safety.

HF Safety: HF is an extremely hazardous acid which may cause severe burns very deep into the tissue. Use of HF requires the utmost care, and special safety precautions must be taken. Protective clothing is essential. In our laboratories, a face shield, neoprene gloves (mid arm length) and neoprene apron are stored under the sink in room 220. Special nalgene labware, including beakers and graduated cylinders are also stored in this room, on the west wall shelves. HF is used only in the hood (room 217) and only when at least one other person is available in our laboratory area. In case of exposure to HF, immediately wash the exposed area of your body with plenty of water. This is very important, since often a burning sensation does not occur until several hours after the exposure. For this reason it is a good practice to wash well after using HF whether you are aware of an exposure or not. If you are aware of an exposure, contact Occupational Medicine and explicitly specify that

the exposure was to HF (not just acid), since the treatment for HF is different than that for other acids. Calcium gluconate gel is available in the first-aid closets for HF burns (EXCEPT in eyes). To use this gel, after washing with water (ca. 20 minutes) shake gel, apply, rub vigorously. You must still report to Occupational Medicine.

Solution Preparation

Prepare two solutions as described in detail below. Adjust ingredients proportionately to meet your requirements of total volume. The recipe below makes 3 l, which is an adequate volume for the Varian 981-0129 LEED screen. Assemble the following ingredients:

Solution 1: 2.5 l deionized, distilled water
1.8 g $Ba(NO_3)_2$

Solution 2: 0.5 l deionized, distilled water
0.18 g silica gel
3.18 g phosphor

A note about the phosphor. We have used RCA-33-Z-151M, a zinc sulphide phosphor activated with Ag, which contains no Cd. This phosphor is commonly used for black and white television screens. It gives bluish LEED spots, to which the camera is sensitive, but not your eyes. The particles of this phosphor are rounded polyhedra, i.e., somewhat

crystalline, that range from 1.5 to 6 microns in diameter. There are, however, quite a number of clustered particles that are approximately 15 to 30 microns. A better phosphor to use is Lumilox® Yellow-Green B20-1B. It is available from Riedel-DeHaan AG, Seelze Hannover, Federal Republic of Germany. This phosphor has a yellow-green emission to which both your eye and the camera are sensitive. However, this phosphor contains beryllium, which is absorbed through the skin and is toxic (especially in this powdered form), and, thus OSHA regulated. This phosphor is made up of highly spherical particles, more uniform in size, 2-3 microns. Again, clusters of 15-30 microns are common. Because of high toxicity, extreme care must be taken to avoid contact with this phosphor. Always wear gloves and avoid breathing the dust.

The object of the following procedure is to get a homogeneous solution of small, fine phosphor particles. A large ultrasonic bath is necessary. A sonic disruptor (also called an ultrasonicator, but not to be confused with an ultrasonic bath) may also be used, and is recommended for preparation of the RCA phosphor. Adjust the procedure to fit whatever equipment is on hand to achieve the final goal: homogeneous solution of small, fine particles. At Ames Laboratory, there was a sonic disruptor in the group of Dr. Burkhart, once located in Metals Development (it may take a bit of searching to find that equipment now). A few words of caution. All water, including rinse water, should be deionized, distilled water. Make sure <u>all</u> of the glassware used is clean and free of dust. Unless specified, do not let the phosphor solution stand. Continue immediately with the next step to prevent settling.

Always cover the solutions to protect from dust. Never put a volumetric flask *with* a stopcock in the ultrasonic bath. The stopcock will get wedged down by the action of vibration and become nearly impossible to remove.

Solution 1:

Add the $Ba(NO_3)_2$ to a convenient amount of water in an Erlenmeyer or volumetric flask (300-500 ml). Shake vigorously by hand for 2 minutes. Put in the ultrasonic bath until ready to use, anywhere from 10 minutes (minimum) to 2+ hours. The solutions will get hot after some time in the ultrasonic bath, so be sure to periodically (ca. every 10-30 minutes) check the bath temperature and replace the bath water with cool water as necessary. Also, periodically shake the solution vigorously by hand. Shake vigorously before using.

Solution 2:

Because aggregated particles are prevalent in the RCA phosphor, we use a sonic disruptor to prepare this solution. In a beaker, make a solution of the silica gel and phosphor with 150 to 175 ml of water. Use the sonic disruptor at 30 % duty cycle on a setting of 4, while stirring vigorously with a magnetic stirbar. Continue for about 5 minutes. Stop to let the solution cool if necessary. Continue for about another 6 minutes. Use immediately. If using the Lumilox® phosphor, combine water, phosphor + silica gel in a volumetric or Erlenmeyer. Shake vigorously by hand for ca. 2 minutes. Put in

ultrasonic bath for ca. 5 minutes. Repeat the hand-shaking and ultrasonic steps. Use immediately.

Transfer the phosphor solution into a large Erlenmeyer (≥ 1 l) using the rest of the 500 ml total of water in a squirt bottle to completely transfer the solution from the beaker. Add the $Ba(NO_3)_2$ solution, using water to rinse and make a final volume of ca. 1 l. Shake vigorously by hand 1-2 minutes. Put in ultrasonic bath for 10 minutes. Shake vigorously again by hand for 1-2 minutes. Pour into a 3 or 4 l beaker (a 4 l beaker is available from Dr. Gerstein's group). Rinse the flask several times with deionized, distilled water adding the wash to the beaker. Fill to 3 l with deionized, distilled water to make 3 l. Using a large stirbar (ca. 3 inch), stir on highest setting of stirplate for 5-10 minutes. When the vortex disappears, let the solution settle for 10 minutes. This allows for the sedimentation of large particles. (Be sure that the solution is covered to prevent dust contamination.) Time the settling period. If this period is too long, the desired, finer particles will settle. Carefully decant the solution into another beaker. Do not stir up the bottom of the solution while pouring, and leave enough solution behind to avoid pouring out larger particles. Cover the decanted solution and let settle for 7 minutes. Using a funnel, and directing the solution away from the screen, carefully decant this solution into the sedimentation beaker (in which the LEED screen is already suspended, as described below). It is important to pour evenly

and continuously, to avoid introducing air into the solution. Trapped air may form bubbles which adhere to the LEED screen.

Sedimentation Process

The sedimentation beaker is a 3 l beaker with a stopcock glassblown in the center of the bottom. Set the beaker on a ringstand, or other appropriate holder, as level as possible. Use an area that is as free of vibration as possible, perhaps in an unused room on a thick neoprene mat. Suspend the LEED screen about 3/4 (or slightly more) the distance to the bottom of the beaker using 3 hooks made from stiff wire. Attach the hooks to the screen through the holes near the perimeter of the screen, and bending them around the sides of the beaker (see Figure 1). Do not support the screen in any other way, and do not let the screen hang too low. The goal is that nothing will disrupt the flow of the solution past the LEED screen while draining. Take care to level the screen. The hole in the screen for the electron gun invariably leaves a lingering drop which depletes/disrupts the coating around the hole. A level screen will leave this area is as small and symmetric as possible. Cover the beaker to prevent dust from settling.

Let the solution stand at least 5 hours, until it is very clear (we have used ~ 11 hours). After this time, carefully adjust the stopcock until the solution just begins to slowly drip out. Do not disturb the solution in any way which might disrupt the settled coating. This coating is very fragile, *especially* when it is wet. Set a flow rate to

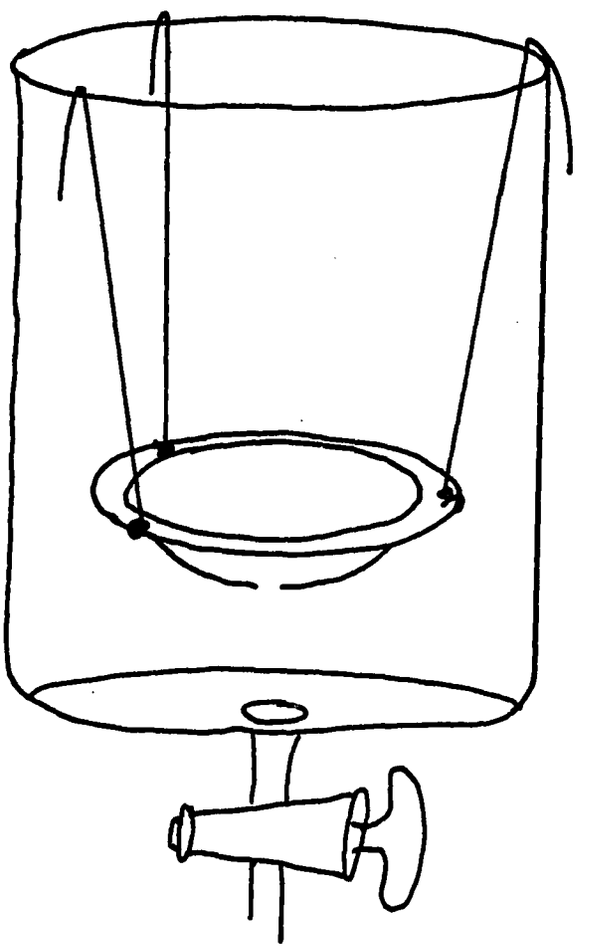

Figure 1. Beaker setup

3 l beaker adapted with a straight-through valve for draining. LEED screen is suspended in the beaker by three stiff wires shaped into hooks.

drain the entire solution in 3 or more hours. We have used ca. 1 drop per second to drain a 3 l solution.

Drying

After draining is complete, let the screen stand (covered) several hours, or overnight. When the screen appears dry, carefully lift it out of the sedimentation beaker and bake for half an hour at 80 C. Keep the screen covered to prevent dust from settling on it. Store the screen in a dust-free desiccator if necessary.

Results

The screen should look homogeneous, with no large particles, dust, bare or thin patches. The sedimentation process may be repeated up to 4 times, if necessary, to get a sufficiently thick coat. However, each time the process is repeated, there is a risk of "lifting" the previous coating, especially when filling the sedimentation beaker. It may be better to restart the procedure with more solution (i.e., in a taller beaker) and/or a more concentrated solution.

We have successfully used this technique to recoat the Varian 981-0129 LEED screen. We prepared the solutions in one day. Sedimentation proceeded overnight. The next day was devoted to draining, followed by room-temperature drying overnight. The third morning the screen was baked. Organization is important, since it is imperative the solutions are used immediately upon preparation. It is helpful if two people work together if time is essential. One person should prepare the solutions,

the other should prepare the screen and set up the sedimentation beaker. If two people are not available, prepare the screen and sedimentation beaker *before* preparing the solutions.

CONCLUSIONS

We examine the epitaxial growth of thin metal films via low-energy electron diffraction (LEED). In particular, we consider Pt and Pd on Pd(100) in an attempt to understand the basic growth processes and the potential of this technique. The main conclusions of this dissertation are summarized below:

(a) We demonstrate the use of a *conventional* LEED apparatus in monitoring diffracted intensity oscillations during the growth of Pt and Pd films on Pd(100). Despite the rather short coherence length of commercial instruments, our LEED profiles are adequately resolved into two separate components at out-of-phase energies. With LEED, we observe intensity oscillations during metal film growth, analogous to those measured with reflection high-energy electron diffraction during the epitaxial growth of semiconductors. The oscillations of the central-spike intensity are damped due to the growth of Pt and Pd/Pd(100) and rather short-lived. We show that only small deviations from perfect layer-by-layer growth severely diminish the central-spike intensity.

(b) The equilibrium growth mode both for Pt and Pd on Pd(100) is layer-by-layer. At low and intermediate temperatures, the system is kinetically limited by the barrier to surface diffusion. From distinct changes in the profile lineshapes with temperature, we estimate the diffusional barrier to be ca. 10 kcal/mol for Pt on Pd(100) and ca. 13 kcal/mol for Pd on Pd(100). At high temperatures, Pt reconstruction interferes with the growth of pseudomorphic layers on Pd(100). For Pd on

Pd(100), growth proceeds via "step propagation" at high temperatures. In this mechanism, nucleation of new layers begins only on very large terraces, thus the initial morphology is more or less maintained throughout growth.

(c) We observe oscillations in the out-of-phase diffracted intensity for the growth of Pt and Pd on Pd(100) at substrate temperatures as low as 95 K. We show intensity oscillations are *predicted* for random deposition at low temperatures, *even in the absence of surface diffusion.* This is in contrast to the assertion by other authors (22) that deposited atoms use their latent heat of condensation (ca. 70 kcal/mol for metal systems) and are transiently mobile, aiding in the development of quasi-layer-by-layer growth. We demonstrate that the *necessity* of creating the fourfold-hollow adsorption site for the birth of an upper layer is sufficient to instill a quasi-layer-by-layer quality to the growth.

(d) Ring-structure in the profile lineshape develops at ca. 200 K for the growth of Pd on Pd(100), and is associated with the onset of diffusion. Indicative of a more uniform growth, ring-structure is evident between ca. 200 and 400 K. Herein is the first report of oscillations in the ring intensity as a function of coverage, demarking the detailed filling of individual layers. Although central-spike intensity oscillations show substantial damping, the *existence* of oscillations in the ring intensity indicates a growth mechanism quite close to perfect layer-by-layer.

(e) Based on the temperature- and coverage-dependence of the in-phase intensity during the epitaxial growth of Pd(100), we propose that in the limit of *very small* islands (one to a few atoms), the interlayer spacing is dependent on the number of atoms in the island. Recent molecular-dynamics simulations, showing that single Pd atoms on Pd(100) are 14 % closer to the Pd substrate than would be predicted from the first Pd(100) interlayer spacing support our postulate (23).

(f) We develop a model to clarify the role diffusion plays in initially enhancing the layer-by-layer quality of thin film growth on fcc(100) surfaces. Interlayer diffusion augments layer-by-layer growth for obvious reasons. Surprisingly, both intralayer and interlayer diffusion result in clustering which *reduces* the layer-by-layer quality. However, the net result of surface diffusion in the onset regime is to enhance the layer-by-layer quality of the growing film, as is observed in our experimental investigation.

(g) We present a novel, graphical representation for the layer-converges during thin film growth. This representation is not restricted to fcc(100) geometry, and can be generally applied to epitaxial growth systems. Deviations from layer-by-layer growth and the onset of diffusion are among the types of information that can be extracted from this new representation.

(h) We present a new procedure to experimentally determine out-of-phase energies suitable for monitoring intensity oscillations during thin film growth. This method, called the Spike-Difference, is based on the energy-dependence of the central-spike intensity, and appears to be less

sensitive to the coverage distribution than the FWHM or A/A_0 methods. The Spike-Difference may be used in conjunction with, or in place of, the FWHM and A/A_0 techniques.

In summary, we show conventional LEED is a useful technique in the investigation of epitaxial growth. A wealth of information is contained in the spot profile, and we are only now learning how to fully evaluate this information. Understanding the growth processes in the simple systems studied here is essential in furthering our knowledge of the creation of interfaces, making possible the development of new materials with novel physical and chemical properties.

REFERENCES

1. A. G. Sault and D. W. Goodman, in Advances in Chemical Physics, edited by K. P. Lawley (John Wiley and Sons, New York, 1989).
2. C. T. Campbell, in Advances in Catalysis, Volume 36, edited by D. D. Eley, H. Pines and P. B. Weisz, (Academic Press, Inc., San Diego, 1989).
3. J. H. Sinfelt, Bimetallic Catalysts (John Wiley and Sons, New York, 1983).
4. J. W. A. Sachtler, M. A. Van Hove, J. P. Biberian and G. A. Somorjai, Phys. Rev. Lett. 45 (1980) 1601.
5. J. W. A. Sachtler, M. A. Van Hove, J. P. Biberian and G. A. Somorjai, Surface Sci. 110 (1981) 19.
6. J. W. A. Sachtler, J. P. Biberian and G. A. Somorjai, Surface Sci. 110 (1981) 43.
7. J. W. A. Sachtler and G. A. Somorjai, J. Catalysis 81 (1983) 77.
8. D. W. Goodman and J. E. Houston, Science 236 (1987) 403.
9. D. W. Goodman and C. H. F. Peden, Ind. Eng. Chem. Fundam. 25 (1986) 58.
10. J. E. Houston, C. H. F. Peden, D. S. Blair, D. W. Goodman, Surface Sci. 167 (1986) 427.
11. C. H. F. Peden and D. W. Goodman, J. Catalysis 100 (1986) 520.
12. J. E. Houston, C. H. F. Peden, P. J. Feibelman, D. R. Hamann, Phys. Rev. Lett. 56 (1986) 375.

13. Magnetic Properties of Low-Dimensional Systems, edited by L. M. Falicov and J. L. Moran-Lopez (Springer-Verlag, Berlin, 1986).

14. J. J. Krebs, B. T. Jonker and G. A. Prinz, in Materials Research Society Proceedings, Volume 151, edited by B. T. Jonker, J. P. Heremans and E. E. Marinero (Materials Research Society, Pittsburgh, 1989) and references therein.

15. B. T. Jonker, K.-H. Walker, E. Kisker, G. A. Prinz, C. Carbone, Phys. Rev. Lett. 57 (1986) 142.

16. J. Gay and R. Richter, Phys. Rev. Lett. 56 (1986) 2728.

17. T. K. Gaylord and K. F. Brennan, Appl. Phys. Lett. 53 (1988) 2047.

18. C. R. O'Dell, Physics Today 43 (1990) 32.

19. E. Bauer and J. H. van der Merwe, Phys. Rev. B 33 (1986) 3657.

20. J. B. Pendry, Low Energy Electron Diffraction (Academic Press, New York, 1974).

21. L. J. Clarke, Surface Crystallography, An Introduction to Low Energy Electron Diffraction (John Wiley and Sons, Chichester, 1985).

22. W. F. Egelhoff, Jr. and I. Jacob, Phys. Rev. Lett. 62 (1989) 921.

23. D. E. Sanders and A. E. DePristo, Iowa State University, Chemistry Department, manuscript in preparation.

ACKNOWLEDGEMENTS

I thank my advisor, Pat Thiel, for her supervision and support throughout this work. She always saw the perspective when I found myself concentrating too much on details. I thank her for her guidance and the many skills she has helped me develop.

I am indebted to Dr. Jim Evans and Dr. Michael Tringides for inspiring discussions of the data and direction in the interpretation. I express gratitude to those who helped with the experiments: Wendi Wang, Dr. Wai Leung, Dr. NaiJuan Wu and Oden Warren. I extend a special appreciation to Oden Warren, who untiringly helped with equipment repairs. I must also mention Dr. Sheng-Liang Chang, a man of exemplary patience and perseverance, whom I'd often think of when frustrated by delicate clean-room tasks. In addition, I thank Jim Anderegg, for consultation over electronic and interfacing problems, and Charlie Burg, for skillful welding.

I thank the past and present members of the Thiel group, who made my work here enjoyable. Assistance was offered whenever requested, and I am most grateful. The comradery among group members made this place more than "just work". Fond memories will be held for the 5:00 "J" meetings. Special thanks to those who made birthdays in the Thiel group deliciously delightful: Mike Columbia, Pam Leavitt, Barb Nielsen, Mary Walczak and to the newest members who will carry on the tradition: Anna Crabtree and the "microwave king" Mark Jensen.

I thank my mother and father, Mary Ann and James, for their encouragement, love and support through all of my endeavors. I especially appreciate the love and patient understanding of my husband, David. His faith in me helped me to strive further.

I am grateful for the opportunity to work in Munich at the Institute of Physical Chemistry in the Spring of 1986. I enjoyed working with Dr. Jürgen Behm and Dr. Keith Jamison. The investigation of K on Ni(110) and Au(110), which is not included in this dissertation, was supported by the Alfred P. Sloan Foundation and the Deutscher Akademischer Austauschdienst.

I thank the Iowa State University Committee for Women in Science and Engineering, Procter and Gamble Company, Association for Women in Science Educational Foundation, American Vacuum Society and Dow Corning Corporation for financial assistance. This work was supported by the Ford Motor Company and the National Science Foundation, Grant No. CHE-8451317 and performed at Ames Laboratory under contract No. 7405-ENG-82 with the U.S. Department of Energy. This dissertation is assigned DOE Report No. IS-T-1415.